

The effects of local fibre steering

Reducing gaps and overlaps
by compensating for tow width fluctuation
in automated fibre placement

J.M.W. van Kollenburg

Technische Universiteit Delft

Local fibre steering

Reducing gaps and overlaps
by compensating for tow width fluctuation
in automated fibre placement

by

J.M.W. van Kollenburg

to obtain the degree of Master of Science at the Delft University of Technology, to be defended
publicly on Friday January 22, 2021 at 9:30 AM.

Student number: 4362594
Project duration: January 6, 2020 – December 4, 2020
Thesis committee: Prof. C.A. Dransfeld, TU Delft, chair
Dr. ir. D.M.J. Peeters, TU Delft, supervisor
Dr. ir. O.K. Bergsma, TU Delft
ir. R. Tonnaer, SAM|XL

An electronic version of this thesis is available at <http://repository.tudelft.nl/>.

Cover illustration: Coriolis Composites [8]

Preface

The year 2020 has definitely not been easy for many of us. After finishing my literature study I started working on my thesis in January not knowing what would be ahead. It quickly became clear that I would have to do a lot of work from home which certainly had not my preference. Fortunately, there were many people that made the job a lot more comfortable.

First and foremost I would like to express how thankful I am for all the effort done by my supervisor Daniël Peeters. Just as quickly as we found a thesis topic of my interest, he adapted the project to make it more suitable for a pandemic. I recognise that I probably cost him a lot of time with our meetings almost every week. He not only offered a lot of professional guidance but often there was also time for some chatting that I would otherwise have had in and around the faculty. Something that is very much appreciated in the times of social distancing.

I am sure I would have learnt even more from Rik Tonnear, lead automated manufacturing engineer at SAM|XL, if it were not for COVID-19. Nevertheless, I would like to thank him for all his help during throughout the project.

Of course, there were also people that supported me more personally, my friends and family whom I could not have done this without. Especially my grandmothers for always checking up on me. Their weekly updates definitely made the year less lonely for both of us. Some special thanks to Willem for his help with illustrations and for being my sparring partner whenever I needed one. There are many more people I should not forget to mention. Such as my fellow ASM students in room NB1.07, or the ones that kept me company at a safe distance in the library. Of course, I will not forget my roommates that made working from home a lot more pleasant. Lastly, Coldplay, for all the hours that one of their albums was my background music.

The report is written for other people in the field of aerospace structures and materials, so some prior knowledge is expected. However, many concepts are shortly explained before going more into detail.

I wish you much joy in reading

*J.M.W. van Kollenburg
Delft, November 2020*

Abstract

The aerospace industry increasingly uses fibre-reinforced plastics that are manufactured using automated fibre placement (AFP). A common problem in AFP is the occurrence of defects. The most frequent defects are gaps and overlaps [18]. Especially narrow systemic gaps and overlaps are important. Narrower gaps and overlap cause more fibre waviness [9]. The most significant effect of gaps and overlaps is a compressive strength reduction mainly driven by fibre waviness [42, 53]. Randomly distributed defects probably have no considerable negative effect. Systemic defects appear frequently at the same planar location causing them to build up and lead to a knockdown in strength [9]. Tow width fluctuation is an important cause of gaps and overlaps. Moreover, the resulting defects are narrow and systemic.

Two developments in manufacturing are combined to create a new mitigation method for gaps and overlaps. One development is fibre steering, which harnesses the flexibility of AFP to vary the fibre orientation within the ply. Traditionally, all fibres within a single layer have the same orientation. There are still many challenges that need to be faced before these so-called variable stiffness laminates become widely used. Another development is smart manufacturing which means moving from a traditional, linear and sequential supply chain to a dynamic interconnected system. The increased usage of data allows it to respond to changes real-time.

The suggestion is to use fibre steering locally to place tows adjacent to each other to compensate for tow width fluctuation. Local fibre steering can be considered a form of smart manufacturing as the tow paths in the laminate construction respond to change in the material input. The research question is: how effective is local fibre steering in increasing the structural performance of composite laminates by reducing gaps and overlaps through compensating for tow width fluctuation in automated fibre placement? The question is answered in the three steps.

Firstly, it is determined to what extent gaps and overlaps are reduced by constructing a conventional and a steered laminate. The tow width is modelled using a cubic spline with nodes at a constant distance from each other and their values taken from a normal distribution described by mean tow width and standard deviation. Literature indicated that a typical tow width tolerance for a 6.350 mm tow is 0.254 mm (4 %) [21]. In the conventional laminate, the tow paths are straight and at a constant distance from each other. The steered laminate uses numerical approximations of the equations for parallel parametric curves. A problem is that the curvature accumulates leading to self-intersections and cusps. Also, large angle deviations are experienced. The curvature accumulation is tackled by smoothing a tow path iteratively with a smoothing spline until the minimum radius of curvature (ROC) is reached. Theoretically, the lowest minimum ROC is about 50 mm to avoid self-intersections and cusps. Practically, automated fibre placement prescribes 400 mm to avoid tow wrinkling or upfolding [38]. The maximum fibre angle deviation can be limited by levelling the tow path by taking a weighted average in the transverse direction.

Secondly, the tow width model is validated by measuring the tow width of two different materials. The material is unwinded from a spool that is connected to an electric brake to maintain tension. A different spool rewinds the material using a stepper motor after passing it by a laser-line scanner to measure the tow width. The mean tow width and standard deviation can be derived directly from the measurements. The spline node distance is found iteratively by varying it until the roughness measure tow model is sufficiently close to that of experimental data. The roughness measure is the average of the second derivative squared. Unfortunately, the data quality was not as expected. The tow width was expected to be normally distributed. Therefore, a moving average was applied until the probability density of the tow width resembled more that of a normally distributed variate. The mean tow widths of the two materials that were tested deviate only slightly from what the supplier prescribed. Before smoothing, the standard deviation is about five times smaller than literature indicated. The spline node distance is roughly around one millimetre. Afterwards, the standard deviation is about ten times smaller than expected. The spline node distance is in the order of millimetres.

Thirdly, the effect of the reduction in gaps and overlaps and the fibre angle deviation on the structural performance is calculated using a finite element method (FEM). The basis is the defect layer method

introduced by Fayazbakhsh et al.. Because the fibre orientation is not a direct function of the planar location, each ply is separated into two layers: the material layer and the overlap layer. The elastic properties in the material layer are scaled proportionally to the amount of gaps using the rule of mixtures. The thickness of the overlap layer is scaled to the amount of overlaps. The fibre orientation in each layer is determined by taking the average weighted by the area. The buckling load and the effective stiffness are calculated. The finite element method is in good agreement with analytical results.

The results from the laminate model showed that local fibre steering is not able to eliminate gaps and overlaps completely because it is limited by the minimum radius of curvature. The structural analysis showed that local fibre steering can achieve a higher effective stiffness. The positive effect of reducing gaps surpasses the negative effect of the induced fibre angle deviation. The conventional laminate did have a higher buckling load than the steered laminate. This is ascribed to the fact that it depends on the flexural stiffness which is proportional to the thickness cubed, so in the current model, overlaps have a large positive effect on the buckling load.

The following recommendations are discussed. The ability of local fibre steering to reduce gaps and overlaps can be improved by either lowering the minimum ROC required by the AFP process or by improving the material quality to slow curvature accumulation by having smoother edges. Gaps and overlaps especially have an effect on the compressive strength through induced fibre waviness, so incorporating the fibre waviness and the damage behaviour of laminates can demonstrate the potential of local fibre steering even more. Also, the productivity must be considered in order to more accurately examine the real costs of local fibre steering. Future work should focus more on the practical side of local fibre steering including what is necessary to employ it.

Contents

List of Figures	ix
List of Tables	xi
Nomenclature	xiii
1 Introduction	1
1.1 Automated fibre placement	1
1.2 Fibre steering	2
1.3 Smart manufacturing	3
1.4 Local fibre steering	4
2 Gaps and overlaps	5
2.1 Other defects in automated fibre placement	5
2.2 Causes	8
2.2.1 Skew ply boundaries	8
2.2.2 Shifted method	8
2.2.3 Tow width fluctuation	9
2.3 Effects	10
2.4 Modelling	13
2.5 Mitigation	14
3 Research outline	17
4 Model	19
4.1 Tow model	19
4.2 Conventional laminate	20
4.3 Parallel curve construction	22
4.4 Minimum radius of curvature	24
4.5 Fibre angle deviation	29
4.6 Preliminary results: defect area percentages	31
5 Validation of tow model	33
5.1 Method	33
5.1.1 Material	34
5.1.2 Sensor	35
5.2 Validation results: tow width fluctuation	37
6 FEM	41
6.1 Fibre angle	41
6.2 Mapping	42
6.3 Analysis	43
6.4 Results: structural performance	46
6.4.1 Cases	46
6.4.2 Coverage strategies	47
6.4.3 Layup	48
6.4.4 Maximum fibre angle	48
6.4.5 Minimum radius of curvature	49
6.4.6 Individual defect types	50
7 Conclusion	53
7.1 Reduction of gaps and overlaps	53
7.2 Structural performance	53
7.3 Tow width fluctuation	54

8 Recommendations	55
8.1 Improve the current research	55
8.2 Improve local fibre steering	55
Bibliography	57
A MATLAB code	63

List of Figures

1.1	Main manufacturing processes for composite laminates	1
1.2	Fibre placement head [11]	2
1.3	A section of a conventional laminate versus local fibre steering	4
2.1	Fibre angle deviation due to finite course width [29]	5
2.2	Tow misalignment causing a gap [18] (Courtesy of Netherlands Aerospace Centre (NLR))	6
2.3	Fibre waviness as defined by Heinecke and Willberg (adapted from:[18])	6
2.4	Tow upfolding due to lack of tackiness [18] (Courtesy of Netherlands Aerospace Centre (NLR))	7
2.5	Fuzzball that contaminates the laminate formed by abrasion of fibre material [18] (Courtesy of Netherlands Aerospace Centre (NLR))	7
2.6	Different coverage strategies at ply boundaries (Adapted from: [33])	8
2.7	Shifted method with different configurations (adapted from: [45])	9
2.8	Cross-sectional shape of fibre placement materials [49]	9
2.9	Defect configurations used by Croft et al. (Adapted from: [9])	11
2.10	Microstructural SEM observations of different defect regions (adapted from: [26])	11
2.11	Defect layer method compared to previously existing approaches for different mesh sizes	13
2.12	The effect of staggering on the thickness distribution of variable-stiffness laminates [44]	14
2.13	Different ply construction methods (adapted from: [25])	16
3.1	Research outline	18
4.1	Rough tow model	19
4.2	Smooth tow model ($dl = 10$ mm)	20
4.3	An example of a single ply of the conventional laminate	21
4.4	The centreline distance d between tows and the resulting gaps and overlaps	21
4.5	Coordinate system	23
4.6	Loop in the construction of a parallel curve	24
4.7	Local fibre steering resulting in self-intersections and cusps	24
4.8	Accumulation of curvature: self-intersections and cusps	25
4.9	Distribution of applied in-plane stress for different values of α [2]	25
4.10	Young's modulus and shear modulus of unidirectional composite material as a function of fibre orientation (AS4/ 3501-6 carbon/epoxy) (adapted from: [10])	30
4.11	The effect of levelling on a simple sine curve	31
5.1	Render of the tow width measurement setup	33
5.2	Single point optical triangulation based on a single laser beam and a position-sensitive detector (Adapted from: [51])	35
5.3	Screen capture of scanCONTROL Configuration Tools	36
5.4	A section of prepreg tape measured twice	38
5.5	Probability density distribution before and after smoothing	39
6.1	Tow element	42
6.2	Determining which tow elements intersect with a certain mesh element	42
6.3	Separating into a material and overlap layer and scaling the properties	43
6.4	Buckling analysis	44
6.5	Static analysis	45
6.6	The structural performance for different cases	46
6.7	The effect of different coverage strategies on the structural performance	47

6.8	The effect of local fibre steering on a quasi-isotropic and a cross-ply layup	48
6.9	The effect of a maximum fibre angle on the structural performance ($ROC_{min} = 400$ mm)	48
6.10	The effect of the minimum radius of curvature on the structural performance	49
6.11	Mesh element with individual defect types excluded	50
6.12	Individual defect types excluded in the calculation of the buckling load	51
6.13	Individual defect types excluded in the calculation of the effective stiffness	51

List of Tables

2.1	Tow width and respective tolerance according to different sources	10
4.1	Standard tow and laminate parameters	20
4.2	Minimum radii of curvature for different tow widths using a 102 mm-wide course [6]	26
4.3	Defect area percentages	31
5.1	Material 1: Toray Cetex TC1320 PEKK [47]	34
5.2	IM7 carbon fibre properties [10]	35
5.3	PES polymer properties [3]	35
5.4	Results of the validation of the tow width fluctuation before smoothing	37
5.5	Results of the validation after smoothing	39
6.1	Composite material properties carbon-reinforced epoxy (AS4/3501-6) [10]	43
6.2	Matrix material properties epoxy (3501-6) [10]	44

Nomenclature

The next list describes several symbols and acronyms that will be later used within the body of the document. The list does not include all symbols but only the ones used by the tow model, laminate model or structural model directly. Some may be reused in other equations or text. When a symbol is used for another purpose it is always specified locally.

γ	Tow path data point
μ	Mean tow width
ν	Poisson's ratio
ρ	Density
σ	Standard deviation
θ	Fibre angle
a	Plate dimension
d	Centreline distance or half tow width
dl	Spline node distance
dx_0	Step size
E	Stiffness modulus
f	Tow model function
G	Shear modulus
h	Laminate thickness
i	Length index
j	Tow index
k	Curvature
l	Tow length
m	Number of points per tow
n	Number of tows
p_θ	Levelling parameter
p_k	Smoothing parameter
r	Radius
S	Smoothing splines
s	Distance travelled along the tow material
t	Ply thickness
v	Volume fraction

w	Tow width
x	Reference coordinate
y	Reference coordinate
AFP	Automated fibre placement
ATL	Automated tape laying
CPS	Cyber-physical system
CTS	Continuous tow shearing
DAP	Defect area percentage
FEM	Finite element method
IoT	Internet of things
OHC	Open hole compression
PEKK	Polyetherketoneketone
ROC	Radius of curvature
RTD	Room temperature dry
UD	Unidirectional
VSL	Variable stiffness laminate

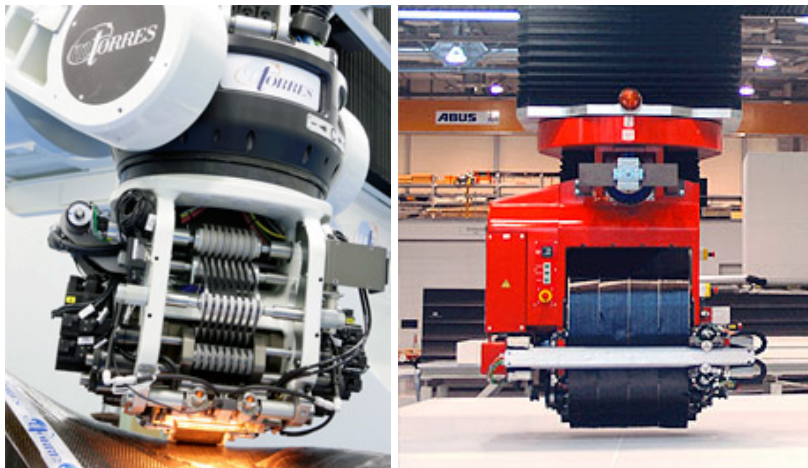
Introduction

Fibre-reinforced plastics have a higher weight-specific stiffness and strength compared to historically used materials in aerospace structures like aluminium alloys. The adoption of these light-weight materials enables a reduction in the fuel consumption of aircraft and ultimately results in a lower operational cost.

To benefit from these properties, the aerospace industry has increased its use of composite materials over the past decades. Approximately half of the aircraft's structural weight of recently introduced models, such as the Boeing 787 Dreamliner, consist of fibre reinforced plastics [17]. In other sectors, for instance, automotive and renewable energy, composites are also of growing interest.

1.1. Automated fibre placement

Two common production methods for composite structures are automated tape laying (ATL) and automated fibre placement (AFP) which can be seen in Figure 1.1. Both use tapes of continuous fibres that are impregnated with a polymer resin which are placed alongside each other to form one layer known as a ply. The plies are stacked in a certain sequence to form a laminate. Until recently all fibres within a layer had the same orientation, typically 0° , $\pm 45^\circ$, or 90° .



(a) Automated Fibre Placement [36]

(b) Automated Tape Laying [35]

Figure 1.1: Main manufacturing processes for composite laminates

Automated tape laying uses prepreg that is typically 75, 150, or 300 mm wide which is similar to the material used for manual layup. For automated fibre placement, the tapes are slit into smaller tows. Common tow widths are 3.175 mm (1/8 in), 6.35 mm (1/4 in), and 12.7 mm (1/2 in). To maintain the productivity up to 32 tows are placed simultaneously in one so-called course. The tows are guided from a creel cabinet, where the material is stored, to the robot system on which an end effector is

mounted that deposits the material on a mould. A schematic overview of such a fibre placement head can be seen in Figure 1.2. The material can also be stored on the head directly, but this usually requires a more expensive gantry type system due to the increased weight [33].

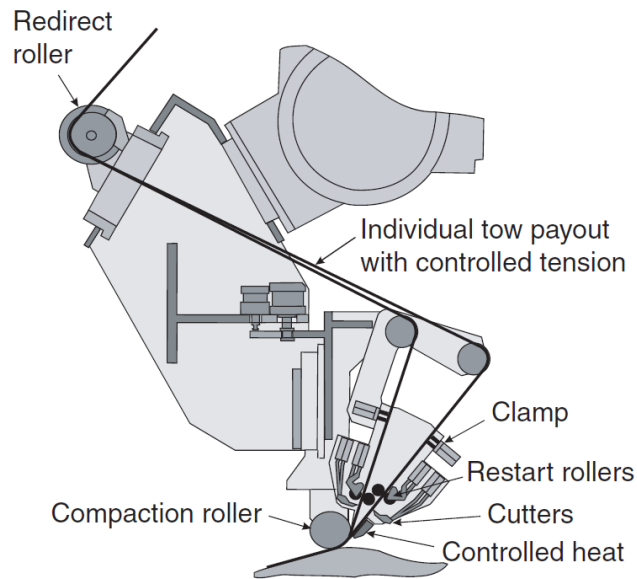


Figure 1.2: Fibre placement head [11]

Two important elements on the AFP head are the compaction roller and the heating element. The compaction roller applies pressure on the fibre course to make it conform to the shape of the mould. The compression by the roller also reduces the amount of trapped air in the composite. The reason for the controlled heat depends on the material that is used in the process. For thermoset composites, the heater is used to increase the tackiness to adhere the tows to the previous layer or the tool surface. The laminate is after placement cured in an autoclave where heat and pressure cause consolidation. When laying thermoplastic material, the heat together with the compaction from the roller is generally sufficient for in-situ consolidation. Independent of the material used, the purpose of the compaction roller and the heater is to make one single product from separate layers that has a minimal amount of voids and the required dimensions [41].

Before the heater and compaction roller, the material has gone through the cut, clamp and restart module. It enables each tow to be controlled individually which is an important advantage of AFP. The waste at the edges of products can be substantially reduced by being able to cut or restart each tow separately. The same goes for cut-outs such as windows and doors in a fuselage section. It can also regulate the speed with which each distinct tow is deposited.

1.2. Fibre steering

The differential tow payout capability, i.e. the ability to control the deposit rate of each tow, is especially important for curvilinear paths. At a curvature the inner and outer edge of the material experience different radii. As a result, one side is under tension while the other is under compression which can cause wrinkling. Because AFP uses more narrow tows, that can be dispensed at different rates, higher curvatures can be achieved.

Since manual and automated tape laying use wider tapes the design freedom in composite laminates has traditionally been restricted to straight fibre paths. On top of that, stacking sequences have generally been only a combination of four conventional fibre orientation: 0° , 45° , -45° , or 90° . Over time a lot of knowledge and experience has been gained about conventional straight-fibre laminates and consequently the design of fibre-placed composites is still often limited. Therefore the potential of automated fibre placement is not fully utilised, but fortunately, it is changing.

Today, more research is done on using the flexibility of AFP to vary the fibre orientation within the ply which is called fibre steering. A laminate where the fibre orientation in each ply is not uniform is

known as a variable stiffness laminate (VSL). Allowing curvilinear tow paths enables the tailoring of load paths that leads to an improved stress distribution and ultimately a higher laminate performance [31]. The laminate can virtually be designed to conform to the local stress state [16].

There are numerous examples of research that have proven the advantages of fibre steering. Variable stiffness laminates can have a significantly higher buckling load compared to their constant stiffness counterparts according to numerical analysis [31, 43]. Also post-buckling, an improvement of the failure load has been shown experimentally [30, 54] as well as numerically [31]. Furthermore, curvilinear-fibre panels can be designed to have an increased tolerance to central holes relative to straight-fibre laminates [30]. This can only be achieved by the ability to tailor load paths. For example, in a plate with a hole under compression, the load is redistributed from the critical regions using fibre steering and consequently, damage can be postponed [23, 31]. Not only the response to a single load case can be improved but varying the fibre angle within the ply makes it easier to balance different design objectives. For instance, for a certain VSL there exist many configurations with equal buckling load yet different values for axial stiffness or vice versa [15], while for a comparable CSL a compromise must be made. The decoupling of the design goals makes it easier to optimise for multiple conditions.

However, this freedom comes at a cost. The larger design space makes it difficult for the design to converge to a practical solution. Another disadvantage of fibre steering is the difficulty of transforming the design into an actual part that can be manufactured using automated fibre steering [16]. As a result, the number of practical applications of variable stiffness laminates is limited and at the moment the industry is not fully embracing the technology [32]. It can take a long time for manufacturers to adopt fibre steering in composite laminates.

1.3. Smart manufacturing

Next to the employment of fibre steering, another development is happening in the world of manufacturing. Throughout history, there have been three industrial revolutions. The First Industrial Revolution is marked by mechanisation, the transition from work by hand or with animals to the use of machines often using steam power or water power. The Second Industrial Revolution, or Technological Revolution, is characterised by electrification and mass production enabled by the introduction of the production line. The Third Industrial Revolution, or Digital Revolution, features automation facilitated by the use of information and communications technology and electronics [50].

Currently, manufacturing is undergoing the Fourth Industrial Revolution, typically referred to as Industry 4.0. The transformation is about manufacturing becoming *smart*. The major technologies driving this are IoT (Internet of things), and CPS (Cyber-physical system) [24]. Previously seen automation enable elements in the manufacturing process to operate with a defined set of rules or thresholds. Smart manufacturing differentiates itself from this by an increased usage of data that enables elements to respond more flexibly and even make predictions and decisions in order to optimise the process.

This requires a complete redesign of the supply chain. A traditional supply chain is linear and sequential and consists of discrete processes such as the planning phase, the actual manufacturing and the product distribution [7]. To achieve smart manufacturing a supply chain must become a dynamic interconnected system. According to the vision of the National Institute of Standards and Technology, smart manufacturing aims to have fully integrated, collaborative systems that can respond real-time to changes in the customer requirements, supply network or manufacturing process [37]. Responding directly to customer requirements allows manufacturers to move from standard mass production to producing customised, yet high-volume, products.

IoT is an important technology in smart manufacturing because it enables each element to be connected to a network. CPS is more about the relations between the elements. The interconnection blurs the boundaries between physical processes, often seen in the actual manufacturing, and digital systems that are more common in the design and logistics.

1.4. Local fibre steering

The thesis topic is local fibre steering, which is a different application of fibre steering that fits within the context of smart manufacturing. As mentioned, many challenges need to be faced before variable stiffness laminates will become broadly used. Therefore, the focus is on improving fibre-placed constant stiffness laminates. The next chapter will explain that tow width fluctuation is an important cause of gaps and overlaps which severely affect the performance of composite laminates. The suggestion is to use fibre steering locally to compensate for tow width fluctuation to reduce gaps and overlaps.

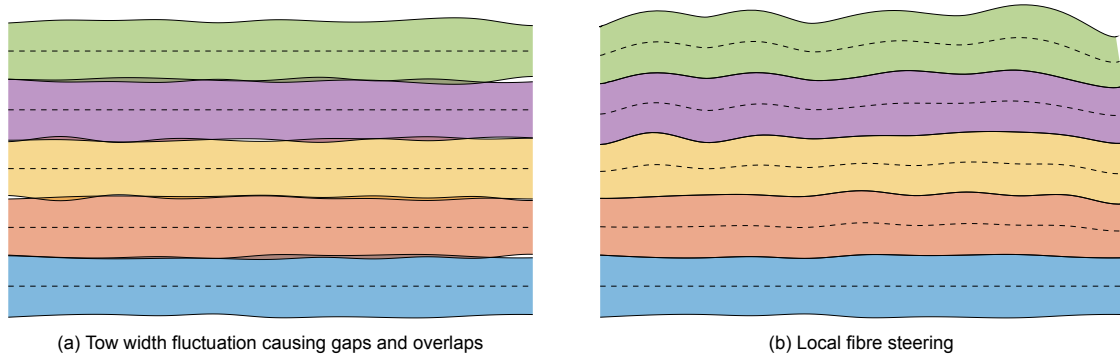


Figure 1.3: A section of a conventional laminate versus local fibre steering

The result is visualised in Figure 1.3. On the left-hand side, the changing width leads to tows overlapping or tows forming long narrow gaps between one another. On the right, local fibre steering is applied. First, the lower tow is laid down straight. Next, the tow above follows the edge of the previous tow. The following tows repeat this in such a way that each tow is adjacent to the preceding one. The benefit is that no gaps or overlaps appear.

Compensating for the tow width fluctuation by local fibre steering to reduce gaps and overlaps can be considered an example of smart manufacturing. Information is gathered about the inputs of the system, in this case, the tow width. As a response, the tow paths laid down by the automated fibre placement machine are adapted. The research question is: how effective is local fibre steering in increasing the structural performance of composite laminate by reducing gaps and overlaps through compensating for tow width fluctuation in automated fibre placement.

2

Gaps and overlaps

Gaps and overlaps are the defect types that local fibre steering aims to mitigate. Therefore this chapter covers their causes and effects in section 2.2 and 2.3. It moves on with current methods of modelling and mitigation of gaps and overlaps in section 2.4 and 2.5 respectively. But, the chapter starts with other defects that occur in automated fibre placement.

2.1. Other defects in automated fibre placement

Just like any other manufacturing process AFP is not perfect. There are many imperfections that can occur. Heinecke and Willberg made a clear overview of these defects that will be summarised here [18]. The seven most relevant types of defects will be discussed. The first four are relatively well-understood. The last three types of imperfections are seldom researched. One reason for this is that these defects emerge less frequently. Another reason is that it is difficult to reproduce and control them.

The first defect to be treated is angle deviation. Often the fibre angle is optimised as a function of the planar coordinates. An example of such a solution is visualised in Figure 2.1a. However, due to the finite width course, the specified fibre paths cannot be followed as they are, but need to be converted into a manufacture ply as in Figure 2.1b. It can be observed that only the centreline of the AFP head is able to follow the ideal paths while the course edges deviate from the locally specified fibre orientation. Reducing the fibre course width reduces the fibre angle deviation but also the fibre deposition rate and thus the productivity of the process.

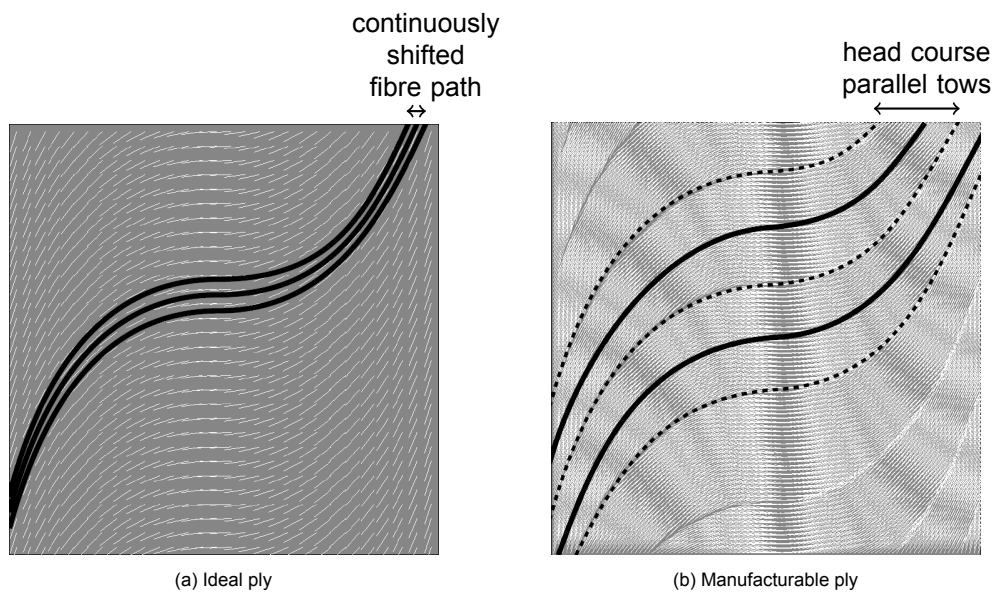


Figure 2.1: Fibre angle deviation due to finite course width [29]

The second is fibre tow misalignment. This is the error between the projected and actual fibre path due to the positioning accuracy of the end effector. The sources of error can be divided into three groups [39]. One is stationary geometric. It is basically the inherent and inevitable error that the robot has even when it is standing still. Another occurs when the robot is moving and is labelled dynamic. It includes vibration resulting from motion and interaction with other objects such as the mould. It highly depends on the inertia of the robot and the quality of the bearings. Another important factor is the production speed which is always part of the trade-off with product quality. The final source of error is thermal which essentially includes the thermal deformations in the robot. Fibre steering increases the risk of fibre tow misalignment since the robot's motion becomes more complex. Fibre tow misalignment causes gaps and overlaps as can be seen in Figure 2.2.

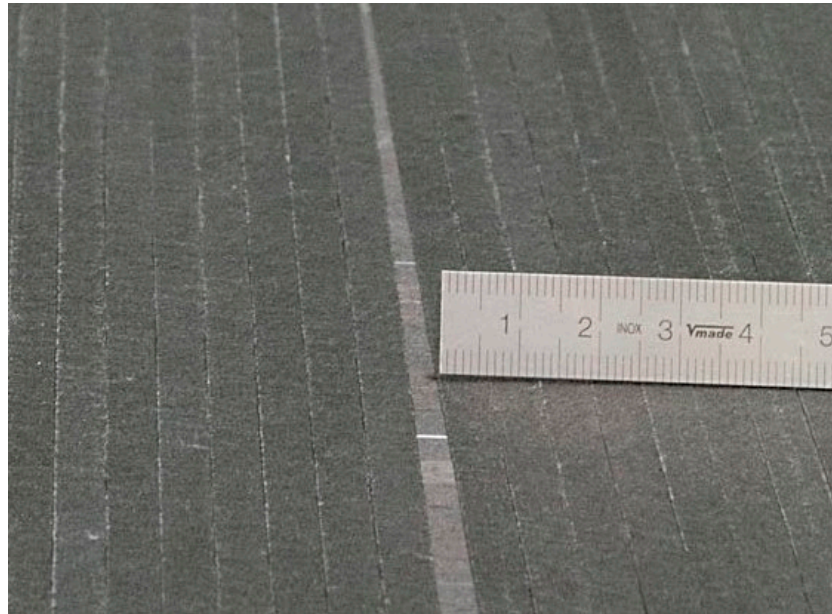


Figure 2.2: Tow misalignment causing a gap [18] (Courtesy of Netherlands Aerospace Centre (NLR))

The third is fibre waviness. In-plane waviness occurs due to fibre steering and complex surfaces. Out-of-plane waviness often emerges as a secondary phenomenon of, for example, the later mentioned inclusion. A schematic illustration of fibre waviness is given in Figure 2.3

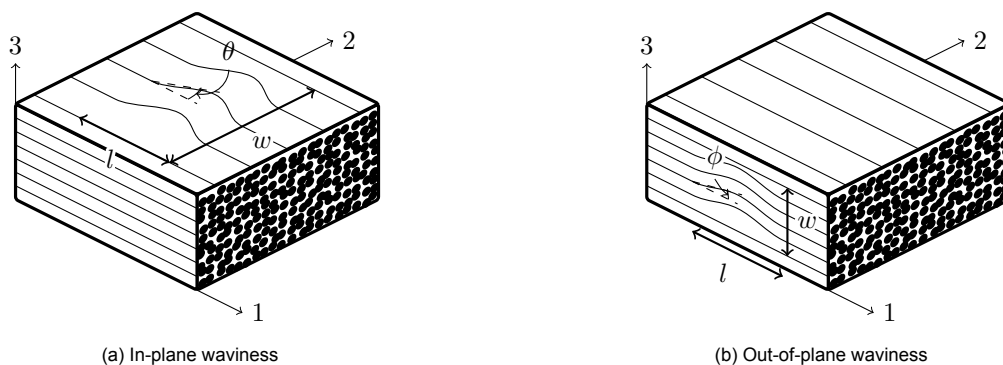


Figure 2.3: Fibre waviness as defined by Heinecke and Willberg (adapted from:[18])

The fourth is tow twisting. It can already occur in the material supply. Tow width fluctuation can be a cause because it allows the material to move sideways. However, it can also occur during the deposition due to the movement of the end effector along the fibre path. Fibre steering consequently increases the risk of twisted tows.

Another defect type includes bridging and crowning. Bridging often occurs as a result of too much tension on a concave surface while crowing happens due to too little tension on a convex surface. To prevent it the fibre tension needs to be regulated throughout the production process.

Furthermore, there is a defect type containing tow wrinkling or upfolding. This is caused by insufficient adhesion. An example of upfolding is shown in Figure 2.4. Fibre steering increases the risk of wrinkling due to the bending of tows in curves.



Figure 2.4: Tow upfolding due to lack of tackiness [18] (Courtesy of Netherlands Aerospace Centre (NLR))

The last defect that deserves to be mentioned is inclusions. The most common inclusion is in the form of air often referred to as voids. One of the most important factors in the formation of voids is the material quality [22]. The void content that is already present at the beginning of the process can only be slightly reduced by compaction. Gaps and overlaps can cause voids as they hinder compaction. The inclusion of foreign bodies is rather rare. Though often fuzzballs appear through the accumulation of frayed fibre material (see Figure 2.5). Fuzzballs sometimes do get included in the product and cause fibre waviness.



Figure 2.5: Fuzzball that contaminates the laminate formed by abrasion of fibre material [18] (Courtesy of Netherlands Aerospace Centre (NLR))

2.2. Causes

Gaps and overlaps are the most frequently occurring imperfections in automated fibre placement [18]. Even in an ideal manufacturing process gaps and overlaps cannot always be avoided, because a complex geometry or layup cannot be translated into a perfectly aligning configuration of tows. Plus there is the fact that gaps and overlaps often bring other defects with them. There are three main causes of gaps and overlaps that will be discussed here, not in the order of prevalence.

2.2.1. Skew ply boundaries

The first is skew ply boundaries which means that the ply boundary is not perpendicular to the direction of the tows. As a result, the fibre course width needs to be varied. The number of tows in a course is discrete and the cutting is typically done perpendicular to the tow edge. Therefore so-called tow drop areas appear where no material is present. To what extent gaps or overlaps occur is dependent on the coverage strategy as illustrated in Figure 2.6. It could be that the ply boundary is a free edge of the laminate that can be trimmed later. Another possibility is that multiple fibre directions are present in one ply and that they coincide. This especially occurs often when fibre steering is used to make a variable stiffness laminate.

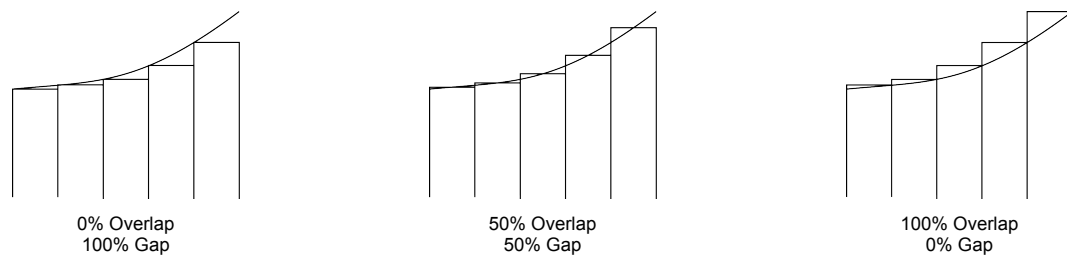


Figure 2.6: Different coverage strategies at ply boundaries (Adapted from: [33])

2.2.2. Shifted method

The second cause of gaps and overlaps is the shifted method. Fibre steering has a large design space as a result. In order to decrease the number of variables often a reference curve is introduced. The reference curve defines a single pass of the AFP head in a ply. To complete the layer a so-called ply construction method is used. The shifted method is a common way to construct a ply. Each course is identical to the reference path but translated with a certain distance. Because of the finite width of a course, the inner and outer edges at a curve are different during steering. This means that two courses do not fit exactly next to each other without the creation of gaps or overlaps. As with the skew ply boundary, one can adopt a certain coverage strategy to choose a ratio between gaps and overlaps as is illustrated in Figure 2.7.

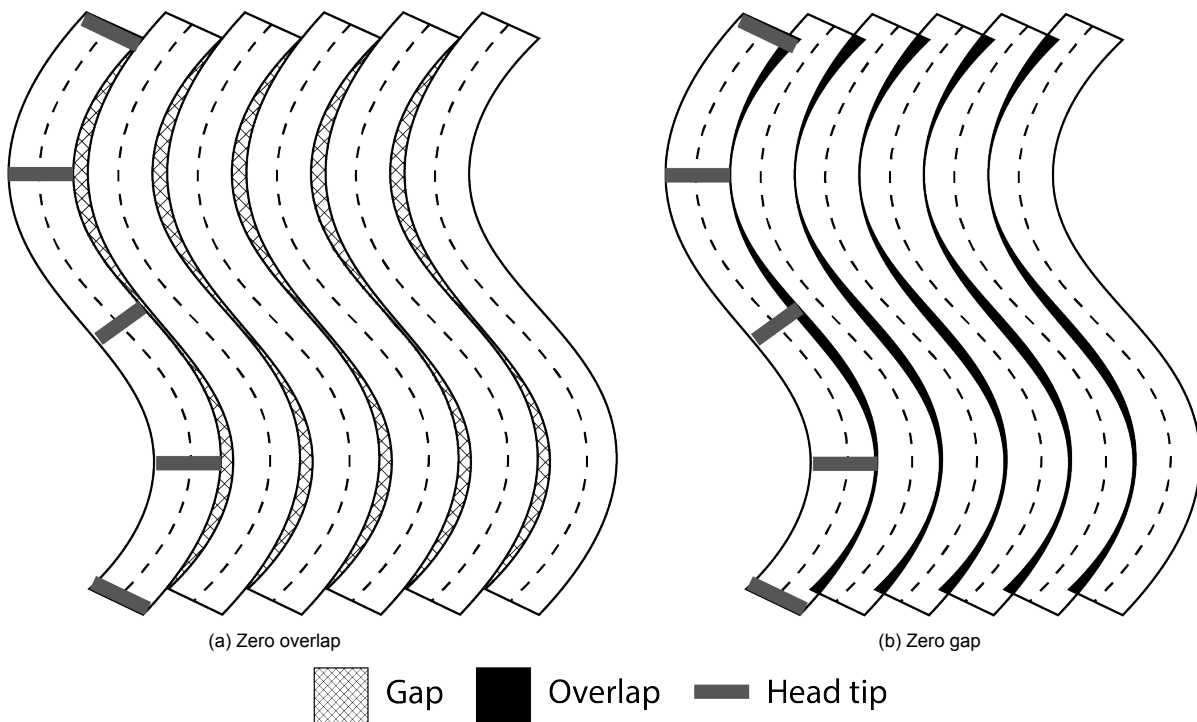


Figure 2.7: Shifted method with different configurations (adapted from: [45])

2.2.3. Tow width fluctuation

The third cause of gaps and overlaps is tow width fluctuation which is the most relevant for this thesis. Typically in constant stiffness laminates, tows are placed with a set distance with respect to each other. The tow width, however, is not constant and therefore the edges are never perfectly straight. This leads to overlapping tows and longitudinal gaps between tows depending on the distance between them.

The severity of the tow width fluctuation depends on the material quality and the product form. There are two product forms available in the manufacturing process: towpreg and slit tape. Both are carefully described by a Composite Materials Handbook by the United States Department of Defense which is summarised below [49].

Towpreg, also known as prepreg tow, is manufactured by impregnating bundles of dry fibre and forming them to the desired width. It is commonly used in filament winding. Because the width is specified, the thickness depends on the size of the fibre bundles. Even when a die is used to shape the tow, the edges will still taper slightly resulting in a cross-section as illustrated in Figure 2.8a. Because of this, precisely controlling the width is of the product is still the biggest challenge for suppliers. After shaping the towpreg is spooled, often without the use of a backing film or separator sheet.

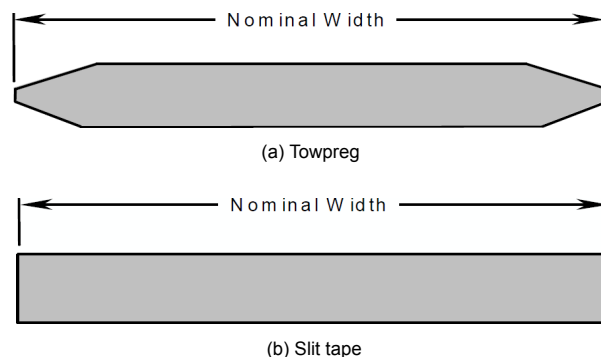


Figure 2.8: Cross-sectional shape of fibre placement materials [49]

Slit tape is, as the name suggests, conventional unidirectional tape slit to a specified width. Similar to towpreg, the parent tape is produced by impregnating dry fibres with resin at a high temperature and pressure. The maximum length of the product is limited to either the amount of resin available or the length of continuous fibre present on the bobbin. A range of widths can be chosen, sometimes up to 1.5 m. The sides of the master roll are trimmed and ultimately it is slit into smaller strands ready to be used in the AFP machine. Due to the slitting, the cross-sectional shape is more rectangular as illustrated in Figure 2.8b. When slit tape is spooled it is common to use a backing sheet centred over the material to aid in separation. Because both a backing sheet as well as secondary slitting is required, slit tape is generally more expensive than towpreg.

Typical tow widths and tolerances are displayed in Table 2.1. Only the handbook by the United States Department of Defense distinguishes between the two product forms. Some sources do not specify to which tow width the tolerance applies. According to Gruber et al. the width tolerance is ten times bigger than the tolerance of the AFP machine [14].

Table 2.1: Tow width and respective tolerance according to different sources

Source	Tow width		Tolerance			
	in	mm	in	mm	%	
United States Department of Defense [49]	0.125	3.175	0.005	0.1270	4.0	(Slit tape)
			0.007	0.1778	5.6	(Towpreg)
Hulcher et al. [21]	0.250	6.350	0.010	0.2540	4.0	
Evans [11]	0.125	3.175	0.015	0.3810	12.0	
Gruber et al. [14]	-	-	0.010	0.2540	-	
Grant and Benson [13]	-	-	0.025	0.6350	-	

Tow width fluctuation is especially important because it also occurs often in straight-fibre laminates. Local fibre steering is maybe an effective mitigation method for the gaps and overlaps caused by width variation. To make clear why it is important to these defects the next section will discuss their effects.

2.3. Effects

To understand the effect of gaps and overlaps it is essential to look at the defects at a smaller scale. The work relating to real defect geometries of Croft et al. and Lan et al. is summarised below.

Croft et al. tested four different defect configurations: gap, overlap, half gap/overlap, and twisted tow. The defects have been introduced in a symmetric and balanced layup. For the gap, a pair of tows has been removed. For the overlap, two tows have been introduced and for the half gap/overlap, they have been shifted by half a tow width. The two tows each come from one of the two middle layers. This is done for two reasons. The first to maintain symmetry to avoid coupling between in-plane loading and out-of-plane deformation. The second is to increase the defect area. The assumption is that the effect of a single defect is small. That is also why the defect width is one tow width which is rather large relative to what would naturally occur during manufacturing. For the twisted tow, only one layer is modified because it is difficult to accurately place two defects on top of one another and a twisted tow rarely occurs twice at the same location.

Micrographs have been made using a scanning electron microscope (SEM) to investigate the real defect geometries. The assumption is often made that gap areas are totally filled with resin, known as resin-rich areas. However, this was not the case for the gap configuration as the pressure of the autoclave helps tows to fill the gaps. It depends on the defect size because a smaller defect yield higher curvatures and thus makes it harder to deform the tows into the gap region. In the half gap/overlap configuration, for example, resin accumulation was observed as the pressure was not sufficient for the tows to fill the defect [9]. Even though the defects may seem to have disappeared, on a larger level fibre waviness is observed. The fibre waviness is caused by the fibres being pushed towards a gap or away from an overlap. As will become clear below, waviness appears to be an important factor for the compressive strength.

Lan et al. published two articles considering the effects of defects on tensile [26], and shear and compression properties [27]. Five different defect configurations were tested. The first is the pristine laminate made with manual layup used as a reference. The second was made with automated fi-

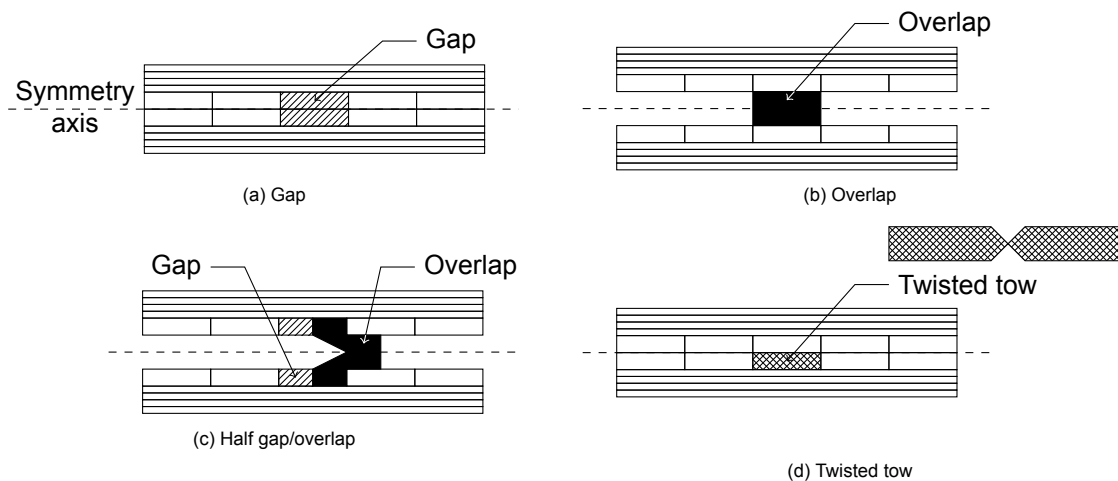


Figure 2.9: Defect configurations used by Croft et al. (Adapted from: [9])

bre placement leaving a 0.5 mm gap between each course, which is considered the industry standard for AFP. The third and fourth configuration has a single gap with a width of half a tow and a full tow respectively. The final configuration contains a half-tow wide overlap.

Each defect configuration is investigated in two different layups. The first layup is $[0^\circ/90^\circ_5/0^\circ]$, where the defect is superimposed in the five middle layers. The second layup is $[(90^\circ/0^\circ)_2/90^\circ]$ and contains only a single defect in the middle layers. Each combination of defect and layup is manufactured with and without caul plate. A caul plate transmits normal pressure and provides a flat and smooth surface. The caul plate reduces the thickness variation. The alternating plies in the second layup restrict material movement and therefore the defects were not filled successfully even with the caul plate.

Figure 2.10 shows a selection of the micrographs from Lan et al.. The first four show the difference between five superimposed gaps and a single gap horizontally and between with and without caul plate vertically. Cross-sections without the caul plate show a large thickness variation. The superimposed gaps even show that the gap has been pushed apart. This does not happen in the superimposed gaps with a width of half a tow (see Figure 2.10e). A large thickness increase can be seen in the overlap (2.10f).

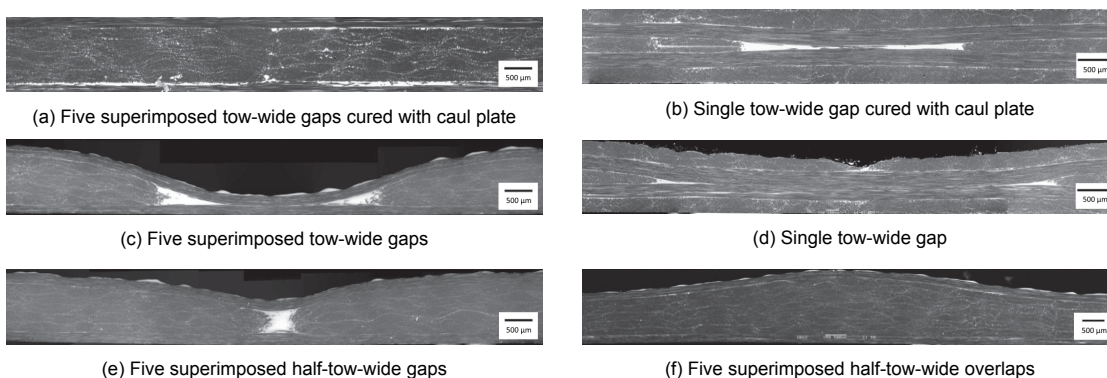


Figure 2.10: Microstructural SEM observations of different defect regions (adapted from: [26])

Previous paragraphs the geometry of the defects. The rest of the section will discuss how they affect the structural performance. Several studies are summarised below.

Sawicki and Minguet tested specimens under compression with many variables [42]. Two different specimen types were tested: unnotched and with an open hole. The specimens were tested in two different environments: room temperature with ambient humidity and 82.2°C (180°F) with 95% relative humidity. Three different layups were used and the defect width varied between zero defect, narrow defects of 0.762 mm (0.03 in), and wider defects of 2.540 mm (0.10 in).

The defects were introduced by leaving out one tow in each 90° ply and adding it after the ply is finished with the above-mentioned defect width as the offset. Because the layups contain a different number of 90° plies, the number of defects is also varied. The defects are present in the transverse plies to cause the maximum out-of-plane waviness in the adjacent longitudinal plies, because the assumption is that waviness is the most important cause of compressive strength reduction.

The compressive strengths of the unnotched and open hole specimens were similar. In the 82.2 °C environment the strength reduction was greater than at room temperature. For example, in an unnotched compression test, a 0.762 mm gap resulted in an 8.6 % decrease of strength at room temperature, but 19.7 % at 82.2 °C. It indicates that the failure mechanisms were matrix-dominated. The compressive strength decreased significantly with the presence of 0.762 mm-wide defects, but the reduction was not significantly different for larger defects sizes. Also, the number of defects turned out to have little effect. From these observations, it was concluded that it was indeed the out-of-plane waviness in adjacent 0° plies that cause the compressive strength reduction.

Woigk et al. experimentally tested four different defect configurations: gaps, overlaps, staggered gaps and a combination of staggered gaps and overlaps [53]. Tests were done for both tensile as well as compressive strength and they came to the same conclusion about the failure mechanism as Sawicki and Minguet. The out-of-plane waviness causes interlaminar shear stresses and out-of-plane normal stresses that lead to failure. However, they found only significant strength reductions for the specimen containing both gaps and overlaps. The results agree with previous research that found that isolated defects do not cause a major knockdown in strength [9]. Nevertheless, it was not the amount of imperfection, but the resulting level of fibre waviness that is the main driver behind strength reductions.

Hsiao and Daniel specifically studied the effects of fibre waviness [20]. They too found it causes serious degradation of the compressive strength as well as the Young's modulus. The dominant failure mechanism under compressive loading was found to be interlaminar shear failure.

The research above showed what the defects look like and how they lead to failure. The next step is to see how this influences the structural properties. Sawicki and Minguet found a significant reduction in compressive strength (5- 27%) caused by gaps of at least 0.762 mm [42]. The testing of Croft et al. concluded that the effect on the specimens with an open hole was larger (up to 13%) compared to specimens without it (overall less than 5%) [9]. Marouene et al. performed both experimental and numerical studies on the effects of gaps and overlaps on the open-hole compressive strength [34]. They concluded that the effect varies, and can even become positive, depending on the location of a defect relative to the hole. Li et al. found that the effect of gaps and overlaps also depends on the orientation of the ply in which they are present [28].

The problem is that most of the research until now focused on isolated defects in laminates under single loading conditions. Woigk et al. concluded that these do not cause a major knockdown in strength [53]. Instead, future research should focus on systemic defects. Tow width fluctuation, for instance, causes many small defects instead of a large single defect. Some studies simulated gaps and overlaps by removing or adding a tow. Others, such as Blom et al. focused on tow drop regions and concluded that the stiffness reduction is proportional to the tow drop area [5]. Neither, however, specialised in the long narrow gaps and overlaps caused by tow width fluctuation. Gaps as wide as a tow may be filled with material, but thinner gaps may stay resin-rich.

Though more research needs to be done on complex defect configuration under combined loading the information summarised above indicates that gaps and overlaps have a severe effect on the mechanical properties and that is necessary to find a way to mitigate them.

2.4. Modelling

In this section, it will be explained how the effects of gaps and overlaps can be incorporated in a structural model. Previously, a gap was often modelled by changing the properties of a number of elements to that of the matrix or no material at all. Similarly, overlaps were modelled by doubling the thickness. Such a binary approach requires the mesh to be fine enough to accurately represent the shape of the defect. The problem is illustrated in Figure 2.11b where the geometry of a defect cannot be described properly. Figure 2.11a solves the issue but requires a large number of elements and thus a high computational effort.

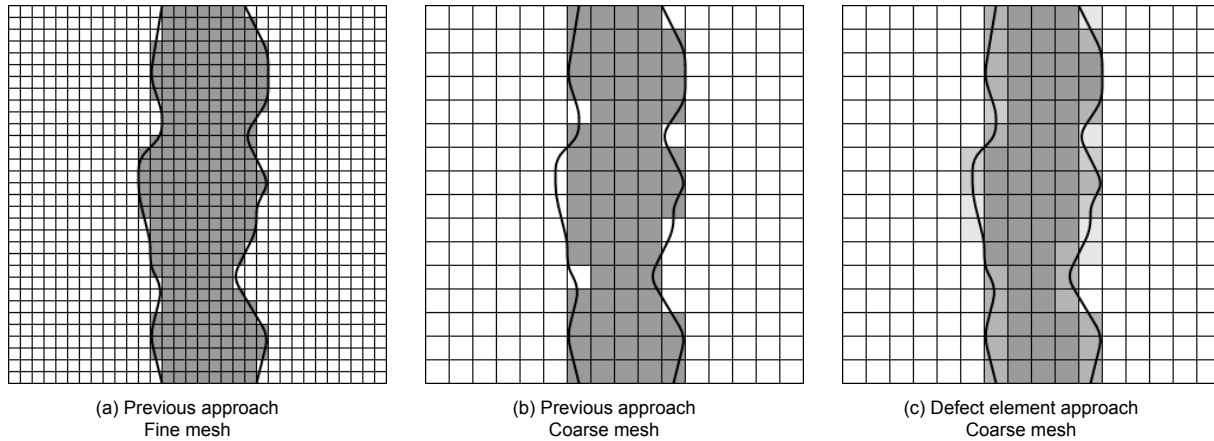


Figure 2.11: Defect layer method compared to previously existing approaches for different mesh sizes

Fortunately, Fayazbakhsh et al. introduced a solution: the defect layer method. The method is able to represent the defects more accurately using the same mesh as the previous approach. Instead of an element either having the properties of the default material or that of a gap, the elastic properties are scaled to the amount of gap present in an element. Likewise, the thickness is not simply doubled but rather scaled to the amount of overlap in an element. This is illustrated in Figure 2.11c where elements on the boundary of the material and the defect are not one of the two but something in between, proportional to the defect area percentage.

For the scaling of the elastic properties to the gap area percentage Fayazbakhsh et al. use a graph. The graph can be shown to correspond to the rule of mixtures. The rule of mixtures is used to predict a property of a composite material. There are two forms of the rule of mixtures. The Voigt model assumes that reinforcement and matrix experience equal uniform strain and is used for the longitudinal elastic properties [10]. This results in the rule of mixtures as used for the longitudinal modulus in Equation 2.1.

The Reuss model assumes equal uniform stress experienced by the constituents that leads to the inverse rule of mixtures that can be used for parallel properties such as the transverse modulus (E_2) and the in-plane shear modulus (G_{12}) as in Equation 2.2 and 2.3.

$$E_1 = v_c E_{1c} + v_m E_m \quad (2.1)$$

$$\frac{1}{E_2} = \frac{v_c}{E_{2c}} + \frac{v_m}{E_m} \quad (2.2)$$

$$\frac{1}{G_{12}} = \frac{1}{G_{13}} = \frac{v_c}{G_{12c}} + \frac{v_m}{G_m} \quad (2.3)$$

In these equations v_c stands for the composite volume fraction, in other words, the amount of material present. Also, v_m does not refer to the actual matrix volume fraction, but the gap area percentage that is assumed to be filled with resin.

There are two important elastic properties that are not present in the graph by Fayazbakhsh2013. The first is the Poisson's ratio, which is identical for the composite and matrix in the paper, so no rule of mixtures is required. The second is G_{23} which is the out-of-plane shear modulus. The rule of mixtures for the two are shown below. The other out-of-plane shear modulus G_{13} can be assumed to be identical to G_{23} . It is important to mention that the equations for G_{12} and G_{23} are not very reliable since neither the Voigt nor the Reuss model accurately represent what happens with a fibre reinforced composite when it is loaded in shear [1].

$$\nu_{12} = \nu_c \nu_{12c} + \nu_m \nu_m \quad (2.4)$$

$$G_{23} = \nu_f G_{23c} + \nu_m G_m \quad (2.5)$$

2.5. Mitigation

It might also be interesting to mention that local fibre steering is not the first attempt in reducing gaps and overlaps or their effects. Four methods have been identified in literature and will be discussed here.

The first method is staggering, which means shifting plies of the same orientation with respect to each other. Research on the effects of staggering is summarised below.

Tatting and Gürdal used a finite element model to investigate the stress distribution of curvilinear fibre laminates with a central hole under axial loading [44]. They refer to staggering as the interwoven technique. Staggering successfully reduced the thickness variations caused by overlaps which is illustrated in Figure 2.12. On the left side, a laminate is present where no staggering is applied. The darker the colour of an element the more plies are present on top of each other and the larger the thickness. On the right, the same laminate can be seen but with staggering. It is evident that the overlaps are more distributed over the composite. However, the difference in the buckling load between the two was negligible. It was suggested that staggering could not only be used for distributing the thickness variation caused by overlaps but also caused by gaps such as tow drop areas.

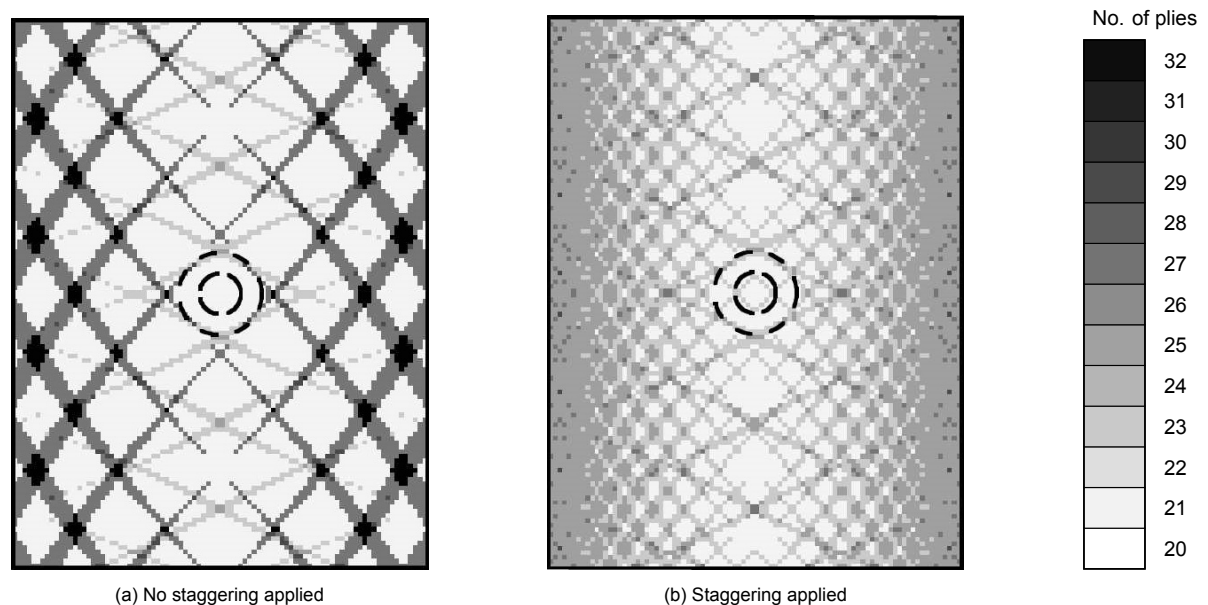


Figure 2.12: The effect of staggering on the thickness distribution of variable-stiffness laminates [44]

Blom et al. performed a numerical analysis on the effect of tow drop area on stiffness and strength of variable stiffness laminates [5]. It included the effect of staggering. In their approach, when there are two plies with the same orientation present, then one is shifted by half a course width. If four plies have the same orientation the shift between each of them is one-quarter of the course width. This assures that course gaps, overlaps and course boundaries, of identical plies are not at the same planar location.

The study concluded that failure occurs at tow drop locations in both inner and outer plies. Staggering had a positive effect on the strength of the laminates while the improvement was less decisive. The increase in strength is explained by the distribution of tow drop areas over the laminate and through it reducing stress concentrations and postponing failure. The effects are confirmed by the increase in the number of failed elements and the failure load. Even laminates containing no tow drop areas benefited from staggering. This is understood to be due to the distribution of angle deviation caused by the finite course width occurring in variable stiffness laminates.

Turoski performed open hole compression (OHC) test with three different variables [48]. The first is the gap width which in this case is the distance between tapes. The second is the stagger repeat number: the number of plies with the same orientation between two plies with the same in-plane location. The third is the in-plane distance between two sequential plies of the same orientation.

The study found no strength increase when staggering was applied. In fact, it is even questioned if staggering is worthwhile considering the increased constraints on the stacking sequences and the effort of additional programming of the AFP machine that is required.

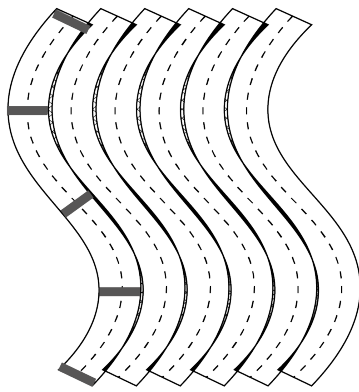
The second method has been studied by Rakhshbahar and Sinapius [40]. The study aims to eliminate gaps by detecting them with a profile sensor after tow placement and filling them with continuous fibre reinforced plastic using a 3D printer. Unfortunately, there is no 3D printer capable of directly printing material in the gaps, so they are printed on a separate panel and then inserted at the defect locations. The five specimens used in the study used a nominal tow width of 6.35 mm and the gaps had a width of 3 mm and a depth of 0.36 mm. Gaps as narrow as 1 mm can be printed in different shapes. The mechanical performance of the specimen with gaps filled with a 3D printer was nearly identical to the pristine specimen [40].

The method still faces many challenges. Though the material that is 3D printed is a continuous fibre reinforced plastic, there are still discontinuities present at the edges of the gap. Besides, the method does not eliminate overlaps but solely gaps. Also, it requires an additional step in the production using material that is added under different conditions. The results may be promising, but the exact effects are complex and therefore it is difficult to verify the method to use it commercially.

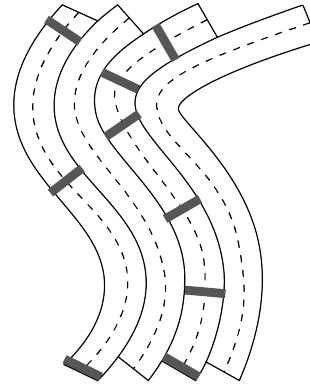
The last to methods to mitigate gaps and overlaps is by applying a different ply construction. As discussed in section 2.2 a common way to overcome the difficulty of translating a design into a part that can be manufactured is by the use of a reference path. The often-used shifted method causes gaps and overlaps as can be seen in Figure 2.13a.

One option is the parallel method displayed in Figure 2.13b. Tows are placed parallel to one another to align their edges. This is similar to the local fibre steering that will be studied in this thesis. Here the centreline of the reference path is curved and the edges are assumed to be perfectly parallel to it. In local fibre steering, the centreline of the first tow is assumed to be straight and it is the edges that are curved. A problem that can occur using the parallel method is the accumulation of curvature. This can be observed in the top half of the figure where the curvature of the right tow is much higher than the left tow. Eventually, the curvature becomes so high that it leads to tow wrinkling. The problem of curvature accumulation and its effect on local fibre steering will be discussed in section 4.4.

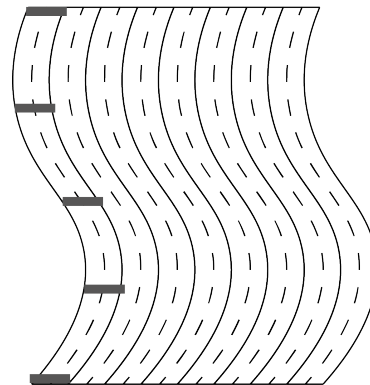
Another option has been introduced by Kim et al. named continuous tow shearing (CTS) [25]. Traditionally, AFP steers tows by rotating the end effector and thereby applying an in-plane bending deformation on the tow. The compression caused by the bending can result in fibre buckling. Instead, CTS steers tows by applying a shear deformation that avoids fibre buckling. A special end effector is required. A compaction shoe compresses the end of the tow to maintain its position while at the other end a pinching device moves along with the head. Continuous tow shearing also asks for a different material. The matrix in conventional composite material is too viscous for the fibres to be easily sheared. Because of the curvature accumulation in the parallel method and the required equipment and material for CTS, both are not considered feasible mitigation methods at the moment.



(a) Shifted method



(b) Parallel method



(c) Continuous tow shearing (CTS)

Figure 2.13: Different ply construction methods (adapted from: [25])

3

Research outline

In the first chapter, the problem of gaps and overlaps was introduced as well as a possible solution: local fibre steering. The second chapter dived deeper into gaps and overlaps. It discussed their causes, effects and methods for modelling and mitigation. This chapter will explain the path forward. The introduction ended with the following main research question:

How effective is local fibre steering in increasing the structural performance of composite laminates by reducing gaps and overlaps through compensating for tow width fluctuation in automated fibre placement?

Local fibre steering in the context of this thesis is defined as using steering capability of automated fibre placement locally to compensate for the tow width fluctuation. To answer the main research question, three sub-questions need to be answered first:

1. To what extent can gaps and overlaps be reduced using local fibre steering?

The goal of chapter 4 is to answer this question by constructing the conventional and steered laminate. The resulting defect area percentage of the conventional and steered laminate are presented in section 4.6.

2. What is the effect of the reduction in gaps and overlaps and the fibre angle deviation on the structural performance?

A finite element analysis will calculate whether the decrease of the defect area percentage improves the structural performance. This will be discussed in Chapter 6. The model will calculate the buckling load and effective stiffness of the conventional and steered laminate which are presented in section 6.4.

It is known that local fibre steering comes at a cost. Deviating from the tow path to compensate for the tow width fluctuation causes the fibre orientation to vary which affects the stiffness locally. The effects of fibre angle deviation are included in the model that calculates the structural performance using a finite element method (FEM).

3. How accurate is the current understanding of tow width fluctuation?

The laminate model that constructs the tow paths uses a model of the tow material. Assumptions were made to determine the values for the tow width fluctuation. Chapter 5 attempts to validate the assumptions. The results of the validation are discussed in section 5.2

Eventually, the research objective is...

...to determine to which extent local fibre steering can reduce gaps and overlaps and what the effects are on the structural performance.

The practical side of local fibre steering, e.g. the technologies necessary to employ local fibre steering, is determined to be out of the scope of this thesis. When it is determined how effective local fibre steering is, it can be decided whether the research and development of the required technologies are worthwhile.

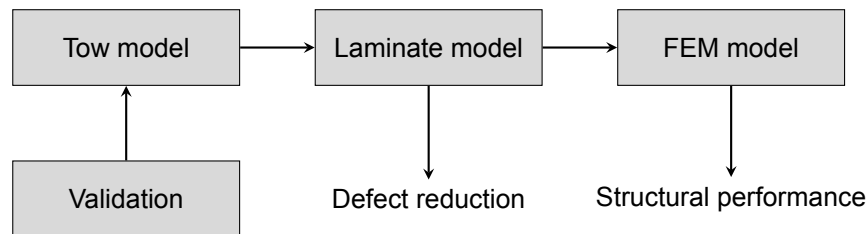


Figure 3.1: Research outline

The way forward is visualised in Figure 3.1. The amount of gaps and overlaps is expressed in the so-called defect area percentages (DAPs). Chapter 4 calculates the DAPs of a conventional laminate and a laminate where local fibre steering is applied. To do that, first, the tow material that is used is modelled in Section 4.1. The tow model is then used to construct the conventional laminate in Section 4.2. The rest of the chapter explains how the steered laminate is constructed and finishes with preliminary results containing the defect area percentages of both laminates.

The values for the parameters in the tow model are based on assumptions or taken from literature presented in Chapter 2 about tow width fluctuation. The goal of Chapter 5 is to validate the assumptions by measuring the actual width of different tow materials.

Chapter 6 will calculate the structural performance of the laminates, more specifically, the buckling load and the effective stiffness. It can be used to compare the conventional laminate with the steered laminate to assess the effectiveness of local fibre steering.

The conclusions that can be drawn from the defect area percentages, validation of the tow width fluctuation and the structural performance are covered in Chapter 7 which is followed by Chapter 8 discussing any recommendations for future work.

4

Model

This chapter explains how the laminates are constructed. The first section describes the model for the tow material. In the second section, the tow model is used to construct the conventional laminate. The tow model continues to be used in the third section in which parallel curves are constructed to create a model of the steered laminate. The two subsequent sections cover challenges that were faced in the process of local fibre steering: the exceedance of the minimum radius of curvature and the large fibre angle deviations. At the end of this chapter, a comparison of the defect area percentages of both laminates is presented as a preliminary result.

4.1. Tow model

The tow model represents the material that is used in the automated fibre placement. Section 2.2.3 has already discussed the current knowledge of tow width fluctuation. The tow model will use a typical value of 6.35 mm (0.25 in) for the tow width. The standard deviation is assumed to be 0.254 mm (0.01 in) which is 4% of the tow width, because Table 2.1 showed that this is common.

The mean width μ and standard deviation σ are not sufficient to model a realistic tow width fluctuation. Figure 4.1 shows a tow with a length l of 100 mm. Using the mean width and standard deviation mentioned above, a random tow width is generated for every step in the longitudinal direction x with a step size dx_0 of one millimetre. It can be observed that the tow edge is very rough. Upcoming sections will show that large changes in the tow width and large rates of changes can become a problem when attempting to construct parallel tows.

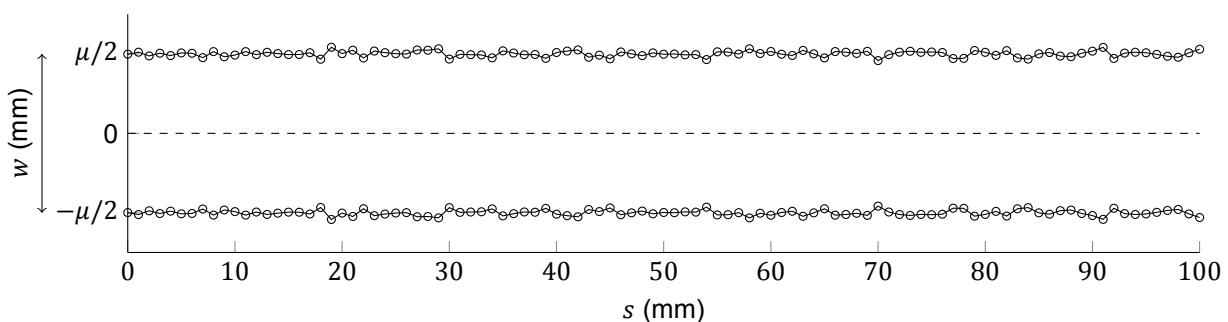


Figure 4.1: Rough tow model

Because of this a tow model needs to be created that can take into account these properties. Therefore, a third parameter is introduced, dl , which is the distance along the tow path between the point for which a random width is generated. Through these points a set of natural cubic splines is constructed. This tow model is visualised in Figure 4.2. It is important to notice that for cubic splines to be a realistic representation of the tow width the edge of the material needs to be smooth. In Chapter 5 the tow model will be validated including the assumption about the smoothness.

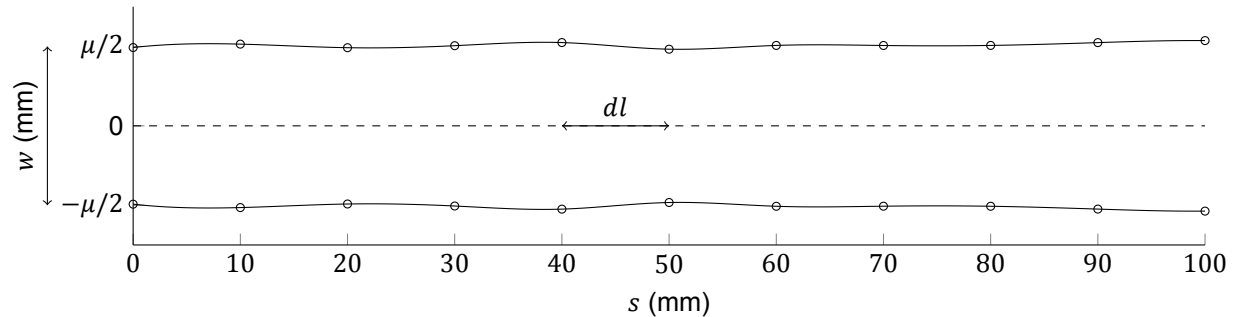


Figure 4.2: Smooth tow model ($dl = 10$ mm)

4.2. Conventional laminate

With the established tow model, the conventional laminate can be constructed. This is done as follows. For each ply and its fibre orientation, the tow length l and the number of tows n necessary to cover the laminate are calculated. Some margins are included. The first tow of each layer is placed with its centerline along the x axis from $x = -l/2$ to $x = l/2$. The consecutive tows are placed alternating above or below the existing group of tows. The centreline of all tows are all spaced a constant distance d apart. The result of one ply (see Figure 4.3) can be transformed to the required ply orientation according to the stacking sequence. The parameters used are shown in table 4.1.

Table 4.1: Standard tow and laminate parameters

Description	Symbol	Value	Unit
Mean tow width	μ	6.35	mm
Standard deviation	σ	0.254	mm
Spline node distance	dl	10	mm
Step size	dx_0	1	mm
Tow length	l	500	mm
Centreline distance	d	6.35	mm

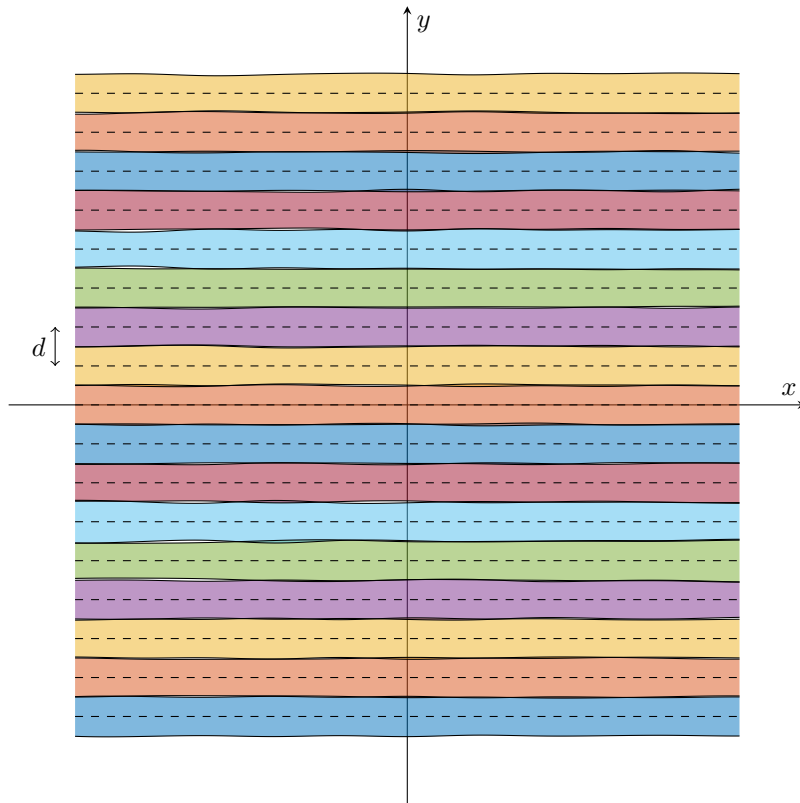


Figure 4.3: An example of a single ply of the conventional laminate

The centreline distance d is chosen to be equal to the mean tow width. This means the probability of a gap or an overlap are equal. A manufacturer can, however, choose to change the distance to prefer one over the other. The paragraph below will explain how the distance d is connected to the conventional one-, two- and three-sigma heuristics. The tow width is assumed to be normally distributed. Algebraically, this can be written as below.

$$w \sim \mathcal{N}(\mu, \sigma^2) \tag{4.1}$$

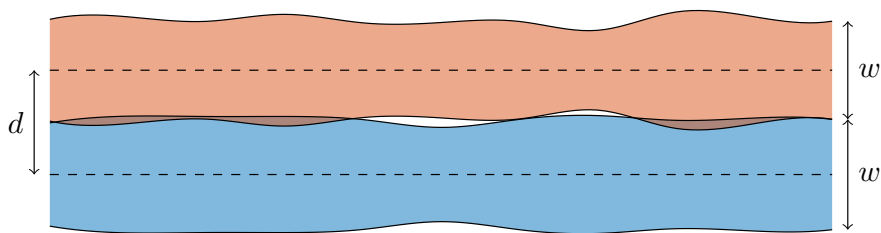


Figure 4.4: The centreline distance d between tows and the resulting gaps and overlaps

Figure 4.4 shows two tows of width w with distance d between them. The linear transformation of a normal distribution goes as follows.

$$aX + b \sim \mathcal{N}(a\mu + b, a^2\sigma^2) \tag{4.2}$$

This means the upper edge of the first tow and the lower edge of the second tow can be described using the following two equations.

$$y_1^u = \frac{1}{2}w \sim \mathcal{N}\left(\frac{1}{2}\mu, \frac{1}{4}\sigma^2\right) \tag{4.3}$$

$$y_2^l = -\frac{1}{2}w + d \sim \mathcal{N}\left(-\frac{1}{2}\mu + d, \frac{1}{4}\sigma^2\right) \quad (4.4)$$

The following is true for the subtraction of two normally distributed variates.

$$X - Y \sim \mathcal{N}(\mu_X - \mu_Y, \sigma_X^2 + \sigma_Y^2) \quad (4.5)$$

Applying this to the two tow edges gives

$$y_1^u - y_2^l \sim \mathcal{N}\left(\frac{1}{2}\mu - \left(-\frac{1}{2}\mu + d\right), \frac{1}{4}\sigma^2 + \frac{1}{4}\sigma^2\right) = \mathcal{N}\left(\mu - d, \frac{1}{2}\sigma^2\right) \quad (4.6)$$

This can be used to set the distance d for the desired heuristic (1σ , 2σ , or 3σ) and defect type (gap or overlap). The derivation continues with an example for the probability of an overlap set at the three-sigma boundary, but a similar method can be used to derive any other specification.

$$\Pr(\text{overlap}) = \Pr(y_1^u > y_2^l) = \Pr(y_1^u - y_2^l < 0)$$

$$\Pr(X \leq \mu_X + 3\sigma_X) = \Pr(y_1^u - y_2^l < 0)$$

$$\mu_X + 3\sigma_X = 0 \quad (4.7)$$

$$\mu - d + 3\sqrt{\frac{1}{2}}\sigma = 0$$

$$d = \mu + 3\sqrt{\frac{1}{2}}\sigma$$

4.3. Parallel curve construction

The construction of the steered laminate begins from the same starting point: a tow aligned with the x -axis from $x = -l/2$ to $x = l/2$. It continues differently. The next centreline is placed parallel to the previous one with the distance being the sum of the half widths of both tows. This is done as follows.

Imagine if the curve representing the centerline of a tow would be described by the parametric function as in Equation 4.8.

$$\gamma(t) = (x(t), y(t)) \quad (4.8)$$

A parallel curve $\gamma_d(t) = (x_d(t), y_d(t))$ at distance d can then be described with

$$x_d(t) = x(t) + \frac{d \cdot y'(t)}{\sqrt{x'(t)^2 + y'(t)^2}} \quad (4.9)$$

$$y_d(t) = y(t) - \frac{d \cdot x'(t)}{\sqrt{x'(t)^2 + y'(t)^2}} \quad (4.10)$$

These formulae, however, require an analytical description of the tow path. One could describe the initial tow paths analytically, but the solution for the next centreline becomes complicated. The result becomes more cumbersome as more curves are constructed. Therefore the model uses a numerical approach. Before the approach can be explained first the notation must be described which is best done visually as in Figure 4.5.

In γ , index j indicates the tow and index i the point in the tow, so $\gamma_{3,5}$ represents the third point in the fifth tow. The last point in a tow located at $i = m$ and the last tow has number n . Now that this is defined the analytical parallel curve construction can be rewritten to a numerical form as in Equation 4.11 and 4.12.

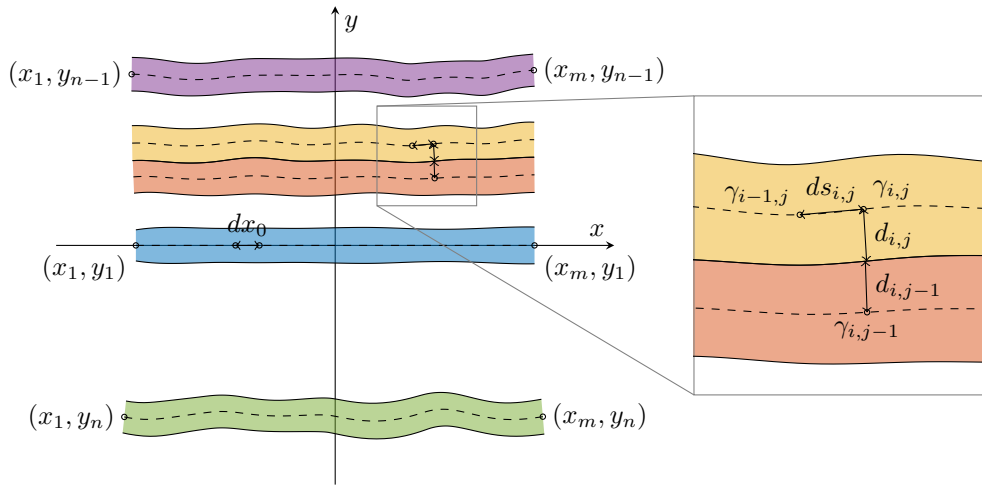


Figure 4.5: Coordinate system

$$x_{i,j} = x_{i,j-1} - \frac{(d_{i,j} + d_{i,j-1}) \cdot dy_{i,j-1}}{\sqrt{dx_{i,j-1}^2 + dy_{i,j-1}^2}} \quad (4.11)$$

$$y_{i,j} = y_{i,j-1} + \frac{(d_{i,j} + d_{i,j-1}) \cdot dx_{i,j-1}}{\sqrt{dx_{i,j-1}^2 + dy_{i,j-1}^2}} \quad (4.12)$$

One problem that is encountered is that the construction is a loop. The new point $\gamma_{i,j}$ is computed using point in the previous tow $\gamma_{i,j-1}$ and the distances $d_{i,j-1}$ $d_{i,j}$. However, the latter depends on the location in the tow model referred to as s . It can be calculated summing the euclidean distances between all the points including the distance between the current point $\gamma_{i,j}$ and its preceding point in the tow $\gamma_{i-1,j}$, which means the location of the new point depends on itself. The complexity is better illustrated using the flowchart in Figure 4.6.

The loop asks for the code to do the process iteratively, but this becomes computationally expensive. Furthermore, the tow width at the spline nodes in the tow model is a random variable. Because of the required effort and the randomness in the tow model, it is not considered worthwhile doing multiple iterations, but it is something that can be done to improve the accuracy of the laminate model.

Last but not least it needs to be mentioned how the derivatives are calculated. The denominator of the difference quotient is not used as it would be cancelled out in the fraction. A forward or central numerical difference method is not possible, since only preceding points are known. This means the derivative is simply calculated using the primary backward numerical difference method in Equation 4.13

$$d\gamma = \gamma_{i,j} - \gamma_{i-1,j} \quad (4.13)$$

Using the standard tow parameters from Table 4.1 and the method stated above one can try to construct the steered laminate. A typical result is displayed in Figure 4.7.

There are two problems that can be observed in this laminate. The first is the high curvatures that are causing self-intersection and cusps. What this means and how this can be avoided will be discussed in the next section. The second is the occurrence of large angle deviations. Why and how this will be addressed in section 4.5.

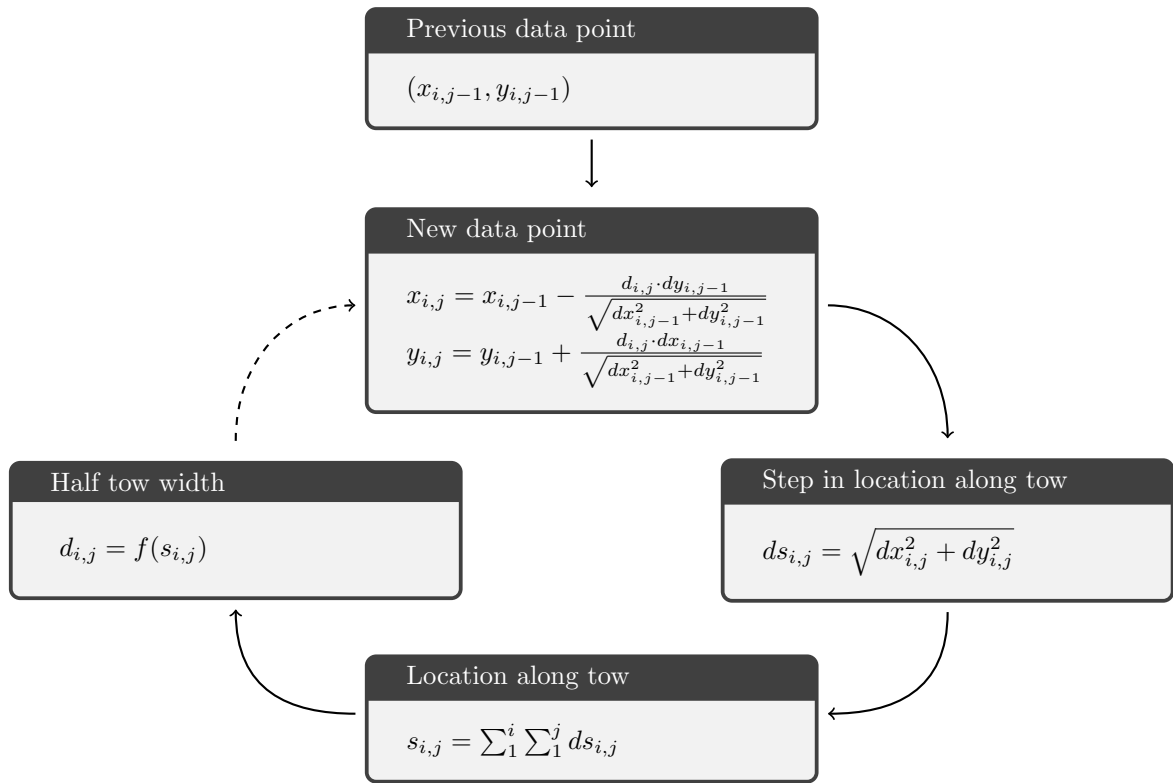


Figure 4.6: Loop in the construction of a parallel curve

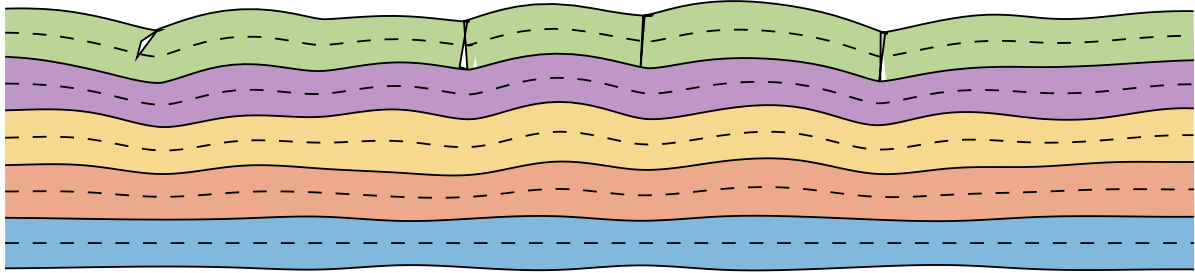


Figure 4.7: Local fibre steering resulting in self-intersections and cusps

4.4. Minimum radius of curvature

If nothing is done, the curvature of the tow paths can become too high. Two indications of that are self-intersections and cusps. A self-intersection is when the tow path forms a loop where it crosses itself. A cusp is a singularity that can be considered an earlier form of a self-intersection as is shown in Figure 4.8. The graph depicts a simple sine in blue and a circle which best approximates the function at its maximum. The radius of this circle is called the radius of curvature (ROC) which is the reciprocal of the curvature. The curvature of a parametric function can be calculated using Equation 4.14. The centre of the circle is called the centre of curvature.

$$k = \frac{x'y'' - y'x''}{(x'^2 + y'^2)^{\frac{3}{2}}} \quad r = \frac{1}{k} \quad (4.14)$$

Under the sinusoid, three parallel curves are constructed using the analytical method described in the previous section. What is interesting is that a point on a curve always shares its centre of curvature with the same point on a parallel curve and the ROC decreases with the offset distance d . As can be

seen in the figure, a cusp occurs when the distance is equal to the ROC and when d increases even more a self-intersection occurs.

What is important to remember is that the curvature increases with the offset distance. So if there is some curvature present in a tow path, then, even without introducing additional fluctuations, self-intersections and cusps will appear at a certain number of tows. This will be referred to as curvature accumulation. However, in an ideal situation, the curvatures as a result of tow width fluctuation cancel each other out. If there is sufficient balance the curvatures would stay within limits for enough tow paths to be constructed to form a laminate of the required dimensions.

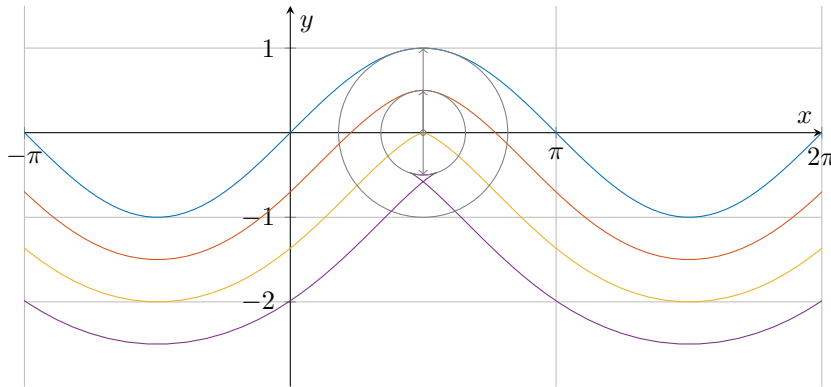


Figure 4.8: Accumulation of curvature: self-intersections and cusps

Unfortunately, even if self-intersections and cusps can be avoided the curvatures are still too high for a laminate to be manufactured. In automated fibre placement, the tows are steered by rotating the end effector to cause an in-plane bending deformation. Due to the finite tow width, the inner edge undergoes compression while the outside experiences tension. This leads to tow wrinkling and upfolding respectively [18]. To prevent this a minimum radius of curvature is introduced.

Beakou et al. introduced an analytical solution to calculate the minimum radius of curvature which is shown in Equation 4.15.

$$r = \frac{E_L b h}{2\alpha N_{0cr}} \tag{4.15}$$

Here, E_L , is the longitudinal Young’s modulus, $b/2$, and h , are the width and thickness of the tow respectively, and N_{0cr} is the critical buckling load of the tow. Factor α is a load parameter which is defined as in Figure 4.9.

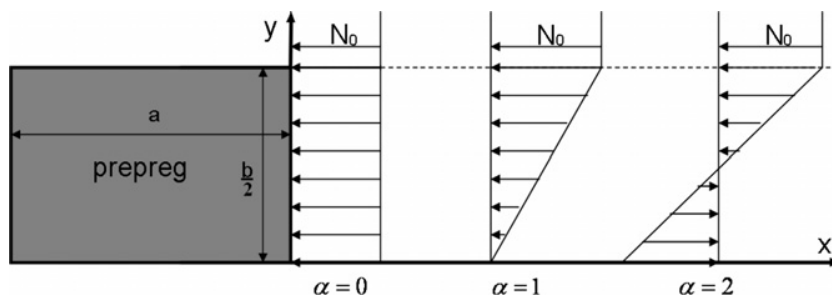


Figure 4.9: Distribution of applied in-plane stress for different values of α [2]

Typical values for the minimum radius of curvature have been given by Blom and are displayed in Table 4.2. From these numbers, it can be concluded that the minimum radius of curvature is related quadratically to the tow width. Typically, automated fibre placement prescribes 400 mm to avoid tow wrinkling or upfolding [38].

Now that is clear that tow paths should conform to the minimum radius of curvature a method should be found to actually reduce the curvatures in a laminate. The methods that have been tried are listed here and are shortly explained below.

Table 4.2: Minimum radii of curvature for different tow widths using a 102 mm-wide course [6]

Tow width $b/2$		Typical minimum turning radius r	
in	mm	in	mm
1/8	3.175	25	635
1/4	6.35	70	1778
1/2	12.7	350	8890

- Increase distance
- Remove points
- Move vertically
- Smoothing spline

The first method to reduce the curvature was to increase the distance d . The idea behind it was to move away from the corner where the curvature is high. However, as explained earlier, the ROC only decreases with the offset distance, so this is actually adversarial.

The second method to limit curvature accumulation was to remove points. This was done either during the curve construction by removing a point when the curvature was too high or by removing the self-intersections as a post-processing step. One thing to say against this method is that it removes information. A tow is represented by a n number of points. If many points will be removed every time a curve is constructed then after a certain number of tows there are not enough points left to realistically represent a tow path. Another reason not to go for this method is that by removing points singularities occur at the edges where data is removed. The transition between the sections actually becomes rough with high curvatures as a result. Thus, removing points is also unsuccessful. Similar to the first method the third aims to move away from the corner where the curvature is high. However, instead of moving perpendicular to the curve, it moves vertically. When a curvature is too high the point is moved away from the previous curve. Then again there is the problem of the transition between the corrected point and the original curve, so in its turn, the points around also have to be moved away vertically. The method actually is proven to be successful, but only sporadically. The challenge is to find how much the point needs to be moved. It can happen that the solution does not converge and the points keep moving further and further away from the original curve.

The fourth and final method is smoothing splines. They can be used to determine how much the points should be moved to correct enough for the curvature and still not differ too much from the original data. Smoothing splines find a balance between having a smooth curve and being close to the original data. The set of splines S is found by minimising the weighted sum of the error measure and the roughness measure displayed in Equation 4.16.

$$p_k \underbrace{\sum_{i=1}^m (y_i - S(x_i))^2}_{\text{error measure}} + (1 - p_k) \underbrace{\int_{x_1}^{x_m} \left(\frac{d^2 S}{dx^2} \right)^2 dx}_{\text{roughness measure}} \quad (4.16)$$

The error measure is the sum of the squared error between the original points y_i and the new points $S(x_i)$ from the spline. The roughness measure is calculated by integrating the second derivative squared of the spline over the domain. The ratio between the two is determined by smoothing parameter p_k . When it is equal to one the solution is a regular cubic spline through the points and the original data remains intact. When $p_k = 0$ the solution will be a linear least-squares estimate since this is infinitely smooth and yet as close to the data as possible. How the minimum of Equation 4.16 is calculated is explained in the next paragraph.

A simple cubic spline is described as shown in Equation 4.17. To demonstrate how the smoothing splines are calculated, the spline needs to be written in the so-called value-second derivative representation. It is assumed that the value ($S(x_i)$) and the second derivative ($S''(x_i)$) are known. Substituting gives the equation for how the entire spline can be plotted using these parameters as shown in Equation 4.18.

$$S_i(x) = a + b(x - x_i) + c(x - x_i)^2 + d(x - x_i)^3 \text{ for } x_i \leq x \leq x_{i+1}, i = 1, \dots, m \quad (4.17)$$

$$S_i(x) = \frac{(x - x_i)S(x_{i+1}) + (x_{i+1} - x)S(x_i)}{x_{i+1} - x_i} - \frac{1}{6}(x - x_i)(x_{i+1} - x) \left\{ \left(1 + \frac{x - x_i}{x_{i+1} - x_i}\right) S''(x_{i+1}) + \left(1 + \frac{x_{i+1} - x}{x_{i+1} - x_i}\right) S''(x_i) \right\} \quad (4.18)$$

for $x_i \leq x \leq x_{i+1}, i = 1, \dots, m$

A requirement for a set of cubic splines is that the first derivatives of neighbouring splines in their common node need to be equal. This is done in the following three equations.

$$S'_i(x_i) = \frac{S(x_{i+1}) - S(x_i)}{x_{i+1} - x_i} - \frac{1}{6}(x_{i+1} - x_i)(S''(x_{i+1}) + 2S''(x_i)) \quad (4.19)$$

$$S'_{i-1}(x_i) = \frac{S(x_i) - S(x_{i-1})}{x_i - x_{i-1}} + \frac{1}{6}(x_i - x_{i-1})(2S''(x_i) + S''(x_{i-1})) \quad (4.20)$$

$$\frac{S(x_{i+1}) - S(x_i)}{x_{i+1} - x_i} - \frac{S(x_i) - S(x_{i-1})}{x_i - x_{i-1}} = \frac{1}{6}(x_i - x_{i-1})S''(x_{i-1}) + \frac{1}{3}(x_{i+1} - x_{i-1})S''(x_i) + \frac{1}{6}(x_{i+1} - x_i)S''(x_{i+1}) \quad (4.21)$$

Let \vec{S} be the vector $(S(x_1) \dots S(x_m))^T$ and \vec{S}'' the vector $(S''(x_1) \dots S''(x_m))^T$. Then the relation above can be displayed in matrix form

$$Q^T \vec{S} = R \vec{S}'' \quad (4.22)$$

where Q is a $m \times (m - 2)$ tridiagonal matrix with the elements

$$q_{i-1,i} = \frac{1}{x_i - x_{i-1}}, \quad q_{ii} = -\frac{1}{x_i - x_{i-1}} - \frac{1}{x_{i+1} - x_i}, \quad q_{i+1,i} = \frac{1}{x_{i+1} - x_i} \text{ for } i = 2, \dots, m - 1 \quad (4.23)$$

and R is a symmetric $(m - 2) \times (m - 2)$ matrix with the elements

$$r_{ii} = \frac{1}{3}(x_{i+1} - x_{i-1}) \quad \text{for } i = 2, \dots, m - 1$$

$$r_{i,i+1} = r_{i+1,i} = \frac{1}{6}(x_{i+1} - x_i) \quad \text{for } i = 2, \dots, m - 2$$

All elements of the two band matrices that are undefined here are equal to zero. The error measure can be written in matrix form as follows.

$$\sum_{i=1}^m (y_i - S(x_i))^2 = (\vec{y} - \vec{S})^T (\vec{y} - \vec{S}) \quad (4.24)$$

Using the relation in Equation 4.22 the roughness measure can also be written in matrix form. The derivation below uses integration by parts and the fact that for a natural set of cubic splines $S''(x_1) = S''(x_m) = 0$ and that S''' is constant on each interval $[x_i, x_{i+1}]$ and zero outside $[x_1, x_m]$.

$$\begin{aligned}
\int_{x_1}^{x_m} (S''(x))^2 dx &= \int_{x_1}^{x_m} S''(x) \frac{d}{dx} (S'(x)) dx \\
&= [S''(x)S'(x)]_{x_1}^{x_m} - \int_{x_1}^{x_m} S'''(x)S'(x) dx \\
&= - \int_{x_1}^{x_m} S'''(x)S'(x) dx \\
&= - \sum_{i=1}^{m-1} S'''(x_i) \int_{x_i}^{x_{i+1}} S'(x) dx \\
&= \sum_{i=1}^{m-1} \frac{S''(x_{i+1}) - S''(x_i)}{x_{i+1} - x_i} (S(x_i) - S(x_{i+1})) \\
&= \sum_{i=1}^{m-1} S''(x_{i+1}) \frac{S(x_i) - S(x_{i+1})}{x_{i+1} - x_i} - S''(x_i) \frac{S(x_i) - S(x_{i+1})}{x_{i+1} - x_i} \\
&= \sum_{i=2}^m S''(x_i) \frac{S(x_{i-1}) - S(x_i)}{x_i - x_{i-1}} - \sum_{i=1}^{m-1} S''(x_i) \frac{S(x_i) - S(x_{i+1})}{x_{i+1} - x_i} \\
&= \sum_{i=2}^{m-1} S''(x_i) \left(\frac{S(x_{i+1}) - S(x_i)}{x_{i+1} - x_i} - \frac{S(x_i) - S(x_{i-1})}{x_i - x_{i-1}} \right) \\
&= (\vec{S}''^T)^T Q^T \vec{S} = \vec{S}^T Q R^{-1} Q^T \vec{S} = \vec{S}^T K \vec{S}
\end{aligned} \tag{4.25}$$

Using the combination of the error and roughness measure expressed in vectors and matrices it can be proven that a unique minimum exists that can be calculated using a linear time algorithm. It starts with introducing $\lambda = \frac{1-p_k}{p_k}$.

$$\begin{aligned}
&\sum_{i=1}^m (y_i - S(x_i))^2 + \lambda \int_{x_1}^{x_m} \left(\frac{d^2 S}{dx^2} \right)^2 dx \\
&= (\vec{y} - \vec{S})^T (\vec{y} - \vec{S}) + \lambda \vec{S}^T K \vec{S} \\
&= \vec{y}^T \vec{y} - 2\vec{y}^T \vec{S} + \vec{S}^T \vec{S} + \lambda \vec{S}^T K \vec{S} \\
&= \vec{S}^T (I - \lambda K) \vec{S} - 2\vec{y}^T \vec{S} + \vec{y}^T \vec{y}
\end{aligned} \tag{4.26}$$

The minimum for this function is located at

$$\vec{S} = (I + \lambda K)^{-1} \vec{y} \tag{4.27}$$

Now that there is a method to calculate the smoothing spline, it can be used for the curve construction. Fortunately, MATLAB has a built-in cubic smoothing spline function called `csaps`. In the script, the smoothing parameter p_k is calculated iteratively. After each tow path, the smoothing is applied, starting at $p_k = 0$ e.g. no smoothing. The parameter gradually decreases until the lowest radius of curvature in the tow path is below the minimum ROC.

Note that the roughness measure uses only the second derivative which is an approximation of the actual curvature in Equation 4.14. However, it is only used to smooth the curves and the amount of smoothing is still defined by a numerical approximation of the curvature. This approximation is displayed in Equation 4.28. It shows that differences can be used instead of the derivatives because the time steps cancel each other out.

$$k = \frac{x'y'' - y'x''}{(x'^2 + y'^2)^{\frac{3}{2}}} = \frac{\frac{dx}{dt} \frac{d^2y}{dt^2} - \frac{dy}{dt} \frac{d^2x}{dt^2}}{\left(\left(\frac{dx}{dt} \right)^2 + \left(\frac{dy}{dt} \right)^2 \right)^{\frac{3}{2}}} = \frac{dx \cdot d^2y - dy \cdot d^2x}{(dx^2 + dy^2)^{\frac{3}{2}}} \quad (4.28)$$

For calculating the curvature, the backward, central, and forward difference methods are used that are displayed respectively in Equation 4.29 for both the first-order as second-order difference. The central difference methods are used except for γ_1 and γ_m where this is impossible.

$$\begin{aligned} \nabla\gamma &= \gamma_i - \gamma_{i-1} & \delta\gamma &= \frac{\gamma_{i+1} - \gamma_{i-1}}{2} & \Delta\gamma &= \gamma_{i+1} - \gamma_i \\ \nabla^2\gamma &= \gamma_i - 2\gamma_{i-1} + \gamma_{i-2} & \delta^2\gamma &= \gamma_{i+1} - 2\gamma_i + \gamma_{i-1} & \Delta^2\gamma &= \gamma_{i+2} - 2\gamma_{i+1} + \gamma_i \end{aligned} \quad (4.29)$$

Smoothing allows for an infinite amount of tows to be constructed as long as the minimum radius of curvature is large enough. Defect area percentages for different amounts of smoothing will be covered in section 4.6.

4.5. Fibre angle deviation

The second problem is the occurrence of large angle deviations. In the conventional laminate, there might be a large amount of gaps and overlap but, at least in an ideal situation, the fibres are aligned in one direction. In the steered laminate the tows move away from the paths to reduce the gaps and overlaps. The fibre angle is sacrificed for the defect area percentage which might, as will be explained in this section, not be worth it.

Automated fibre placement uses orthotropic continuous fibre reinforced plastic material. Orthotropic means the mechanical properties depend on the orientation. The stiffness, for example, is often more than ten times higher in the direction of the fibres compared to the other directions.

The strains and stress referred to the principal axes are related as in

$$\begin{pmatrix} \varepsilon_1 \\ \varepsilon_2 \\ \gamma_{12} \end{pmatrix} = \begin{bmatrix} S_{11} & S_{12} & 0 \\ S_{21} & S_{22} & 0 \\ 0 & 0 & S_{66} \end{bmatrix} \begin{pmatrix} \sigma_1 \\ \sigma_2 \\ \tau_{12} \end{pmatrix} = \begin{bmatrix} \frac{1}{E_1} & \frac{\nu_{21}}{E_2} & 0 \\ \frac{\nu_{12}}{E_1} & \frac{1}{E_2} & 0 \\ 0 & 0 & \frac{1}{G_{12}} \end{bmatrix} \begin{pmatrix} \sigma_1 \\ \sigma_2 \\ \tau_{12} \end{pmatrix} \quad (4.30)$$

The engineering constant referred to the principal axes

$$\begin{pmatrix} \sigma_1 \\ \sigma_2 \\ \tau_{12} \end{pmatrix} = [T] \begin{pmatrix} \sigma_x \\ \sigma_y \\ \tau_{xy} \end{pmatrix} \quad \begin{pmatrix} \varepsilon_1 \\ \varepsilon_2 \\ \frac{1}{2}\gamma_{12} \end{pmatrix} = [T] \begin{pmatrix} \varepsilon_x \\ \varepsilon_y \\ \frac{1}{2}\gamma_{xy} \end{pmatrix} \quad (4.31)$$

$$[T] = \begin{bmatrix} m^2 & n^2 & 2mn \\ n^2 & m^2 & -2mn \\ -mn & mn & m^2 - n^2 \end{bmatrix} \quad \begin{aligned} m &= \cos \theta \\ n &= \sin \theta \end{aligned} \quad (4.32)$$

The transformation of the stresses and strains can be used to find the transformation of the mathematical constants.

$$\begin{aligned} \begin{pmatrix} \varepsilon_x \\ \varepsilon_y \\ \frac{1}{2}\gamma_{xy} \end{pmatrix} &= [T]^{-1} \begin{pmatrix} \varepsilon_1 \\ \varepsilon_2 \\ \frac{1}{2}\gamma_{12} \end{pmatrix} = [T]^{-1} \begin{bmatrix} S_{11} & S_{12} & 0 \\ S_{21} & S_{22} & 0 \\ 0 & 0 & \frac{1}{2}S_{66} \end{bmatrix} \begin{pmatrix} \sigma_1 \\ \sigma_2 \\ \tau_{12} \end{pmatrix} \\ &= [T]^{-1} \begin{bmatrix} S_{11} & S_{12} & 0 \\ S_{21} & S_{22} & 0 \\ 0 & 0 & \frac{1}{2}S_{66} \end{bmatrix} [T] \begin{pmatrix} \sigma_x \\ \sigma_y \\ \tau_{xy} \end{pmatrix} = \begin{bmatrix} S_{xx} & S_{xy} & S_{xs} \\ S_{yx} & S_{yy} & S_{ys} \\ \frac{1}{2}S_{xs} & \frac{1}{2}S_{ys} & \frac{1}{2}S_{ss} \end{bmatrix} \begin{pmatrix} \sigma_x \\ \sigma_y \\ \tau_{xy} \end{pmatrix} \end{aligned} \quad (4.33)$$

Just like how in Equation 4.30 the mathematical constants are related to the engineering constants referred to the principal this can be done relative to the reference axes in Equation 4.34.

$$\begin{pmatrix} \varepsilon_x \\ \varepsilon_y \\ \gamma_{xy} \end{pmatrix} = \begin{bmatrix} S_{xx} & S_{xy} & S_{xs} \\ S_{yx} & S_{yy} & S_{ys} \\ S_{xs} & S_{ys} & S_{ss} \end{bmatrix} \begin{pmatrix} \sigma_x \\ \sigma_y \\ \tau_{xy} \end{pmatrix} = \begin{bmatrix} \frac{1}{E_x} & \frac{\nu_{yx}}{E_y} & \frac{\eta_{sx}}{G_{xy}} \\ \frac{\nu_{xy}}{E_x} & \frac{1}{E_y} & \frac{\eta_{sy}}{G_{xy}} \\ \frac{\eta_{xs}}{E_x} & \frac{\eta_{ys}}{E_y} & \frac{1}{G_{xy}} \end{bmatrix} \begin{pmatrix} \sigma_x \\ \sigma_y \\ \tau_{xy} \end{pmatrix} \quad (4.34)$$

Substituting gives the direct transformation of the engineering constant from one coordinate system to the other.

$$\begin{aligned} \frac{1}{E_x} &= \frac{m^2}{E_1}(m^2 - n^2\nu_{12}) + \frac{n^2}{E_2}(n^2 - m^2\nu_{21}) + \frac{m^2n^2}{G_{12}} \\ \frac{1}{E_y} &= \frac{n^2}{E_1}(n^2 - m^2\nu_{12}) + \frac{m^2}{E_2}(m^2 - n^2\nu_{21}) + \frac{m^2n^2}{G_{12}} \\ \frac{1}{G_{xy}} &= \frac{4m^2n^2}{E_1}(1 + \nu_{12}) + \frac{4m^2n^2}{E_2}(1 + \nu_{21}) + \frac{(m^2 - n^2)^2}{G_{12}} \end{aligned} \quad (4.35)$$

The transformation of the engineering constants in Equation 4.35 can be plotted resulting in Figure 4.10. It can be observed that the longitudinal stiffness reduces drastically when angle θ increases. At about 15° the Young's modulus has decreased by half.

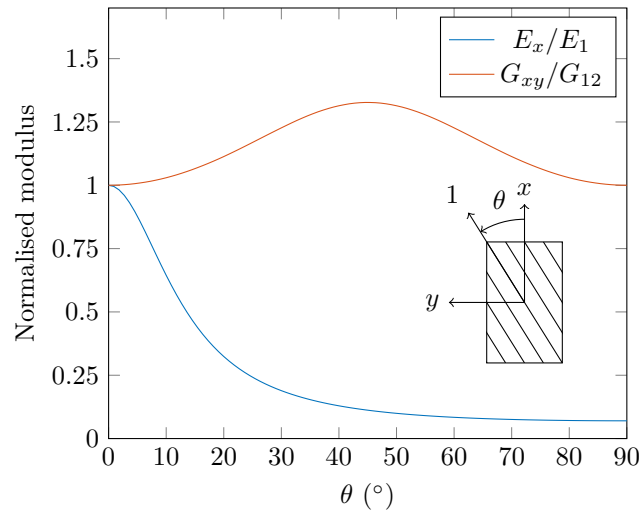


Figure 4.10: Young's modulus and shear modulus of unidirectional composite material as a function of fibre orientation (AS4/3501-6 carbon/epoxy) (adapted from: [10])

The magnitude of this variable should not exceed prescribed requirements for the manufacturing method. The tolerances for fibre angle deviations are generally $\pm 3^\circ$ on short distances and $\pm 2^\circ$ on distances over circa 300 mm [4]. The first would result in a longitudinal stiffness change of -1.78% and the latter -3.91% . Similar to the problem with limiting the radius of curvature a method needs to be found to keep the fibre angle within bounds. This is done using a weighted average of the original values and the mean of all values as displayed in Equation 4.36. This process will henceforth be referred to as levelling, since it actually forces the tow paths to be more horizontal.

$$y = (1 - p_\theta) \cdot \bar{y} + p_\theta \cdot y \quad (4.36)$$

The effect of levelling is visualised in Figure 4.11. Smoothing also levels the data partially and vice versa. Smoothing, however, will be done first, because it essential to construct the laminate. Levelling is optional and balances the fibre angle deviation with the fidelity to the data. As a result, the absolute fibre angle may decrease, but in turn, the defect area percentage will increase as will be shown in the next section.

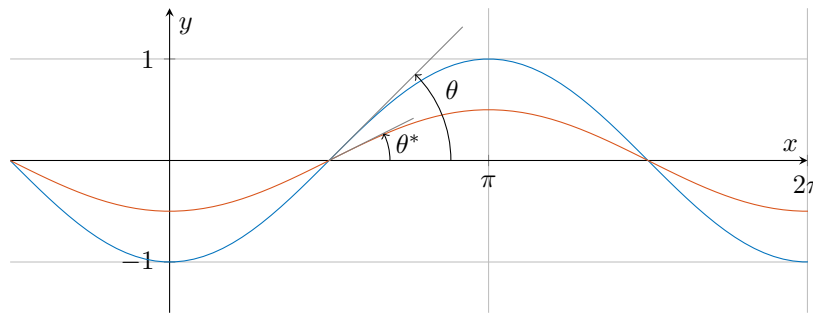


Figure 4.11: The effect of levelling on a simple sine curve

4.6. Preliminary results: defect area percentages

Table 4.3 shows the defect area percentages for different degrees of smoothing and levelling. The standard parameters from Table 4.1 are used for the model. The defect area percentage is the sum of the gap and overlap area divided by the total area of the laminate. The latter is the product of the mean tow width μ , number of tows n , and the tow length l . Vertically different minimum radii of curvature that are required are shown. Horizontally the maximum absolute fibre angle that is allowed is varied. The last column shows the results of no levelling. Next to the defect area percentage it also includes the maximum absolute fibre angle observed in the laminate. The ultimate minimum ROC is about 50 mm, since below that the curvature accumulates and the desired number of tows cannot be constructed. This ROC without levelling shows the lowest theoretical defect area percentage for this input. The negative side-effects are the high angle deviation of up to almost 12 degrees. A minimum ROC of 6400 mm is an interesting case as well. The smoothing is so high that no levelling is required to stay below the often used one-degree limit for the angle deviation. When levelling is used to comply with this constraint a local minimum of the defect area percentage is present around 400 mm for the minimum ROC.

Of course, all these results are preliminary since the input parameters are based on literature and educated guesses. The next chapter will cover the validation of the tow model and the resulting outputs from experimental data.

Table 4.3: Defect area percentages

Minimum ROC [mm]	Maximum absolute fibre angle [°]						∞	
	1	2	3	4	5			
50	1.78%	1.55%	1.37%	1.18%	1.04%	0.98%	11.9°	
100	1.71%	1.45%	1.28%	1.14%	1.17%	1.08%	6.4°	
200	1.65%	1.43%	1.33%	1.32%	1.33%	1.29%	6.1°	
400	1.63%	1.49%	1.45%			1.42%	3.9°	
800	1.67%					1.59%	1.9°	
1600	1.73%					1.72%	1.8°	
6400						1.84%	0.5°	

5

Validation of tow model

The previous chapter explained the model that constructs the laminates. The input, the tow model, still contains a lot of assumptions. The goal of this chapter is to validate the tow model. The tow width fluctuation is measured and compared to the previously chosen parameters. The first section describes the setup, material, and sensor respectively. The second discusses the results of the validation.

5.1. Method

The setup that is used is illustrated in Figure 5.1. Prepreg tow material is unwinded from a spool and passed by a sensor after which it is rewinded on a different spool. The material is kept under tension by an electric brake that controls the torque on the shaft to which the unwinding spool is connected. The rewinding spool is rotated at a constant rotational speed by a stepper motor. Both spools are connected to their shaft using an Uhing Easylock clamping system in order to prevent slipping. The tape is guided by rollers from one end to the other to make sure it does not slide and it is at the right distance from the sensor.

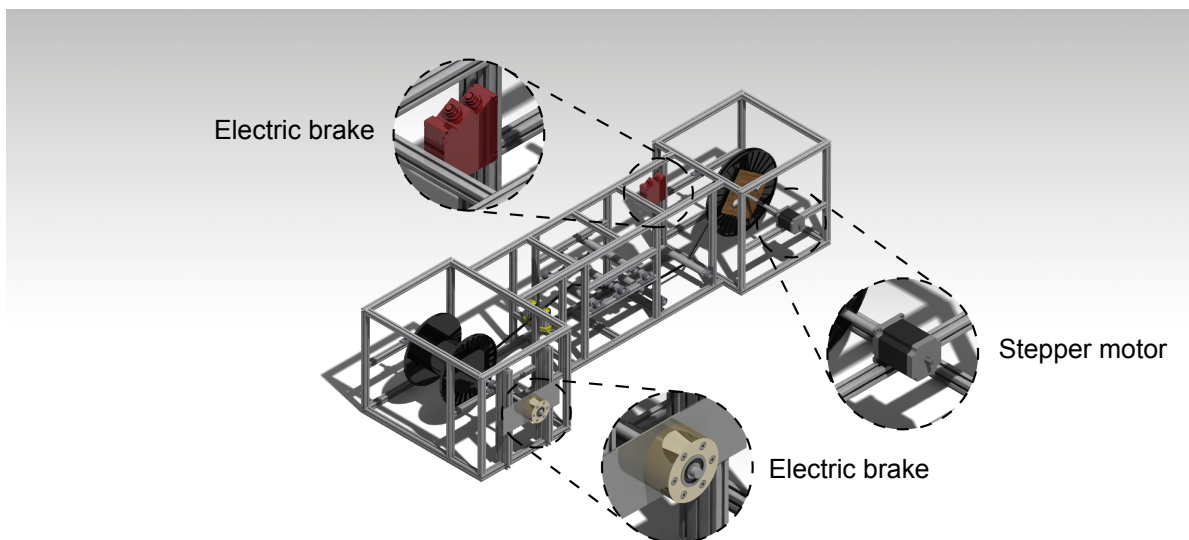


Figure 5.1: Render of the tow width measurement setup

5.1.1. Material

Two different materials are measured separately. Prepreg tapes with a thermoplastic matrix are used because they can be stored for a long period at room temperature. The properties of the first material are shown in Table 5.1. All material is unidirectional (UD).

Table 5.1: Material 1: Toray Cetex TC1320 PEKK [47]

Property	Value
Physical properties	Standard Modulus Carbon UD Tape
Fiber areal weight (FAW)	145 g/m ² (4.28 oz/yd ²)
Weight per ply (PAW)	221 g/m ² (6.52 oz/yd ²)
Resin content by weight (RC)	34%
Consolidated ply thickness (CPT)	0.14 mm (0.006 in)
Density	1.59 g/cm ³ (99.3 lb/ft ³)
Width	6.35 mm (0.25 in)*
	<i>*The original width of the material is 305 mm (12 in)</i>
	<i>Narrower widths are available through secondary slitting</i>
Mechanical properties	Standard Modulus Carbon 145gsm UD Tape (45% RC)*
Tensile Modulus 0°	135 GPa
Tensile Modulus 90°	10 GPa
Compression Modulus 0°	124 GPa
In-Plane Shear Modulus	5.2 GPa
	<i>*Room temperature dry (RTD) condition</i>
	<i>Fiber type AS-4D</i>
Typical neat resin properties	PEKK (Polyetherketoneketone)
Density (specific gravity)	1.30 g/cm ³ (80.5 lb/ft ³)

Note that the table actually contains two different materials, but only the resin content differs. Using the density of the resin and of the composite at a resin content by weight of 34% results in a matrix volume fraction of 42%. It can also be calculated that the density of AS-4D fibres must be 1.80 g cm⁻³. This density agrees with a datasheet from a supplier of AS-4 carbon fibre [19]. Assuming that the variant used for determining the mechanical properties has the same fibre areal weight of 145 g/m² and a resin content by weight of 45% the following properties can be deducted. The fibre volume fraction is estimated to be 47%. The ply thickness is increased to 0.17 mm due to the higher resin content while the grams of fibre per square metre stays the same. The density of the composite material is 1.53 g/cm³.

The second material that is tested is Suprem T62% IM7/PES-4100 where 62% represents the fibre volume content and IM7 is a type of carbon fibre. PES stands for polyethersulfone which is the matrix polymer and 4100 refers to its reduced viscosity (RV) which the supplier uses to categorise the polymer in different grades. According to the product description, the tape is 5 mm wide and 0.16 mm thick. The mechanical properties of the fibres and the polymer are summarised in Table 5.2 and 5.3 respectively.

The shear modulus of PES is calculated using Equation 5.1 which holds for isotropic material. The properties of the reinforcement and the matrix can be combined using the rule of mixtures to determine the properties of the composite as described in section 2.4.

Table 5.2: IM7 carbon fibre properties [10]

Property	Value
Density ρ_f	1.80 g/cm ³
Longitudinal modulus E_{1f}	290 GPa
Transverse modulus E_{2f}	21 GPa
Axial shear modulus G_{12f}	14 GPa
Poisson's ratio ν_f	0.20

Table 5.3: PES polymer properties [3]

Property	Value
Density ρ_m	1.37 g/cm ³
Tensile modulus E_m	2.4 GPa
Shear modulus G_m	0.86 GPa
Poisson's ratio ν_m	0.4

$$G = \frac{E}{2(1 + \nu)} \quad (5.1)$$

5.1.2. Sensor

The sensor that is used to determine the tow width is the Micro-Epsilon scanCONTROL 2950-100/BL laser scanner. It uses the triangulation principle to measure the profile which is shown schematically in Figure 5.2.

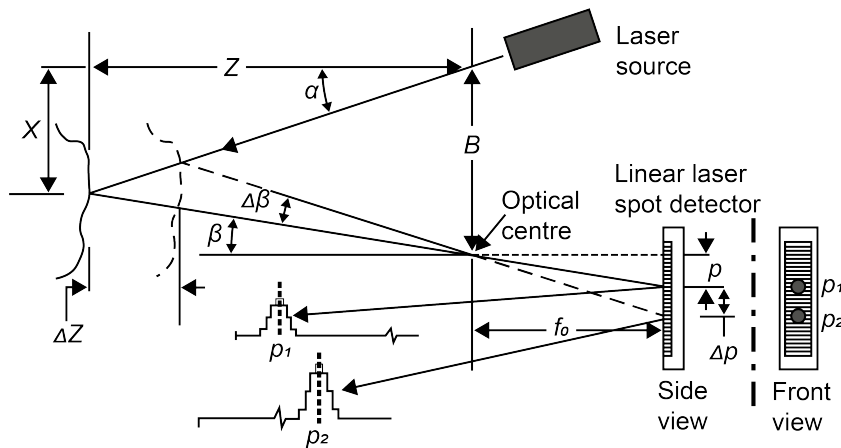


Figure 5.2: Single point optical triangulation based on a single laser beam and a position-sensitive detector (Adapted from: [51])

The laser source projects light at a known projection angle α with respect to the $X - Z$ coordinate system. The light is then reflected by the surface of interest to pass through the collection lens and fall onto the position-sensitive detector. The source, lens and detector are at a fixed location with respect to one another. The distance between the optical centre of the lens and the laser source is known as baseline B . The laser spot detector is at a distance f_0 from the collection lens. From the measured spot position p on the detector, the collection angle β can be determined and using the cosine law the coordinates X and Z of a point on the surface can be derived. The relation can be found in Equation 5.2 and 5.3.

$$X = Z \tan(\alpha) \quad (5.2)$$

$$Z = \frac{B f_0}{p + f_0 \tan(\alpha)} \quad (5.3)$$

A laser-line scanner is chosen as the sensor because a stand-alone camera is not suitable for several reasons. The first is that the camera must be perpendicular to the tow surface. Tow twisting introduces more uncertainty to the measurements. The second reason is that carbon fibre tows have a dark colour and high reflectance. It makes it difficult to get a good contrast between the tow and the background. The third is that if the same method would be used online, during automated fibre placement, the heating element used for consolidation increases the reflections on the material and thus make it even more difficult to detect the width accurately.

Figure 5.3 shows a screen capture of the scanCONTROL Configuration Tools, a software package available from Micro-Epsilon to communicate with the sensor with a Windows PC. The sensor will only

give a 2D profile that is just one slice of the tape at a certain moment in time. From this, the course of the tape is constructed by converting the slices to their locations along the tape.

The connection between the moment in time t and the location along the tape s can be derived as follows. The angular velocity of the spool winding the material is constant. The radius is assumed to increase linearly, approximately the thickness of the tape every revolution. The tangential velocity is linear accordingly.

The speed of the material is measured by placing marking tape of a known width (50 mm) on the roll. Using the time that it takes for the marking tape to pass the sensor, the speed can be derived. This is done at several points along the tow and linear regression is applied to estimate speed over time. Integrating the velocity allows the timestamp of each profile to be translated into a location s .

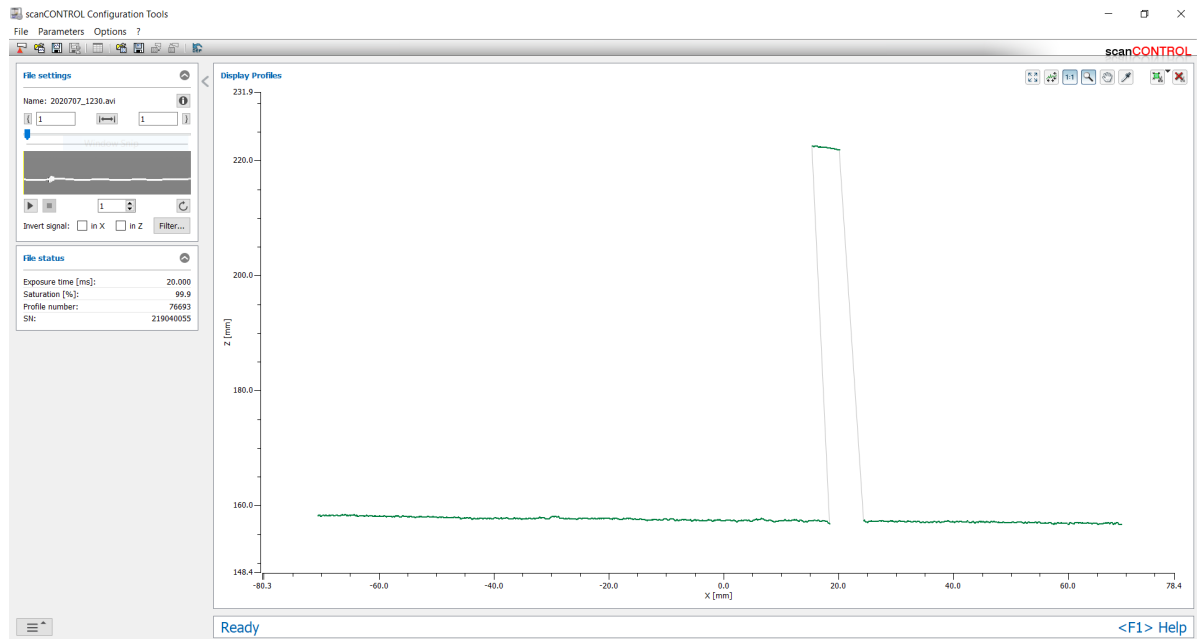


Figure 5.3: Screen capture of scanCONTROL Configuration Tools

5.2. Validation results: tow width fluctuation

In section 4.1 a tow model was introduced that used three parameters: mean tow width, standard deviation and spline node distance. The goal of this section is to examine whether the model accurately represents the tow material and if the values chosen for the parameters are valid.

The first two parameters are the mean tow width μ and standard deviation σ . They can be calculated directly from the data. The results are shown in Table 5.4. The mean tow width of the two materials deviate 2.2 % and 0.1 % from the expected value respectively. The standard deviation is about five times smaller than literature indicated.

The last parameter, spline node distance dl cannot be calculated directly. In some way dl represents how smooth the tow width fluctuates. To derive this parameter from the measurements the roughness of both the measurements and the tow model need to be compared. In Chapter 4 the smoothing spline was introduced which includes a common roughness measure that is repeated below.

$$\int_{x_1}^{x_m} \left(\frac{d^2 S}{dx^2} \right)^2 dx \quad (5.4)$$

Equation 5.4 is the analytical equation for calculating the total roughness from x_1 to x_m for a cubic spline. The integral can be approximated by a summation as shown in eq. (5.5), which is a numerical way to determine the average roughness for a m number of data points of the tow width measurement. The second derivative is calculated in a way similar to the formulae stated in eq. (4.29).

$$\bar{k}^2 = \frac{1}{m} \sum_{i=1}^m \left(\frac{d^2 w_i}{ds_i^2} \right)^2 \quad (5.5)$$

The average roughness \bar{k}^2 can be used to calculate the spline node distance dl as follows. First the average roughness of the measurement data is calculated. Then a tow model is generated using the μ and σ from the same data. Lastly, dl in the tow model is varied until the \bar{k}^2 of the data and the tow model are sufficiently close (three decimal digits). Both are shown in table 5.4.

Table 5.4: Results of the validation of the tow width fluctuation before smoothing

	Material 1	Material 2	Tow model
μ	6.492 mm	5.006 mm	6.350 mm
σ	0.050 mm (0.8 %)	0.039 mm (0.8 %)	0.254 mm (4.0 %)
\bar{k}^2	0.072	0.090	0.081
dl	0.837 mm	0.705 mm	1.842 mm

Unfortunately, the quality of the data is not as anticipated. The data from the experiment shows large variations in the tow width that are not observed visually. The same section of a tape is measured twice and the data is shown in Figure 5.4.

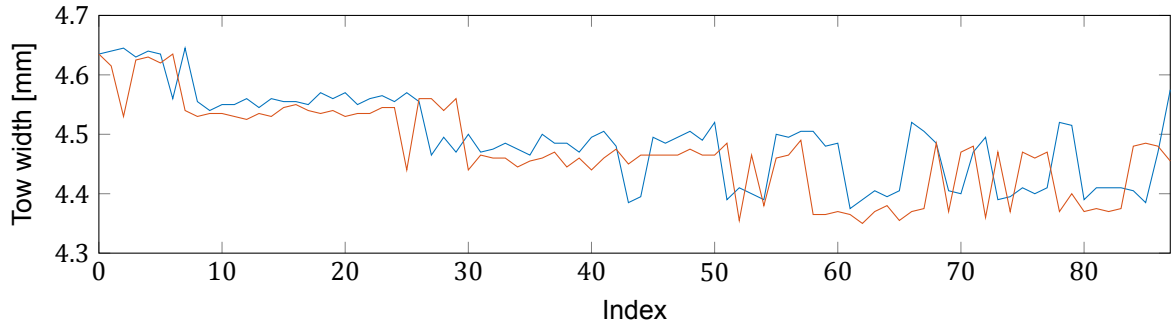


Figure 5.4: A section of prepreg tape measured twice

It shows that the measurements do follow the trend of the tow width, but it is not very accurate. Also, rapid shifts in tow width are observed, which may not have a large effect on the average tow width but the effect is larger on the standard deviation and especially important for the roughness since it depends on the course of the tow width fluctuation. To make the data more suitable, the choice is made to smooth the data.

There are multiple methods to smooth the data to make it more practical. One is the smoothing splines used in the laminate model. This requires the user to balance the fidelity to the data with the smoothness of the spline. However, it is the smoothness of the spline that is important, so it must not be set by the smoothing method, but by the data itself.

Another option is using the moving average. The moving average replaces every data point with the mean of it and several points around it. This is shown mathematically in Equation 5.6.

$$\bar{w}_i = \frac{w_{i-\frac{\Delta m-1}{2}} + \dots + w_{i-1} + w_i + w_{i+1} + \dots + w_{i+\frac{\Delta m-1}{2}}}{\Delta m} \quad (5.6)$$

Here, w_i is the width at a certain point and Δm is the number of points included in the subset over which the average is calculated.

The next step is to determine the sliding window length Δm used for the moving average. The method is based on the chi-square goodness-of-fit test. The test determines if a data sample comes from a normal distribution with the μ and σ estimated from the data. The data is grouped into bins and the observed counts (O_i) and expected counts (E_i) are computed. The formula for the variable χ^2 is shown in Equation 5.7.

$$\chi^2 = \sum_{i=1}^n (O_i - E_i)^2 / E_i \quad (5.7)$$

Here, O_i and E_i are the observed and expected counts of the i -th bin and n is the number of bins. The lower χ^2 the more the data is normally distributed, thus the variable is calculated for different number of Δm until a local minimum is reached.

The results are shown in Figure 5.5. The counts are scaled using the number of bins and the bin width to give the probability density. On the left the distribution of the data before smoothing is shown while on the right the probability density is shown at a local minimum of χ^2 with the required Δm . The blue bars are the scaled observed counts O_i and the red line is the estimated normal distribution from which the values for E_i are derived. The jumps in the tow width observed in Figure 5.4 can also be observed in the distribution before smoothing. However, after smoothing, the tow width resembles much more normal deviate which it is expected to be. The three tow model parameters μ , σ , and dl are also calculated for the smooth data as well as the average roughness. The results of the validation are shown in Table 5.5.

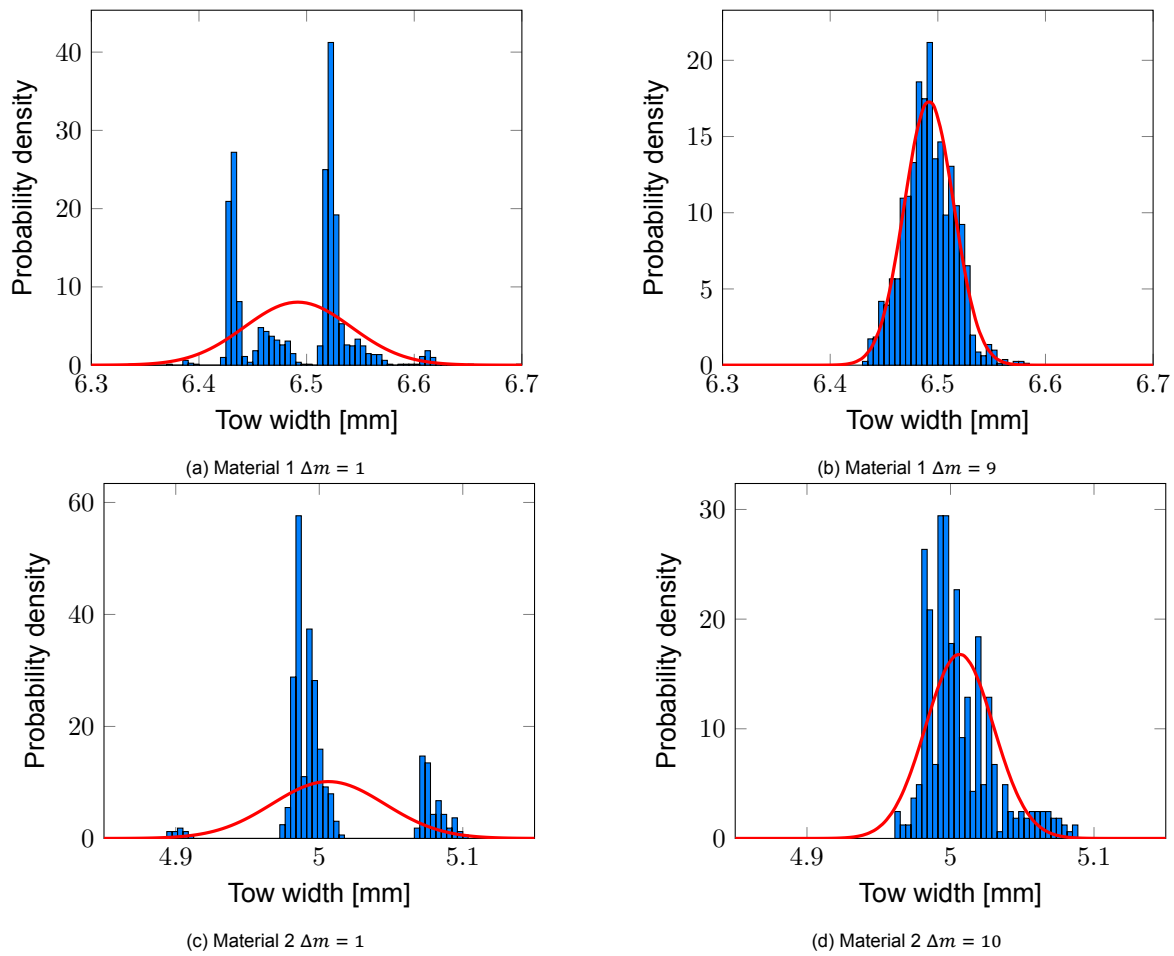


Figure 5.5: Probability density distribution before and after smoothing

Table 5.5: Results of the validation after smoothing

	Material 1	Material 2	Tow model
Δm	9	10	-
μ	6.492 mm	5.006 mm	6.350 mm
σ	0.023 mm (0.4 %)	0.024 mm (0.5 %)	0.254 mm (4.0 %)
\bar{k}^2	6.171×10^{-4}	6.358×10^{-4}	6.265×10^{-4}
dl	1.875 mm	1.896 mm	6.267 mm

6

FEM

In order to make the comparison of the structural performance between local fibre steering and traditional approaches, a finite element analysis is carried out. The basis for the analysis is the defect layer method by Fayazbakhsh et al. explained in section 2.4. Section 4.5 will explain how the fibre angle deviation is incorporated into the method. Section 6.2 discusses how the laminate model is mapped to the finite element mesh. Section 6.3 treats the analysis in the FEM software before section 6.4 shows the results.

6.1. Fibre angle

In section 4.5 about fibre angle deviation it was shown that when the principal axes and reference axes are not aligned the engineering constants can be transformed, the resulting stress-strain relations are repeated below.

$$\begin{Bmatrix} \varepsilon_1 \\ \varepsilon_2 \\ \gamma_{12} \end{Bmatrix} = \begin{bmatrix} \frac{1}{E_1} & \frac{\nu_{21}}{E_2} & 0 \\ \frac{\nu_{12}}{E_1} & \frac{1}{E_2} & 0 \\ 0 & 0 & \frac{1}{G_{12}} \end{bmatrix} \begin{Bmatrix} \sigma_1 \\ \sigma_2 \\ \tau_{12} \end{Bmatrix} \Rightarrow \begin{Bmatrix} \varepsilon_1 \\ \varepsilon_2 \\ \gamma_{12} \end{Bmatrix} = \begin{bmatrix} \frac{1}{E_x} & \frac{\nu_{yx}}{E_y} & \frac{\eta_{sx}}{G_{xy}} \\ \frac{\nu_{xy}}{E_x} & \frac{1}{E_y} & \frac{\eta_{sy}}{G_{xy}} \\ \frac{\eta_{xs}}{E_x} & \frac{\eta_{ys}}{E_y} & \frac{1}{G_{xy}} \end{bmatrix} \begin{Bmatrix} \sigma_x \\ \sigma_y \\ \tau_{xy} \end{Bmatrix} \quad (6.1)$$

It can be observed that with the transformation two engineering constants are introduced. These are the shear coupling coefficients η_{sx} and η_{sy} . η_{xs} and η_{ys} in the right-hand matrix in Equation 6.1 can be derived using the fact that the matrix is symmetric.

The variable that is required to calculate the transformed engineering constants is the fibre orientation. Fayazbakhsh et al. use a fibre path definition where the fibre orientation is directly correlated with a location on the plate. In the laminate model from Chapter 4 tows with different fibre angles can overlap. To solve this the decision was made to take the weighted average of the fibre orientation and use that to do the transformation. This is shown in Equation 6.2 where θ_i is the fibre orientation of each piece of material and v_i is its prevalence in terms of area.

$$\bar{\theta} = \sum v_i \theta_i \quad (6.2)$$

6.2. Mapping

In order to calculate the properties of each mesh element, the defect area percentages are necessary as well as the weighted average of the fibre orientation. This section shows how the tows from the laminate model are mapped to the FEM mesh to be able to calculate the necessary values.

Chapter 4 showed how the tows are constructed. Each tow has m points along its centreline and its edges. The tow is divided into $m - 1$ tow elements. An example of such a tow element is illustrated in Figure 6.1. The four vertices are the transformed coordinates of the tow edge and the fibre orientation θ is determined by calculating the angle of the centreline relative to the laminate coordinates.

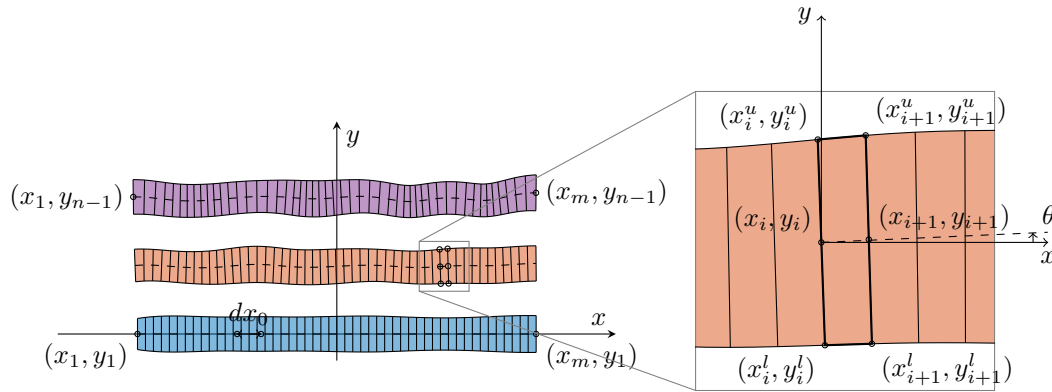


Figure 6.1: Tow element

Now that the tow elements are constructed they can be mapped to the finite element mesh. First is determined for each mesh element which tow elements intersect. The process is visualised in Figure 6.2. On the left, it is checked for every tow element whether it intersects with the mesh. If not, the tow element can be discarded. Then, for each mesh column, it is figured out which tow elements intersect. The same is done for the mesh rows. The two steps are shown in the centre of Figure 6.2. By combining the information of the two steps it can be determined for each mesh element which tow elements intersect. Separating rows and columns is computationally more efficient than determining the intersections of each individual mesh element directly.

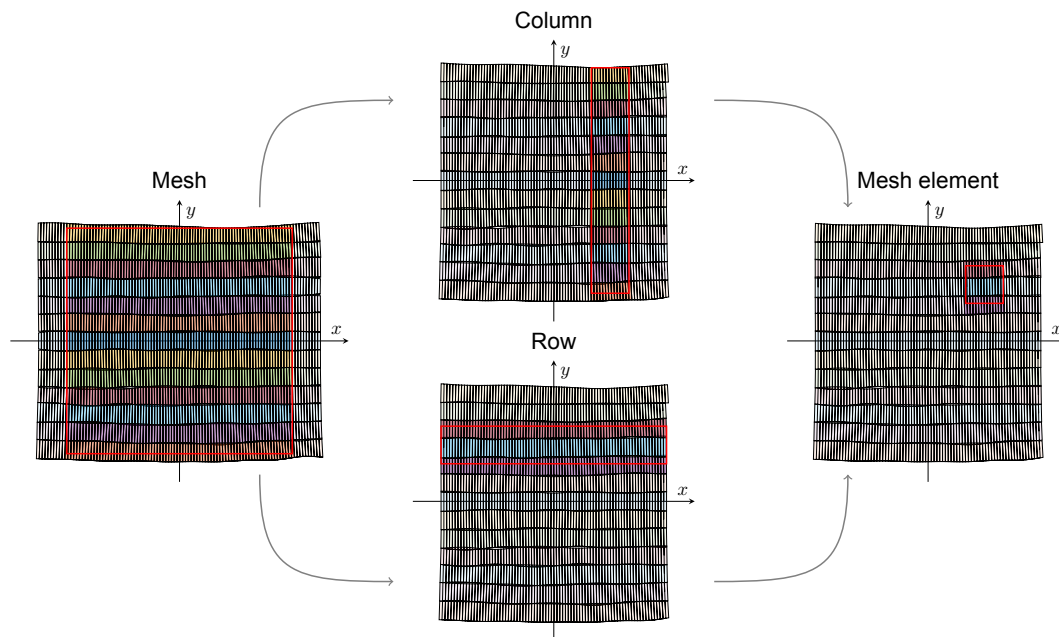


Figure 6.2: Determining which tow elements intersect with a certain mesh element

Currently, it is only known for each mesh element which tow elements intersect, but it is not yet known to what extent. How much a tow element intersects with a mesh element is determined next, together with whether the tow elements overlap. The process is visualised in Figure 6.3. On the left, the intersections are calculated. Then for each tow element, it is computed if and how much it overlaps with tow elements of the previous tow. In the centre of the figure, it can be seen that the overlaps are separated in a different layer from the material without overlaps. On the right, the properties of the two layers are calculated. The overlap layer has its thickness scaled according to the overlap area percentage. The material layer has its elastic properties scaled with the rule of mixtures. For both layers, the average fibre orientation is calculated individually. The whole process from the tow model to the laminate construction and the mapping of the tows to the mesh is done using a script presented in Appendix A.

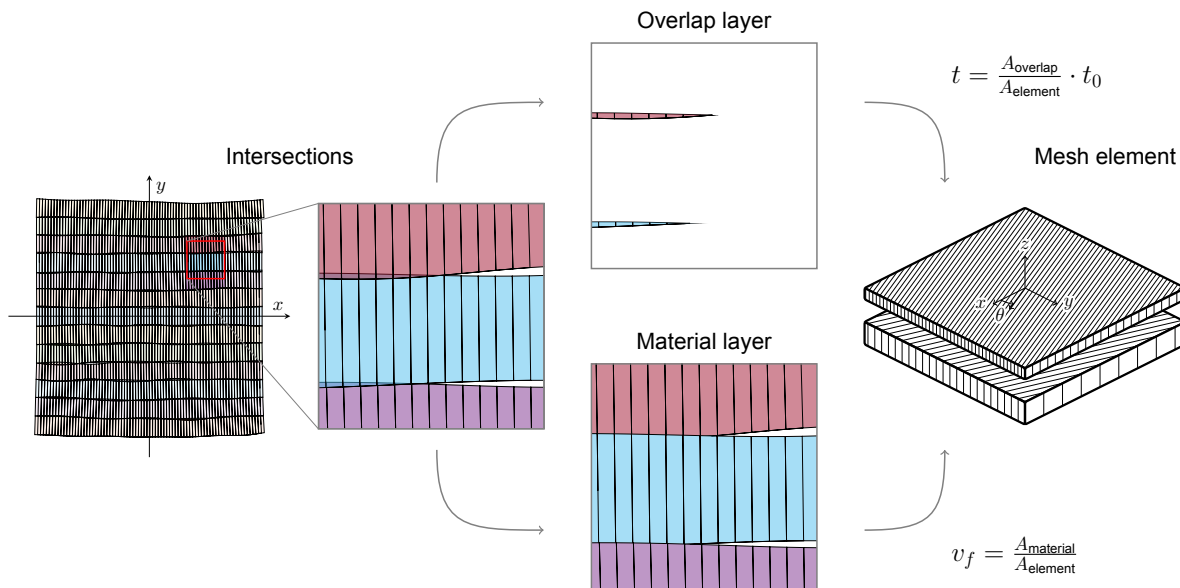


Figure 6.3: Separating into a material and overlap layer and scaling the properties

6.3. Analysis

With the laminate model mapped to the finite element mesh the analysis can finally be performed. This is done in two steps. First, the buckling analysis is performed which gives the buckling displacement. Secondly, the static analysis calculates the buckling load from which the effective stiffness can be derived. The material properties of the composite material are presented in Table 6.1 and of the matrix material in Table 6.2. The ply thickness t is set at 0.1 mm.

Table 6.1: Composite material properties carbon-reinforced epoxy (AS4/3501-6) [10]

Property	Symbol	Unit	Value
Density	ρ	g/cm ³	1.60
Longitudinal modulus	E_1	GPa	147
Transverse in-plane modulus	E_2	GPa	10.3
Transverse out-of-plane modulus	E_3	GPa	10.3
In-plane shear modulus	G_{12}	GPa	7.0
Out-of-plane shear modulus	G_{23}	GPa	3.7
Out-of-plane shear modulus	G_{13}	GPa	7.0
Major in-plane Poisson's ratio	ν_{12}		0.27
Out-of-plane Poisson's ratio	ν_{23}		0.54
Out-of-plane Poisson's ratio	ν_{13}		0.27

Table 6.2: Matrix material properties epoxy (3501-6) [10]

Property	Symbol	Unit	Value
Density	ρ	g/cm ³	1.27
Young's modulus	E_m	GPa	4.3
Shear modulus	G_m	GPa	1.6
Poisson's ratio	ν_m		0.35

In both cases the following boundary conditions are applied. All edges are fixed in the z -direction. This means the plate is simply supported. On the right edge, a displacement is applied. The left edge is also fixed in the x -direction to counter it. Its midpoint is fixed in the y -direction as well to anchor the plate in space.

In the buckling step, the right edge is under a unit displacement. A linear perturbation analysis is performed. The out-of-plane displacement of the first mode is displayed in Figure 6.4. The plate is shown from above where the displacement is plotted on the undeformed shape. The eigenvalue of the first mode gives the first buckling displacement of the laminate.

Figure 6.4 shows that the buckling shape is not completely symmetric, but is different in the two diagonal directions. This can be attributed to the fact that $+45^\circ$ and -45° plies are at different distances to the midplane. The further the distance, the stronger the contribution to the flexural stiffness.

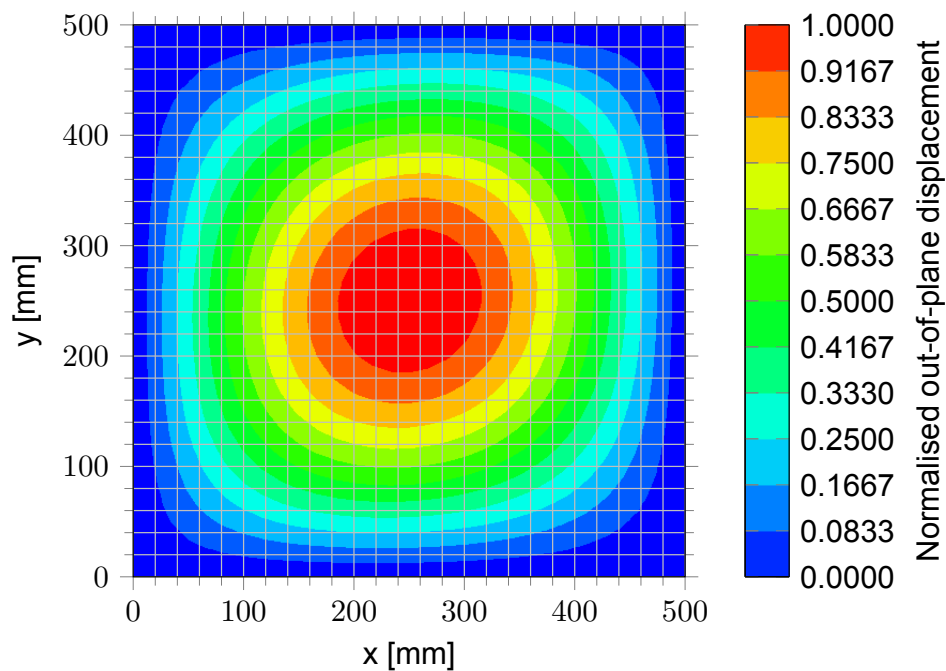


Figure 6.4: Buckling analysis

The buckling displacement is applied on the right edge of the plate in the second, static step. An example of a result of the static step is displayed in Figure 6.5 which shows the longitudinal displacement as a result of the compression. The static analysis also gives the reaction force at the nodes at the left edge. The sum of all the nodes gives the total reaction force as a result of the displacement which is the buckling load of the laminate.

Figure 6.5 does not show the asymmetry observed in the buckling analysis. This due to the fact that axial stiffness is of importance in the static load case which, in a symmetric layup, does not depend on the through-the-thickness location of plies.

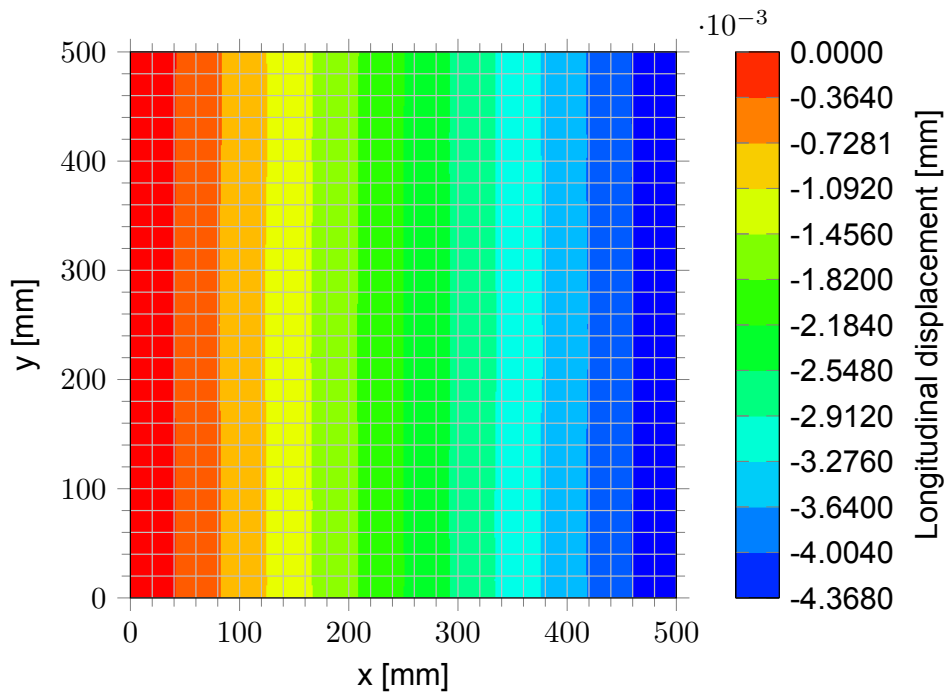


Figure 6.5: Static analysis

The buckling displacement is converted to strain by dividing by the plate length of 500 mm. The stress is calculated by dividing the buckling load by the cross-sectional area of the plate. Though the laminate thickness varies per configuration and differs per location, it is assumed to be constant with 8 plies of 0.1 mm. Multiplied with the plate width this gives a cross-sectional area of 400 mm². Eventually, the effective stiffness E_{eff} can be calculated by dividing the stress by the strain.

6.4. Results: structural performance

The results of the finite element analysis concerning the structural performance are summarised below. Five different comparisons are discussed.

The material uses in the analyses is described in Table 6.1 and 6.2. The tow width fluctuation can be found in Table 4.1. The smoothing and levelling for the local fibre steering use a ROC_{min} of 400 mm θ_{max} of 2° unless stated otherwise. The distance between tow centrelines for the conventional laminate is set at the mean tow width μ unless stated otherwise.

6.4.1. Cases

The first comparison includes four different cases. The first two are ideal which means there are no gaps or overlaps or any fibre angle deviation. The other two are the conventional laminate with its imperfections and a laminate where local fibre steering is applied. The results are summarised in Figure 6.6.

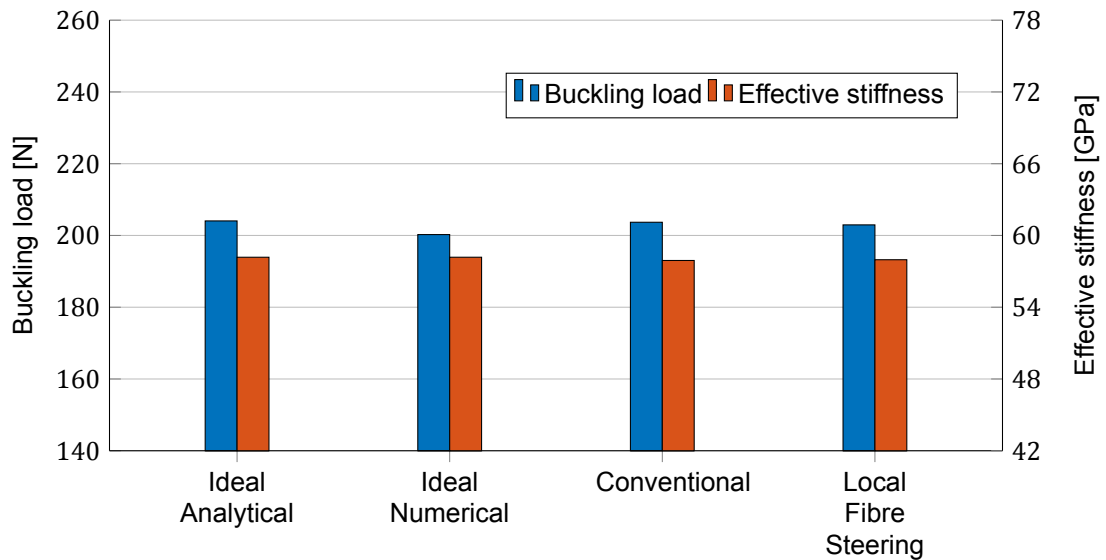


Figure 6.6: The structural performance for different cases

For the analytical case, similar to the numerical analysis, first the buckling load is calculated and then the effective stiffness. The buckling load of a square plate can be calculated using Equation 6.3 [52].

$$N_x = \frac{\pi^2}{a^2} (D_{11} + 2(D_{12} + 2D_{66}) + D_{22}) \quad (6.3)$$

Here, N_x is the buckling load per unit length. D_{ij} are bending or flexural laminate stiffnesses relating moments to curvatures. The latter can be calculated with Equation 6.4.

$$D_{ij} = \frac{1}{3} \sum_{k=1}^n Q_{ij}^k (z_k^3 - z_{k-1}^3) \quad (6.4)$$

Q_{ij} are the transformed stiffnesses of the k -th layer and z_k and z_{k-1} are the locations of its surfaces.

Classical laminate theory gives a general expression relating in-plane forces and moments to reference plane strains and curvatures as shown in Equation 6.5.

$$\begin{bmatrix} N \\ M \end{bmatrix} = \begin{bmatrix} A & B \\ B & D \end{bmatrix} \begin{bmatrix} \varepsilon^o \\ \kappa \end{bmatrix} \quad (6.5)$$

For a symmetric laminate ($B_{ij} = 0$) under axial compression ($N_y = N_s = 0$) the expression can be reduced to

$$\varepsilon^0 = [A]^{-1} \begin{bmatrix} -N_x \\ 0 \\ 0 \end{bmatrix} \quad (6.6)$$

The matrix constituent A_{ij} are the extensional stiffnesses, or in-plane laminate moduli, relating in-plane loads to in-plane strains, which can be calculated using Equation 6.7.

$$A_{ij} = \sum_{k=1}^n Q_{ij}^k (z_k - z_{k-1}) \quad (6.7)$$

Identical to the numerical cases, the effective stiffness E_{eff} can eventually be calculated using the buckling load and the strain.

Figure 6.6 shows a good agreement between the finite element method and the analytical solution. Local fibre steering is able to increase the effective stiffness, but the buckling load of the conventional method remains higher.

6.4.2. Coverage strategies

The second comparison covers different coverage strategies. In this context, it means the distance d between tow centrelines in the conventional laminate. A manufacturer can choose a different value for d in order to avoid the detrimental effects of gaps or the unpredictability of overlaps. The comparison includes seven different coverage strategies for the conventional laminate based on three heuristics commonly used in statistics, namely one, two, or three standard deviations from the mean. How these ranges are converted to different values of d has been explained in section 4.2. The results are shown in Figure 6.7 next to the standard local fibre steered laminate.

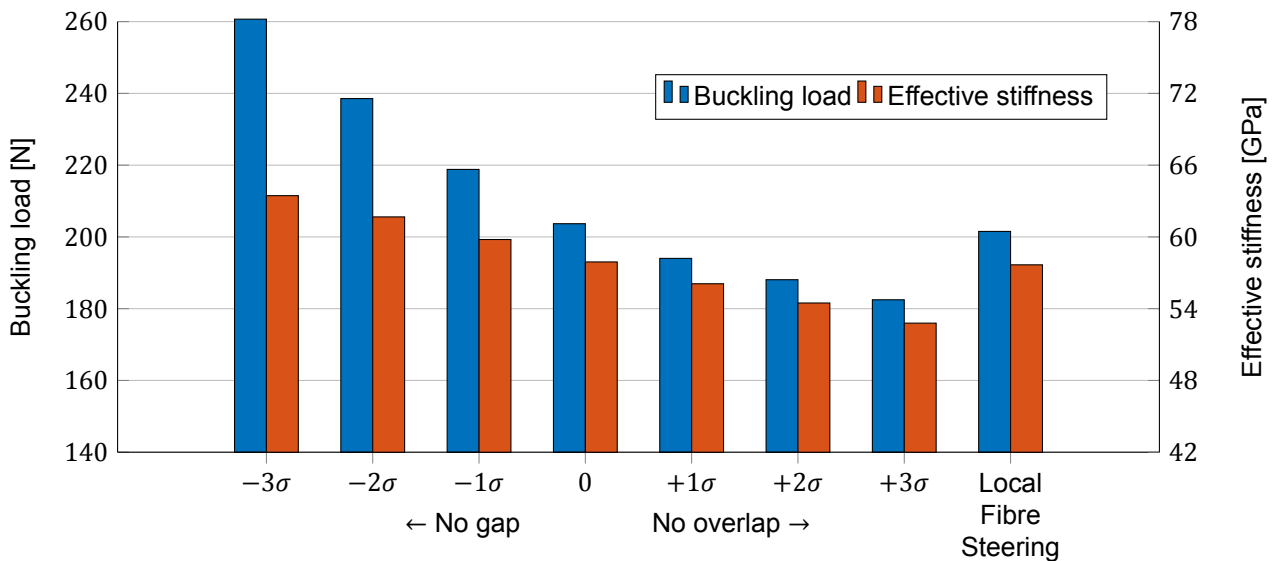


Figure 6.7: The effect of different coverage strategies on the structural performance

6.4.3. Layup

A quasi-isotropic and a cross-ply layup are compared. A cross-ply layup only contains fibre orientations 0° and 90° . The buckling load decreases with 19 % while the effective stiffness increases with 36 % for both methods.

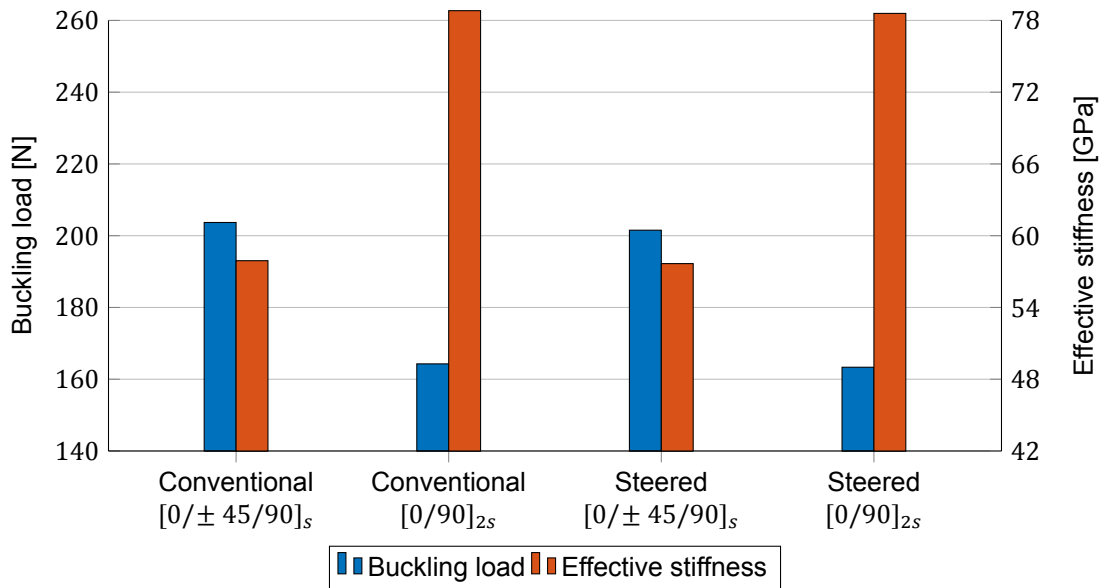


Figure 6.8: The effect of local fibre steering on a quasi-isotropic and a cross-ply layup

6.4.4. Maximum fibre angle

In this subsection, the different grades of levelling are compared to study the effect of the maximum fibre angle. The range displayed on the y-axis is about one per cent of the average value in contrast to 60 % in the other figures. The maximum fibre angle observed without levelling is about four degrees. This explains why levelling to 5° has no effect.

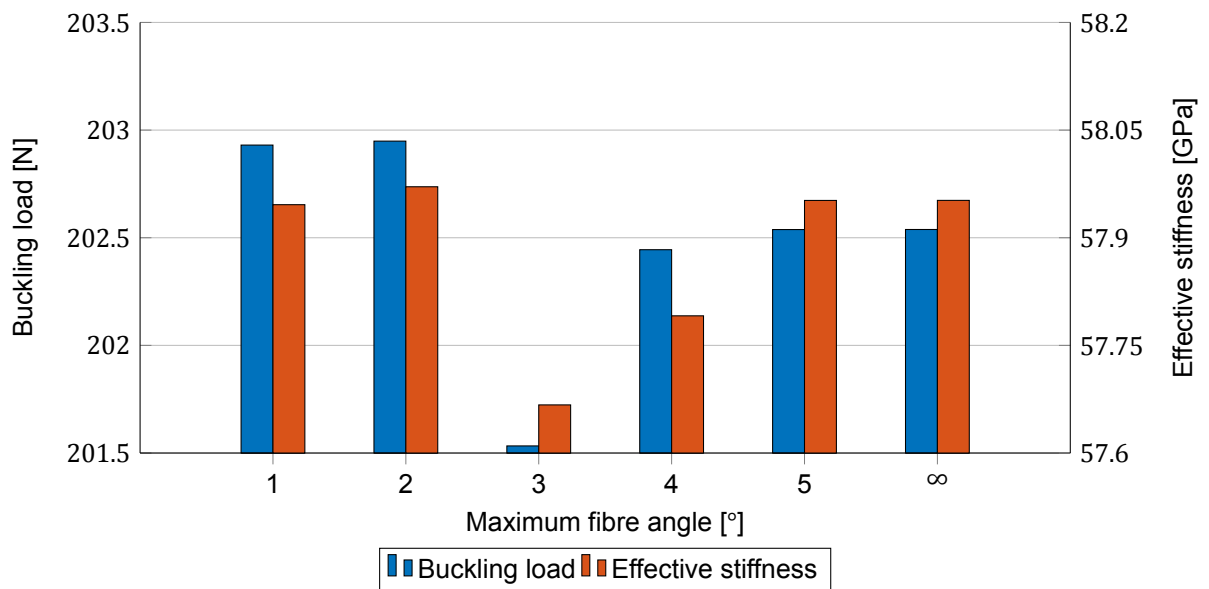


Figure 6.9: The effect of a maximum fibre angle on the structural performance ($ROC_{min} = 400$ mm)

6.4.5. Minimum radius of curvature

The range displayed again is about one percent of the average value. No levelling is applied because it is no requirement for the construction of a laminate. It also helps to show the effects of ROC_{min} separately.

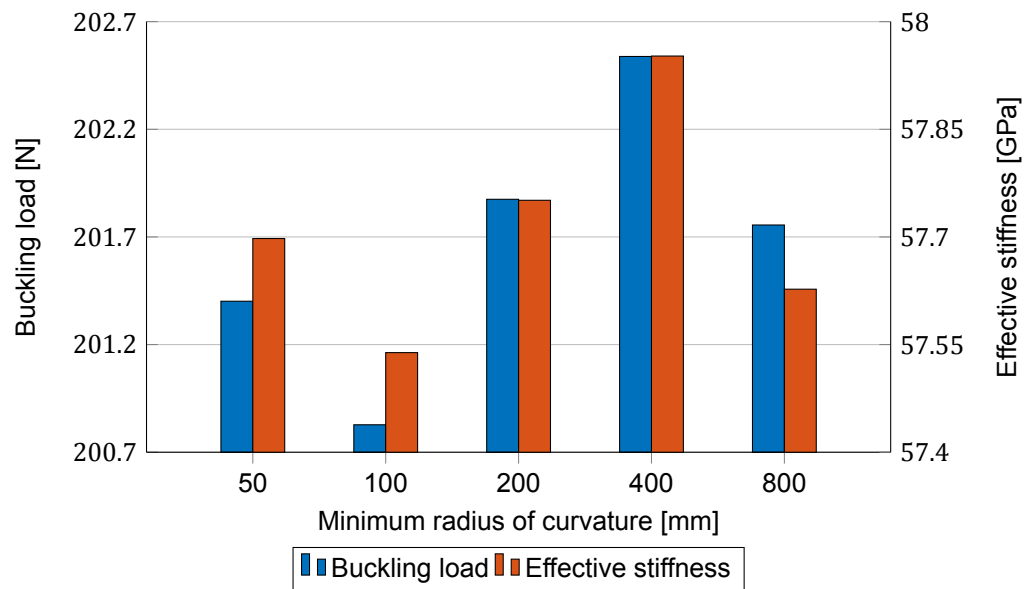


Figure 6.10: The effect of the minimum radius of curvature on the structural performance

6.4.6. Individual defect types

Previous results showed the effect of changing parameters, but they never showed the effects of gaps, overlaps and fibre angle deviation separately. Throughout the report, fibre angle deviation has been treated as a side effect of local fibre steering, but it could also be seen as a defect. In this subsection, the defect types are one by one excluded from the analysis. What this looks like is visualised in Figure 6.11. In the standard situation (a) the fibre angle of both the material layer as well as the overlap layer are calculated separately. The fibre content v_f is visualised by the density of the shading. In the second situation (b) the fibre angle deviation is set to zero and all fibre are aligned in the direction of the ply orientation. In the third situation (c) content of the material layer is reset to one. The last situation (d) the thickness of the overlap layer is set to zero. The results show the conventional laminate and the steered laminate smoothed to $ROC_{min} = 400$ mm and not levelled.

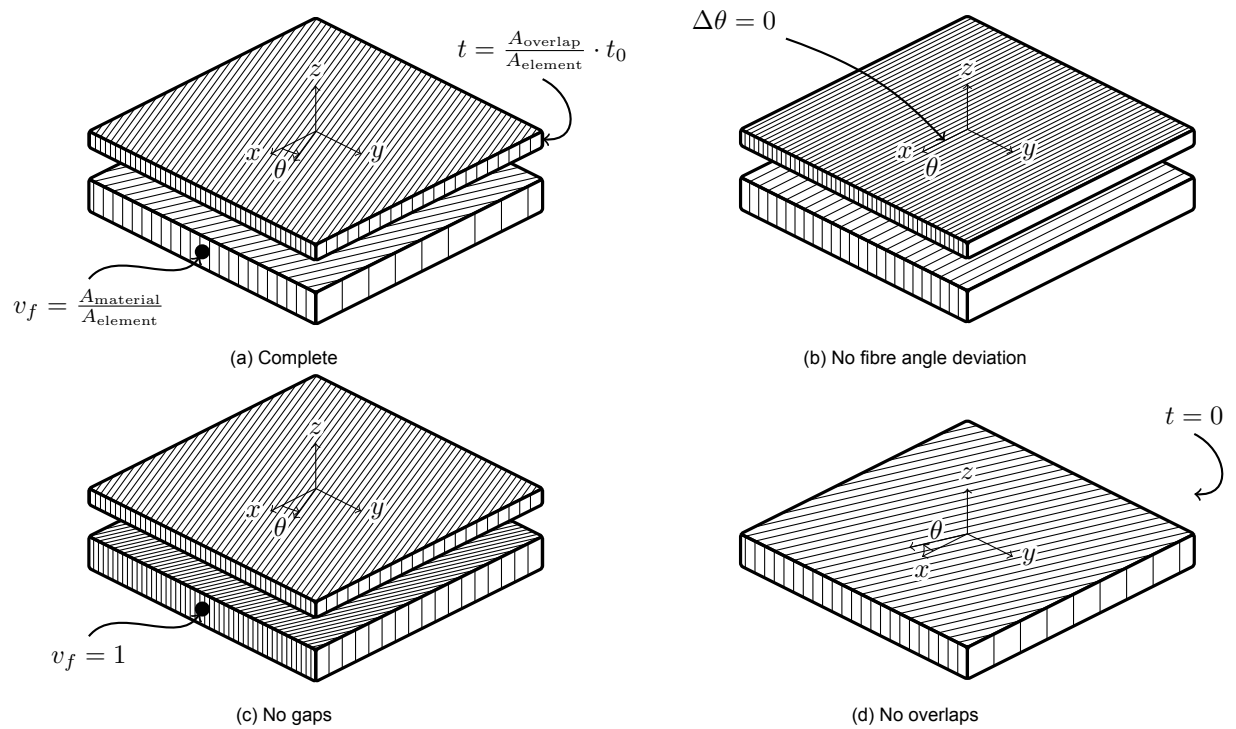


Figure 6.11: Mesh element with individual defect types excluded

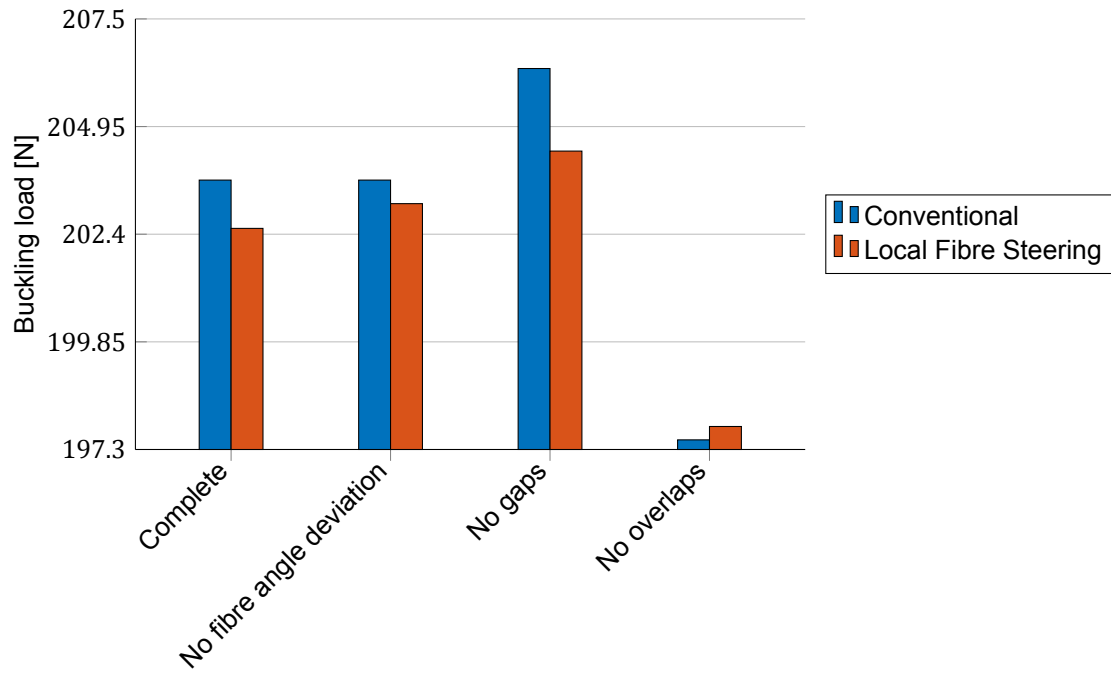


Figure 6.12: Individual defect types excluded in the calculation of the buckling load

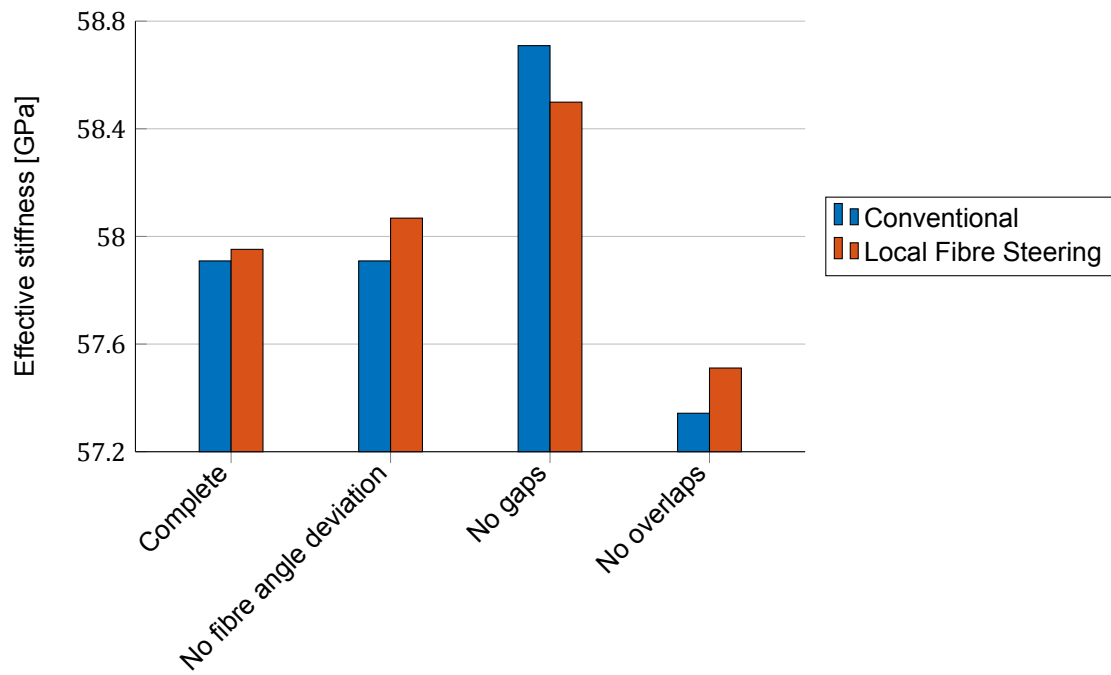


Figure 6.13: Individual defect types excluded in the calculation of the effective stiffness

7

Conclusion

In Chapter 3 the research question has been introduced: *How effective is local fibre steering in increasing the structural performance of composite laminates by reducing gaps and overlaps through compensating for tow width fluctuation in automated fibre placement?* To answer this, the research is divided into three sub-questions:

1. *To what extent can gaps and overlaps be reduced using local fibre steering?*
2. *What is the effect of the reduction in gaps and overlaps and the fibre angle deviation on the structural performance?*
3. *How accurate is the current understanding of tow width fluctuation?*

The answers to these sub-questions will be discussed in the following three sections: reduction of gaps and overlaps, structural performance, and tow width fluctuation.

7.1. Reduction of gaps and overlaps

To what extent local fibre steering can reduce is measured with the defect area percentage. An important conclusion to make is that local fibre steering is not able to eliminate gaps and overlaps completely. Instead, it only decreases the amount of gaps and overlaps, because it is limited by the minimum radius of curvature. The ROC_{min} was introduced as a theoretical limit to avoid cusps and self-intersections. To achieve this the minimal value is around 50 mm. However, in practice, the parameter is defined by the manufacturing process. In automated fibre placement, a typical value is 400 mm.

The defect area percentages resulting from the laminate model are shown in section 4.6. The DAP is indeed not reduced to zero, but at minimal smoothing and levelling it can be reduced from 1.84 % to 0.98 %. It means that the total amount of gaps and overlaps is reduced with 47 %. However, when the more practical minimum radius of curvature of 400 mm is used the DAP only goes down to 1.42 % of the laminate (–23 % relatively).

7.2. Structural performance

The effect of the reduction on structural performance has been analysed with a FEM model in Chapter 6. Two structural properties have been investigated: the buckling load and the effective stiffness. The following conclusions can be drawn.

Firstly, the finite element method of the ideal laminate is in good agreement with the analytical solution. Especially the numerical calculation of the effective stiffness is very accurate compared to the analytical result. Secondly, local fibre steering is able to achieve a higher E_{eff} by reducing the amount of defects. Despite being limited by the minimum radius of curvature, the gaps can be reduced sufficiently to increase the effective stiffness.

This is despite the induced fibre angle deviation. Figure 6.8 showed that the relative decrease of the buckling load and the effective stiffness when going from the quasi-isotropic layup $([0/\pm 45/90]_s)$ to a cross-ply layup $([0/90]_{2s})$ is equal for the conventional and the steered laminate. Figure 6.12 and

6.13 showed that positive effect of reducing gaps surpasses the negative effect of the induced fibre angle deviation.

The effects of varying the maximum fibre angle or the minimum radius of curvature are small compared to changing the layup or coverage strategy or excluding individual defect types. The maximum fibre angle and ROC_{min} limit the ability of local fibre steering to decrease the defect area percentage. There is, however, an optimum between the increase in performance due to the reduced defect area percentage and the decrease due to the fibre angle deviation. The respective optima according to Figure 6.9 and 6.10 are at a maximum angle of 2° and $ROC_{min} = 400$ mm.

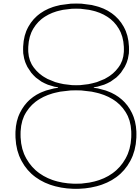
The conventional method has a higher buckling load than local fibre steering as can be seen in Figure 6.6. The buckling load depends on the flexural stiffness. The flexural stiffness is proportional to the thickness cubed. The effect is observed in Figure 6.7. The effective stiffness only linearly increases with distance d as more tows are necessary to cover the same plate width. Some manufacturers choose to increase the distance between tows to avoid overlaps. This comes at a cost as the amount of gaps is increased. Local fibre steering, however, can reduce the amount of overlaps without increasing the gap area percentage.

It is important to reflect on how well the buckling load and the effective represent the structural performance of a composite laminate. They only consider the mechanical properties of a laminate, but not the damage behaviour. Chapter 2 explained that the effect of gaps and overlaps is most seen in the compressive strength as they induce fibre waviness. Fibre waviness and damage behaviour, however, are not included in the model.

7.3. Tow width fluctuation

The initial values of the mean tow width and standard deviations come from literature as has been explained in section 4.1. Though a standard deviation of 4 % of the tow width was chosen, this was actually the lowest result from literature. Tolerances from other studies were up to 12 % of the mean tow width. The absolute standard deviation was expected to be 0.2540 mm for a 6.350 mm tow, while other studies indicated up to two and a half times the value. For the purpose of this research the course of the tow width fluctuation is important. Therefore a third parameter, spline node distance dl has been introduced which was assumed to be 10 mm.

Chapter 5 aimed to validate the assumptions by measuring the tow width fluctuations of two different materials. Both indicated that the standard deviation is in reality 0.4 %, five times smaller than expected. The value for dl was actually more than ten times lower than assumed. The data, however, showed many sudden shifts that are symptoms of a large source of error. Therefore, the data was smoothed using a moving average until it resembles more a normally distributed variable. After smoothing, the standard deviation was about ten times lower than was initially taken from literature. The spline node distance was calculated to be 1.9 mm. To conclude, the variation in tow width appears to be much smaller than literature indicated and the tow width fluctuation is much rougher than assumed.



Recommendations

The recommendations have been divided into two sections. The first section examines the possible improvements for the current assessment of local fibre steering. Making it better strengthens the current judgement on local fibre steering. The second section discusses the way forward. With the shown capabilities of local fibre steering, how could it be employed effectively?

8.1. Improve the current research

The improvements will be covered in the three aspects seen throughout the report. One is the construction of the laminates. The current model only considers individual tows with the goal to decrease gaps and overlaps as much as possible. However, the productivity in the manufacturing process is not taken into account. To harness the flexibility of the AFP process, but still achieve a sufficiently high productivity, tows are typically placed in courses. It is not completely clear how this will affect the laminate model. If tows cannot be steered individually this would simply decrease the ability to reduce gaps and overlaps. Furthermore, deviating from straight fibre paths causes lower deposition speeds to be achieved which ultimately affects the productivity. A future laminate model should consider productivity in order to more accurately examine the real costs of local fibre steering.

Another aspect is the analysis of the structural performance. The numerical analysis benefits from a higher number of elements to be used. The defect layer method divides the gaps and overlaps over the mesh element. By having smaller mesh elements the local effects of defects can be observed. An important change is to include more aspects of the structural performance. The current analysis only considers two mechanical properties: the buckling load and the effective stiffness. Chapter 2 showed that a significant effect of gaps and overlaps is the induced fibre waviness affecting the compressive strength. Reducing gaps and overlaps could decrease the fibre waviness and with it increase the compressive strength. Involving damage behaviour in the structural analysis will more accurately demonstrate the effects of local fibre steering.

Finally, there are a lot of ways the tow model can be improved. It was assumed that the tow width fluctuation is normally distributed. The current tow model validation focused on the values for the parameters in the tow model. Future work, however, should focus on whether the cubic spline accurately describes the actual tow material geometry. Research should not only measure more materials and other types of materials, such as thermoset but also consider the real tow geometry after manufacturing.

8.2. Improve local fibre steering

Local fibre steering is effective in decreasing gaps and overlaps and increasing (some aspects of) the structural performance. Nevertheless, it can still be improved. The ability of local fibre steering to reduce gaps and overlaps is limited by the minimum radius of curvature. It can be extended by either altering the automated fibre placement process to lower the required ROC_{min} or by improving the material quality so that tows have a smoother edge and the curvature accumulates slower. However, to know what would be the most profitable it is necessary to understand how tow width fluctuation is caused in the production of tow material.

Additionally, future work should put more emphasis on how to successfully employ local fibre steering. For now, the technologies required have been left out of the scope of research. Though this research covered more the theoretical side, ultimately the goal is to bring it into practice. Online tow width detection and tow path adjustment is something future work should be dedicated to. Fortunately, this could be combined with current trends in the aerospace industry. One trend has been introduced in Chapter 1: smart manufacturing. Smart manufacturing implies an interconnected supply chain and the sharing of data within the manufacturing process. More information about the variation in the tow material could, for example, come from the supplier. Another trend is the automation of inspection. Much of the manufacturing process in the aerospace industry has become automated, but inspection not so much [46]. Measurement of the tow width could not only be used for local fibre steering but also play a role in automated inspection to share the costs.

Bibliography

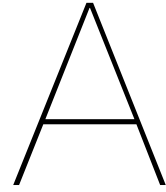
- [1] Holm Altenbach, Johannes Altenbach, and Wolfgang Kissing. *Mechanics of composite structural elements: Second edition*. 2018. ISBN 9789811089350. doi: 10.1007/978-981-10-8935-0.
- [2] A. Beakou, M. Cano, J.-B. Le Cam, and V. Verney. Modelling slit tape buckling during automated prepreg manufacturing: A local approach. *Composite Structures*, 93(10):2628–2635, 9 2011. ISSN 0263-8223. doi: 10.1016/J.COMPSTRUCT.2011.04.030. URL <https://www.sciencedirect.com/science/article/pii/S0263822311001541>.
- [3] Sylvie Béland. Neat Thermoplastic Resins Properties. In *High Performance Thermoplastic Resins and their Composites*, pages 3–52. William Andrew Publishing, Oxford, 1990. ISBN 978-0-8155-1278-3. doi: 10.1016/B978-0-8155-1278-3.50005-1. URL <http://www.sciencedirect.com/science/article/pii/B9780815512783500051>.
- [4] Andreas Björnsson, Marie Jonsson, Daniel Eklund, Jan Erik Lindbäck, and Mats Björkman. Getting to grips with automated prepreg handling. *Production Engineering*, 11(4-5):445–453, 10 2017. ISSN 0944-6524. doi: 10.1007/s11740-017-0763-2. URL <http://link.springer.com/10.1007/s11740-017-0763-2>.
- [5] Adriana W. Blom, Claudio S. Lopes, Peter J. Kromwijk, Zafer Gürdal, and P. P. Camanho. A theoretical model to study the influence of tow-drop areas on the stiffness and strength of variable-stiffness laminates. *Journal of Composite Materials*, 43(5):403–425, 2009. ISSN 00219983. doi: 10.1177/0021998308097675.
- [6] Adriana Willempje Blom. *Structural performance of fiber-placed, variable-stiffness composite conical and cylindrical shells*. PhD thesis, Delft University of Technology, 2010. URL <http://resolver.tudelft.nl/uuid:46f2e44b-1a68-44f8-9633-79490a54e087>.
- [7] Rick Burke, Adam Mussomeli, Stephen Laaper, Martin Hartigan, and Brenna Sniderman. The smart factory. *The smart factory*, page 24, 2017. URL <https://www2.deloitte.com/us/en/insights/focus/industry-4-0/smart-factory-connected-manufacturing.html>.
- [8] Coriolis Composites. Coriolis C1, 2019. URL <https://www.coriolis-composites.com/fiber-placement-machines/coriolis-c1/>.
- [9] Kaven Croft, Larry Lessard, Damiano Pasini, Mehdi Hojjati, Jihua Chen, and Ali Yousefpour. Experimental study of the effect of automated fiber placement induced defects on performance of composite laminates. *Composites Part A: Applied Science and Manufacturing*, 42(5):484–491, 5 2011. ISSN 1359-835X. doi: 10.1016/J.COMPOSITESA.2011.01.007. URL <https://www.sciencedirect.com/science/article/pii/S1359835X11000224>.
- [10] Isaac M. Daniel and Ori Ishai. *Engineering Mechanics of Composite Materials*. Oxford University Press, New York, second edition, 2006. ISBN 9780195150971. doi: 10.1016/s0261-3069(97)87195-6.
- [11] Don O. (Cincinnati Machine) Evans. Fiber Placement. In D.B. Miracle and S.L. Donaldson, editors, *ASM Handbook*, volume 21 - Compo, chapter 60, pages 477–479. ASM International, Materials Park, Ohio, first edition, 2001. doi: 10.1007/978-1-4615-6389-1_{ }23. URL <https://app.knovel.com/hotlink/toc/id:kpASMHVC13/asm-handbook-volume-21/asm-handbook-volume-21>.
- [12] Kazem Fayazbakhsh, Mahdi Arian Nik, Damiano Pasini, and Larry Lessard. Defect layer method to capture effect of gaps and overlaps in variable stiffness laminates made by Automated Fiber Placement. *Composite Structures*, 97:245–251, 3 2013. ISSN 0263-8223. doi: 10.1016/J.COMPSTRUCT.2012.10.031. URL <https://www.sciencedirect.com/science/article/pii/S0263822312005272>.

- [13] Carroll G. Grant and Vernon M. Benson. Automated fiber placement: Evolution and current demonstrations. *Third NASA Advanced Composites Technology Conference*, 1:625–648, 1 1993. URL <https://ntrs.nasa.gov/search.jsp?R=19950022411>.
- [14] M. B. Gruber, M. A. Lamontia, and B. J. Waibel. Automated fabrication processes for large composite aerospace structures: A trade study. In *International SAMPE Symposium and Exhibition*, volume 46 II, pages 1986–1997, Long Beach, CA, USA, 2001. URL <http://www.accudyne.com/wp-content/uploads/2016/02/Automated-Fabrication-Process-For-Large-Composite-Aerospace-Structures-A-Trade-Study.pdf>.
- [15] Z. Gürdal, B. F. Tatting, and C. K. Wu. Variable stiffness composite panels: Effects of stiffness variation on the in-plane and buckling response. *Composites Part A: Applied Science and Manufacturing*, 39(5):911–922, 2008. ISSN 1359835X. doi: 10.1016/j.compositesa.2007.11.015.
- [16] Zafer Gurdal, Brian Tatting, and K. Wu. Tow-Placement Technology and Fabrication Issues for Laminated Composite Structures. In *46th AIAA/ASME/ASCE/AHS/ASC Structures, Structural Dynamics and Materials Conference*, Reston, Virginia, 4 2005. American Institute of Aeronautics and Astronautics. ISBN 978-1-62410-065-9. doi: 10.2514/6.2005-2017. URL <http://arc.aiaa.org/doi/10.2514/6.2005-2017>.
- [17] Justin Hale. Boeing 787 from the ground up. *AERO Magazine*, (24):17–24, 2006. URL https://www.boeing.com/commercial/aeromagazine/articles/qtr_4_06/article_04_1.html.
- [18] Falk Heinecke and Christian Willberg. Manufacturing-Induced Imperfections in Composite Parts Manufactured via Automated Fiber Placement. *Journal of Composites Science*, 3(2):56, 6 2019. ISSN 2504-477X. doi: 10.3390/jcs3020056. URL <https://www.mdpi.com/2504-477X/3/2/56>.
- [19] Hexcel. HexTow AS4, 2020. URL https://www.hexcel.com/user_area/content_media/raw/AS4_HexTow_DataSheet.pdf.
- [20] H. M. Hsiao and I. M. Daniel. Effect of fiber waviness on stiffness and strength reduction of unidirectional composites under compressive loading. *Composites Science and Technology*, 56(5):581–593, 1996. ISSN 02663538. doi: 10.1016/0266-3538(96)00045-0.
- [21] A. Bruce Hulcher, Joseph M. Marchello, Jeffrey A. Hinkley, Norman J. Johnston, and Mark A. Lamontia. Dry Ribbon for Heated Head Automated Fiber Placement. Technical report, NASA Langley Research Center, Hampton, VA, 1 2000. URL <https://ntrs.nasa.gov/search.jsp?R=20040086973>.
- [22] Anthony Bruce Hulcher, David M. McGowan, Brian W. Grimsley, Norman J. Johnston, and Gail H. Gordon. Processing and Testing of Thermoplastic Composite Cylindrical Shells Fabricated by Automated Fiber Placement. In *International SAMPE Symposium and Exhibition*, volume 47 II, pages 1–15, Long Beach, CA, 5 2002. URL <https://ntrs.nasa.gov/search.jsp?R=20020046692>.
- [23] M. W. Hyer and H. H. Lee. The use of curvilinear fiber format to improve buckling resistance of composite plates with central circular holes. *Composite Structures*, 18(3):239–261, 1 1991. ISSN 02638223. doi: 10.1016/0263-8223(91)90035-W.
- [24] Hyoung Seok Kang, Ju Yeon Lee, Sangsu Choi, Hyun Kim, Jun Hee Park, Ji Yeon Son, Bo Hyun Kim, and Sang Do Noh. Smart manufacturing: Past research, present findings, and future directions. *International Journal of Precision Engineering and Manufacturing - Green Technology*, 3(1): 111–128, 2016. ISSN 21980810. doi: 10.1007/s40684-016-0015-5.
- [25] Byung Chul Kim, Kevin Potter, and Paul M. Weaver. Continuous tow shearing for manufacturing variable angle tow composites. *Composites Part A: Applied Science and Manufacturing*, 43(8): 1347–1356, 8 2012. ISSN 1359-835X. doi: 10.1016/J.COMPOSITESA.2012.02.024. URL <https://www.sciencedirect.com/science/article/pii/S1359835X12000929>.

- [26] Marine Lan, Denis Cartié, Peter Davies, and Christophe Baley. Microstructure and tensile properties of carbon–epoxy laminates produced by automated fibre placement: Influence of a caul plate on the effects of gap and overlap embedded defects. *Composites Part A: Applied Science and Manufacturing*, 78:124–134, 11 2015. ISSN 1359-835X. doi: 10.1016/J.COMPOSITESA.2015.07.023. URL <https://www.sciencedirect.com/science/article/pii/S1359835X15002559>.
- [27] Marine Lan, Denis Cartié, Peter Davies, and Christophe Baley. Influence of embedded gap and overlap fiber placement defects on the microstructure and shear and compression properties of carbon-epoxy laminates. *Composites Part A: Applied Science and Manufacturing*, 82:198–207, 2016. ISSN 1359835X. doi: 10.1016/j.compositesa.2015.12.007. URL <http://dx.doi.org/10.1016/j.compositesa.2015.12.007>.
- [28] Xiangqian Li, Stephen R. Hallett, and Michael R. Wisnom. Modelling the effect of gaps and overlaps in automated fibre placement (AFP)-manufactured laminates. *Science and Engineering of Composite Materials*, 22(2):115–129, 2015. ISSN 0334181X. doi: 10.1515/secm-2013-0322.
- [29] C. S. Lopes. *Damage and Failure of Non-Conventional Composite Laminates*. PhD thesis, Delft University of Technology, 2009.
- [30] C. S. Lopes, P. P. Camanho, Z. Gürdal, and B. F. Tatting. Progressive failure analysis of tow-placed, variable-stiffness composite panels. *International Journal of Solids and Structures*, 44(25-26):8493–8516, 12 2007. ISSN 00207683. doi: 10.1016/j.ijsolstr.2007.06.029.
- [31] C. S. Lopes, Z. Gürdal, and P. P. Camanho. Variable-stiffness composite panels: Buckling and first-ply failure improvements over straight-fibre laminates. *Computers and Structures*, 86(9):897–907, 2008. ISSN 00457949. doi: 10.1016/j.compstruc.2007.04.016.
- [32] Gustavo Gonzalez Lozano, Ashutosh Tiwari, Christopher Turner, and Simon Astwood. A review on design for manufacture of variable stiffness composite laminates. *Proceedings of the Institution of Mechanical Engineers, Part B: Journal of Engineering Manufacture*, 230(6):981–992, 2016. ISSN 20412975. doi: 10.1177/0954405415600012.
- [33] Dirk H.-J.A. Lukaszewicz, Carwyn Ward, and Kevin D. Potter. The engineering aspects of automated prepreg layup: History, present and future. *Composites Part B: Engineering*, 43(3):997–1009, 4 2012. ISSN 1359-8368. doi: 10.1016/J.COMPOSITESB.2011.12.003. URL <https://www.sciencedirect.com/science/article/pii/S1359836811005452>.
- [34] Aymen Marouene, Pierre Legay, and Rachid Boukhili. Experimental and numerical investigation on the open-hole compressive strength of AFP composites containing gaps and overlaps. *Journal of Composite Materials*, 51(26):3631–3646, 2017. ISSN 1530793X. doi: 10.1177/0021998317690917.
- [35] MTorres. Automated Tape Layer machine | Torreslayup, 2019. URL <https://www.mtorres.es/en/aeronautics/products/carbon-fiber/torreslayup>.
- [36] MTorres. Automated fiber placement machine | Torresfiberlayup, 2019. URL <https://www.mtorres.es/en/aeronautics/products/carbon-fiber/torresfiberlayup>.
- [37] National Institute of Standards and Technology. Product Definitions for Smart Manufacturing, 2018. URL <https://www.nist.gov/programs-projects/product-definitions-smart-manufacturing>.
- [38] Daniël Maria Jozef Peeters. *Design Optimisation of Practical Variable Stiffness and Thickness Laminates*. PhD thesis, Delft University of Technology, 2017.
- [39] M. Perner, S. Algermissen, R. Keimer, and H.P. Monner. Avoiding defects in manufacturing processes: A review for automated CFRP production. *Robotics and Computer-Integrated Manufacturing*, 38:82–92, 4 2016. ISSN 0736-5845. doi: 10.1016/J.RCIM.2015.10.008. URL <https://www.sciencedirect.com/science/article/pii/S0736584515001209>.

- [40] Mohammad Rakhshbahar and Michael Sinapius. A Novel Approach: Combination of Automated Fiber Placement (AFP) and Additive Layer Manufacturing (ALM). *Journal of Composites Science*, 2(3):42, 7 2018. ISSN 2504-477X. doi: 10.3390/jcs2030042. URL <http://www.mdpi.com/2504-477X/2/3/42>.
- [41] Suranjan Roychowdhury and Suresh G. Advani. An experimental investigation of consolidation in thermoplastic filament winding. *Composites Manufacturing*, 2(2):97–104, 1 1991. ISSN 0956-7143. doi: 10.1016/0956-7143(91)90186-K. URL <https://www.sciencedirect.com/science/article/pii/095671439190186K>.
- [42] A J Sawicki and P J Minguet. The Effect of Intraply Overlaps and Gaps Upon the Compression Strength of Composite Laminates. In *39th AIAA/ASME/ASCE/AHS/ASC Structures, Structural Dynamics, and Materials Conference and Exhibit*, pages 744–754, Long Beach, CA, 1998. American Institute of Aeronautics and Astronautics. doi: 10.2514/6.1998-1786. URL <https://doi.org/10.2514/6.1998-1786>.
- [43] Shahriar Setoodeh, Mostafa M. Abdalla, Samuel T. IJsselmuiden, and Zafer Gürdal. Design of variable-stiffness composite panels for maximum buckling load. *Composite Structures*, 87(1): 109–117, 2009. ISSN 02638223. doi: 10.1016/j.compstruct.2008.01.008.
- [44] Brian F. Tatting and Zafer Gürdal. Design and Manufacture of Elastically Tailored Tow Placed Plates. Technical report, National Aeronautics and Space Administration, Hampton, Virginia, 8 2002. URL <https://ntrs.nasa.gov/search.jsp?R=20020073162>.
- [45] Brian F. Tatting and Zafer Gürdal. Automated Finite Element Analysis of Elastically-Tailored Plates. *Nasa/Cr-2003-212679*, 12 2003. URL <https://ntrs.nasa.gov/search.jsp?R=20040031675>.
- [46] A. Tiwari, K. Vergidis, R. Lloyd, and J. Cushen. Automated inspection using database technology within the aerospace industry. *Proceedings of the Institution of Mechanical Engineers, Part B: Journal of Engineering Manufacture*, 222(2):175–183, 2008. ISSN 09544054. doi: 10.1243/09544054JEM938.
- [47] Toray Advanced Composites. Toray Cetex TC1320 PEKK, 2019. URL https://www.toraytac.com/media/409dcc72-6aff-4643-86b8-20b5f464f038/LVmlmQ/TAC/Documents/Data_sheets/Thermoplastic/UDtapes, prepregsandlaminates/Toray-Cetex-TC1320_PEKK_PDS.pdf.
- [48] Luke Everett Turoski. *Effects of Manufacturing Defects on the Strength of Toughened Carbon/Epoxy Prepreg Composites*. PhD thesis, Montana State University, 2000. URL <https://scholarworks.montana.edu/xmlui/handle/1/8007>.
- [49] United States Department of Defense. *Composite Materials Handbook, MIL-HDBK-17-3F, Polymer Matrix Composites - Materials Usage, Design, and Analysis (CMH-17)*, volume Volume 3. 2002. ISBN 9781566768269. URL <https://app.knovel.com/hotlink/toc/id:kpMHMILH43/military-handbook-mil-3/military-handbook-mil-3>.
- [50] Saurabh Vaidya, Prashant Ambad, and Santosh Bhosle. Industry 4.0 - A Glimpse. *Procedia Manufacturing*, 20:233–238, 2018. ISSN 23519789. doi: 10.1016/j.promfg.2018.02.034.
- [51] George Vosselman and Hans-Gerd Maas. *Airborne and Terrestrial Laser Scanning*, 2010.
- [52] James M. Whitney. *Structural Analysis of Laminated Composites*. Technomic Publishing Company, Lancaster, Pennsylvania, 1987. ISBN 0877625182.
- [53] Wilhelm Woigk, Stephen R. Hallett, Mike I. Jones, Moritz Kultz, Andreas Hornig, and Maik Gude. Experimental investigation of the effect of defects in Automated Fibre Placement produced composite laminates. *Composite Structures*, 201:1004–1017, 10 2018. ISSN 02638223. doi: 10.1016/j.compstruct.2018.06.078. URL <https://www.sciencedirect.com/science/article/pii/S0263822317339946?via%3Dihub>.

- [54] K. Chauncey Wu, Zafer Gürdal, and James H. Starnes. Structural Response of Compression-Loaded, Tow-Placed, Variable Stiffness Panels. In *43rd AIAA/ASME/ASCE/AHS/ASC Structures, Structural Dynamics and Materials Conference*, Denver, Colorado, 2002. American Institute of Aeronautics and Astronautics (AIAA). doi: <https://doi.org/10.2514/6.2002-1512>.



MATLAB code

```
1 %% Layup
2 t = [0 45 -45 90]; % Ply orientation [deg]
3 t = [t flip(t)];
4 t = deg2rad(t);
5 n_k = length(t); % Number of plies
6
7 %% Load tow
8 tow_type = 'spline';
9 tow_name = 'tow_material_20200925_110354';
10
11 f = loadTow(tow_name, tow_type);
12
13 if strcmp(tow_type, 'spline')
14     Mu = mean(f.coefs(:,4)); % Mean tow width [mm]
15     Si = std(f.coefs(:,4)); % Standard deviation [mm]
16 elseif strcmp(tow_type, 'data')
17     Mu = mean(f.Width);
18     Si = std(f.Width);
19 end
20
21 %% Dimensions
22 a = 500; % Plate width [mm]
23 b = 500; % Plate length [mm]
24 da = 1.05;
25 db = 1.05;
26
27 l = da*a*cos(abs(t))+db*b*sin(abs(t)); % Tow length [mm]
28 n = ceil((da*a*sin(abs(t))+db*b*cos(abs(t)))/Mu); % Number of tows
29 n(mod(n,2) == 0) = n(mod(n,2) == 0) + 1;
30
31 %% Mesh
32 m_ = 30; % Number of mesh columns
33 n_ = 30; % Number of mesh rows
34 x_ = linspace(-a/2, a/2, m_+1); % Mesh element coordinates [mm]
35 y_ = linspace(-b/2, b/2, n_+1);
36 mesh = polyshape([x_(1) x_(end) x_(end) x_(1)], [y_(1) y_(1) y_(end) y_(end)
    ]]);
37 mesh_column = polyshape.empty(0, m_);
38 for i_ = 1:m_
```

```

39     mesh_column(i_) = polyshape([x_(i_) x_(i_+1) x_(i_+1) x_(i_)],[y_(1)
        y_(1) y_(end) y_(end)]);
40 end
41 mesh_row = polyshape.empty(0,n_);
42 for j_ = 1:n_
43     mesh_row(j_) = polyshape([x_(1) x_(end) x_(end) x_(1)],[y_(j_) y_(j_)
        y_(j_+1) y_(j_+1)]);
44 end
45 mesh_element = polyshape.empty(m_,0);
46 for i_ = 1:m_
47     for j_ = 1:n_
48         mesh_element(i_,j_) = polyshape([x_(i_) x_(i_+1) x_(i_+1) x_(i_)
            ],[y_(j_) y_(j_) y_(j_+1) y_(j_+1)]);
49     end
50 end
51
52 VariableNames = { 'i', 'j', 'k', 'p', 'E1', 'E2', 'v12', 'G12', 'G13', 'G23', '
    thickness', 'orientAngle' };
53 T = array2table(zeros(0,12), 'VariableNames', VariableNames);
54
55 %% Material
56 % Carbon/Epoxy AS4/3501-6 % Composite material
57 h0 = 0.1e-3; % Ply thickness [mm]
58 pc = 1.60E3; % Density [g/mm3]
59 E1c = 147E9; % Longitudinal stiffness modulus [Pa]
60 E2c = 10.3E9; % Transverse in-plane stiffness modulus [Pa]
61 v12c = 0.27; % Poisson's ratio
62 G12c = 7.0E9; % In-plane shear modulus [Pa]
63 G13c = 7.0E9; % Out-of-plane shear modulus [Pa]
64 G23c = 3.7E9; % Out-of-plane shear modulus [Pa]
65
66 % Epoxy 3501-6 % Matrix material
67 pm = 1.27E3; % Density [g/mm3]
68 Em = 4.3E9; % Stiffness modulus [Pa]
69 Gm = 1.60E9; % Shear modulus [Pa]
70 vm = 0.35;
71
72 %% Generate tow
73 % Mu = 6.350;
74 % Si = 0.2540;
75 % dl = 10; % Spline node distance [mm]
76
77 % f = generateTow(Mu, Si, dl, 2*n_*l*n_k);
78 % saveTow(f)
79
80 %% Parameters
81 % Model
82 dx0 = 1; % Step size [mm]
83 s0 = 0; % Starting position at tow [mm]
84 m = floor(l/dx0)+1; % Number of points per tow
85
86 % Smoothing and levelling
87 pa0 = 1; % Initial value levelling parameter
88 dpa = 0.01; % Step change levelling parameters
89 maxAngle = deg2rad(lmf); % Maximum fibre angle deviation (rad)
90 pk0 = 1; % Initial value smoothing parameter

```

```

91 cpk = 0.99; % Coefficient change smoothing parameter
92 minROC = 50; % Minimum radius of curvature [mm]
93
94 wb = waitbar(0, 'Please wait... ');
95 %% Loop
96 for k = 1:n_k
97     %% Initial tow
98     x = zeros(m(k),n(k));
99     x(:,1) = -l(k)/2:dx0:l(k)/2;
100    y = zeros(m(k),n(k));
101    y0 = y;
102
103    dx = zeros(m(k),n(k));
104    dx(1:m(k),1) = dx0;
105    dy = zeros(m(k),n(k));
106    ddx = zeros(m(k),n(k));
107    ddy = zeros(m(k),n(k));
108
109    ds = dx;
110    dydx = zeros(m(k),n(k)); % Fibre angle deviation [rad]
111    ddyddx = zeros(m(k),n(k)); % Tow path curvature [1/mm]
112    r = zeros(m(k),n(k)); % Radius of curvature [mm]
113    r(1:m(k),1) = Inf;
114
115    pa = ones(n(k)); % Levelling parameter
116    pk = ones(n(k)); % Smoothing parameter
117
118    s = zeros(m(k),n(k)); % Location along tow [mm]
119    d = zeros(m(k),n(k)); % Half tow width [mm]
120
121    s(:,1) = x(:,1)-x(1,1)+s0;
122    d(:,1) = evaluateTow(s(:,1),f,tow_type)/2;
123
124    %% Loop
125    for j = 2:n(k)
126        %% Parallel curve construction
127        s(1,j) = s(end,j-1);
128        for i = 1:m(k)
129            d(i,j) = evaluateTow(s(i,j),f,tow_type)/2;
130            if j == 2
131                x(i,j) = x(i,j-1) - (d(i,j)+d(i,j-1))*dy(i,j-1)/sqrt(dx(i,
132                    j-1)^2+dy(i,j-1)^2);
133                y(i,j) = y(i,j-1) + (d(i,j)+d(i,j-1))*dx(i,j-1)/sqrt(dx(i,
134                    j-1)^2+dy(i,j-1)^2);
135            elseif rem(j,2) == 0
136                x(i,j) = x(i,j-2) - (d(i,j)+d(i,j-2))*dy(i,j-2)/sqrt(dx(i,
137                    j-2)^2+dy(i,j-2)^2);
138                y(i,j) = y(i,j-2) + (d(i,j)+d(i,j-2))*dx(i,j-2)/sqrt(dx(i,
139                    j-2)^2+dy(i,j-2)^2);
140            else
141                x(i,j) = x(i,j-2) + (d(i,j)+d(i,j-2))*dy(i,j-2)/sqrt(dx(i,
142                    j-2)^2+dy(i,j-2)^2);
143                y(i,j) = y(i,j-2) - (d(i,j)+d(i,j-2))*dx(i,j-2)/sqrt(dx(i,
144                    j-2)^2+dy(i,j-2)^2);
145            end
146            if i == 1 && j == 2

```

```

141         dx(i, j) = dx(i, j-1);
142         dy(i, j) = dy(i, j-1);
143     elseif i == 1 && j > 2
144         dx(i, j) = dx(i, j-2);
145         dy(i, j) = dy(i, j-2);
146     else
147         dx(i, j) = x(i, j) - x(i-1, j);
148         dy(i, j) = y(i, j) - y(i-1, j);
149     end
150     if i ~= m(k)
151         ds(i, j) = sqrt(dx(i, j)^2+dy(i, j)^2);
152         s(i+1, j) = s(i, j) + ds(i, j);
153     end
154 end
155
156 %% Smoothing and levelling
157 for i = 1:m(k)
158     if i == 1
159         dx(i, j) = x(i+1, j)-x(i, j);
160         ddx(i, j) = x(i+2, j)-2*x(i+1, j)+x(i, j);
161     elseif i == m(k)
162         dx(i, j) = x(i, j)-x(i-1, j);
163         ddx(i, j) = x(i, j)-2*x(i-1, j)+x(i-2, j);
164     else
165         dx(i, j) = (x(i+1, j)-x(i-1, j))/2;
166         ddx(i, j) = x(i+1, j)-2*x(i, j)+x(i-1, j);
167     end
168 end
169
170 %% Smoothing
171 pk(j) = pk0;
172 smooth = false;
173 y0(:, j) = y(:, j);
174 while ~smooth
175     y(:, j) = csaps(x(:, j), y0(:, j), pk(j), x(:, j));
176     for i = 1:m(k)
177         if i == 1
178             dy(i, j) = y(i+1, j)-y(i, j);
179             ddy(i, j) = y(i+2, j)-2*y(i+1, j)+y(i, j);
180         elseif i == m(k)
181             dy(i, j) = y(i, j)-y(i-1, j);
182             ddy(i, j) = y(i, j)-2*y(i-1, j)+y(i-2, j);
183         else
184             dy(i, j) = (y(i+1, j)-y(i-1, j))/2;
185             ddy(i, j) = y(i+1, j)-2*y(i, j)+y(i-1, j);
186         end
187         ddyddx(i, j) = (dx(i, j)*ddy(i, j)-dy(i, j)*ddx(i, j))/((dx(i, j)
188             )^2+dy(i, j)^2)^(3/2));
189         r(i, j) = 1/ddyddx(i, j);
190     end
191     if min(abs(r(:, j))) < minROC
192         pk(j) = pk(j) * cpk;
193     else
194         smooth = true;
195     end
196 end

```

```

196
197 %% Levelling
198 pa(j) = pa0;
199 level = false;
200 y0(:,j) = y(:,j);
201 while ~level
202     y(:,j) = (1-pa(j))*mean(y0(:,j))+pa(j)*y0(:,j);
203     for i = 1:m(k)
204         if i == 1
205             dy(i,j) = y(i+1,j)-y(i,j);
206         elseif i == m(k)
207             dy(i,j) = y(i,j)-y(i-1,j);
208         else
209             dy(i,j) = (y(i+1,j)-y(i-1,j))/2;
210         end
211         dydx(i,j) = atan2(dy(i,j),dx(i,j));
212     end
213     if max(abs(dydx(:,j))) > maxAngle
214         pa(j) = pa(j) - dpa;
215     else
216         level = true;
217     end
218 end
219 waitbar(j/n(k),wb,['Constructing tows ... (',num2str(k),'/',num2str
220 (n_k),')']);
221
222 end
223
224 s0 = s(end);
225
226 %% Tow edges
227 xl = x + d.*dy./sqrt(dx.^2+dy.^2);
228 yl = y - d.*dx./sqrt(dx.^2+dy.^2);
229 xu = x - d.*dy./sqrt(dx.^2+dy.^2);
230 yu = y + d.*dx./sqrt(dx.^2+dy.^2);
231
232 %% Transformation of tow paths
233 u = x*cos(t(k)) - y*sin(t(k));
234 v = x*sin(t(k)) + y*cos(t(k));
235 ul = xl*cos(t(k)) - yl*sin(t(k));
236 vl = xl*sin(t(k)) + yl*cos(t(k));
237 uu = xu*cos(t(k)) - yu*sin(t(k));
238 vu = xu*sin(t(k)) + yu*cos(t(k));
239
240 %% Tow elements
241 tow_element = polyshape.empty(m(k)-1,0); % Tow element geometry
242 o = zeros(m(k),n(k)); % Tow element orientation
243 [rad]
244 for i = 1:m(k)-1
245     for j = 1:n(k)
246         tow_element(i,j) = polyshape([ul(i,j) ul(i+1,j) uu(i+1,j) uu(i
247             ,j)],[vl(i,j) vl(i+1,j) vu(i+1,j) vu(i,j)]);
248         o(i,j) = atan2(v(i+1,j)-v(i,j),u(i+1,j)-u(i,j));
249         waitbar((i-1+j/n(k))/(m(k)-1),wb,['Generating tow elements ...
250             (',num2str(k),'/',num2str(n_k),')']);
251     end
252 end
253 end

```

```

248
249 %% Trim edges
250 waitbar(0,wb,['Trimming edges... (',num2str(k),'/',num2str(n_k),'')]);
251 M0 = overlaps(tow_element,mesh);
252 M = repmat(M0,[1 1 m_ n_]);
253 waitbar(1,wb,['Trimming edges... (',num2str(k),'/',num2str(n_k),'')']);
254
255 %% Mesh columns
256 for i_ = 1:m_
257     ij = find(M0);
258     TF = ~overlaps(tow_element(ij),mesh_column(i_));
259     [i,j] = ind2sub([m(k)-1,n(k)],ij(TF));
260     M(sub2ind(size(M),repmat(i,n_,1),repmat(j,n_,1),repelem(i_,n_*
        length(i),1),repelem(1:n_,1,length(i)).')) = false;
261     waitbar(i_/m_,wb,['Mapping to mesh columns... (',num2str(k),'/',
        num2str(n_k),'')']);
262 end
263
264 %% Mesh rows
265 for j_ = 1:n_
266     ij = find(M0);
267     TF = ~overlaps(tow_element(ij),mesh_row(j_));
268     [i,j] = ind2sub([m(k)-1,n(k)],ij(TF));
269     M(sub2ind(size(M),repmat(i,m_,1),repmat(j,m_,1),repelem(1:m_,1,
        length(i)).',repelem(j_,m_*length(i),1))) = false;
270     waitbar(j_/n_,wb,['Mapping to mesh row... (',num2str(k),'/',
        num2str(n_k),'')']);
271 end
272
273 %% Material layer
274 material = repmat({polyshape.empty},m_,n_,n(k));
275 o_material = repmat({[]},m_,n_,n(k));
276 for i_ = 1:m_
277     for j_ = 1:n_
278         ij = find(M(:, :, i_, j_));
279         P = intersect(tow_element(ij),mesh_element(i_,j_));
280         o_ = o(ij);
281         [~,ij2j] = ind2sub([m(k)-1,n],ij);
282         for j = unique(ij2j).'.
283             material{i_,j_,j} = [material{i_,j_,j} P(ij2j == j & P.
                area > 0)];
284             o_material{i_,j_,j} = [o_material{i_,j_,j} o_(ij2j == j &
                P.area > 0)];
285         end
286         waitbar((i_-1+j_/n_)/m_,wb,['Mapping to mesh elements... (',
            num2str(k),'/',num2str(n_k),'')']);
287     end
288 end
289
290 %% Overlap layer
291 overlap = repmat({polyshape.empty},m_,n_,n(k)-1);
292 o_overlap = repmat({[]},m_,n_,n(k)-1);
293 material_minus = material;
294 for i_ = 1:m_
295     for j_ = 1:n_
296         for j1 = 2:n(k)

```

```

297         if j1 == 2
298             j2 = j1 - 1;
299         elseif j1 > 2
300             j2 = j1 - 2;
301         end
302         for i = 1:length(material{i_ ,j_ ,j2})
303             P = intersect(material{i_ ,j_ ,j1},material{i_ ,j_ ,j2}(i)
304             );
305             A = area(P);
306             if any(A, 'all')
307                 overlap{i_ ,j_ ,j1-1} = [overlap{i_ ,j_ ,j1-1}; P(
308                 logical(A))];
309                 o_overlap{i_ ,j_ ,j1-1} = [o_overlap{i_ ,j_ ,j1-1};
310                 o_material{i_ ,j_ ,j1}(logical(A))];
311                 material_minus{i_ ,j_ ,j1} = subtract(material_minus
312                 {i_ ,j_ ,j1},P);
313             end
314         end
315     end
316     waitbar((i_-1+j_/n_)/m_,wb,['Calculating overlaps... (',
317     num2str(k), '/', num2str(n_k), ')']);
318 end
319 end
320
321 %% Defect layer method
322 D = zeros(m_*n_*n_k*2,12);
323 for i_ = 1:m_
324     for j_ = 1:n_
325         %%Material layer
326         vf = sum(area(vertpcat(material_minus{i_ ,j_ ,:}))) / area(
327         mesh_element(i_ ,j_ ));
328         o_ = sum(area(vertpcat(material_minus{i_ ,j_ ,:})) .* vertpcat(
329         o_material{i_ ,j_ ,:})) / sum(area(vertpcat(material_minus{i_ ,j_
330         ,:})));
331
332         p = vf*pc+(1-vf)*pm;
333         E1 = vf*E1c+(1-vf)*Em;
334         E2 = (vf/E2c+(1-vf)/Em)^-1;
335         v12 = vf*v12c+(1-vf)*vm;
336         G12 = (vf/G12c+(1-vf)/Gm)^-1;
337         G13 = (vf/G13c+(1-vf)/Gm)^-1;
338         G23 = vf*G23c+(1-vf)*Gm;
339
340         D(sub2ind([m_,n_],i_ ,j_ )*2-1,:) = [i_ j_ k*2-1 p E1 E2 v12 G12
341         G13 G23 h0 o_];
342
343         %%Overlap layer
344         vf = sum(area(vertpcat(overlap{i_ ,j_ ,:}))) / area(mesh_element(i_
345         ,j_ ));
346         o_ = sum(area(vertpcat(overlap{i_ ,j_ ,:})) .* vertpcat(o_overlap{i_
347         ,j_ ,:})) / sum(area(vertpcat(overlap{i_ ,j_ ,:})));
348         h = vf*h0;
349
350         D(sub2ind([m_,n_ ,n_k],i_ ,j_ ,k)*2,:) = [i_ j_ k*2 pc E1c E2c
351         v12c G12c G13c G23c h o_];
352         waitbar((i_-1+j_/n_)/m_,wb,['Calculating section stiffnesses

```

```
... (',num2str(k), '/' ,num2str(n_k),')');
341     end
342 end
343
344 % Convert to table
345 D(D(:,11) == 0,:) = [];
346 D = array2table(D, 'VariableNames',VariableNames);
347 T = [T; D];
348 end
349
350 %% Export
351 writetable(T, strcat('dataset_',datestr(datetime,'yyymmdd_HHMMSS'),' .csv')
)
352 disp('Done!')
```